The 40th ICFA Advanced Beam Dynamics Workshop on High Luminosity e^+e^- Factories

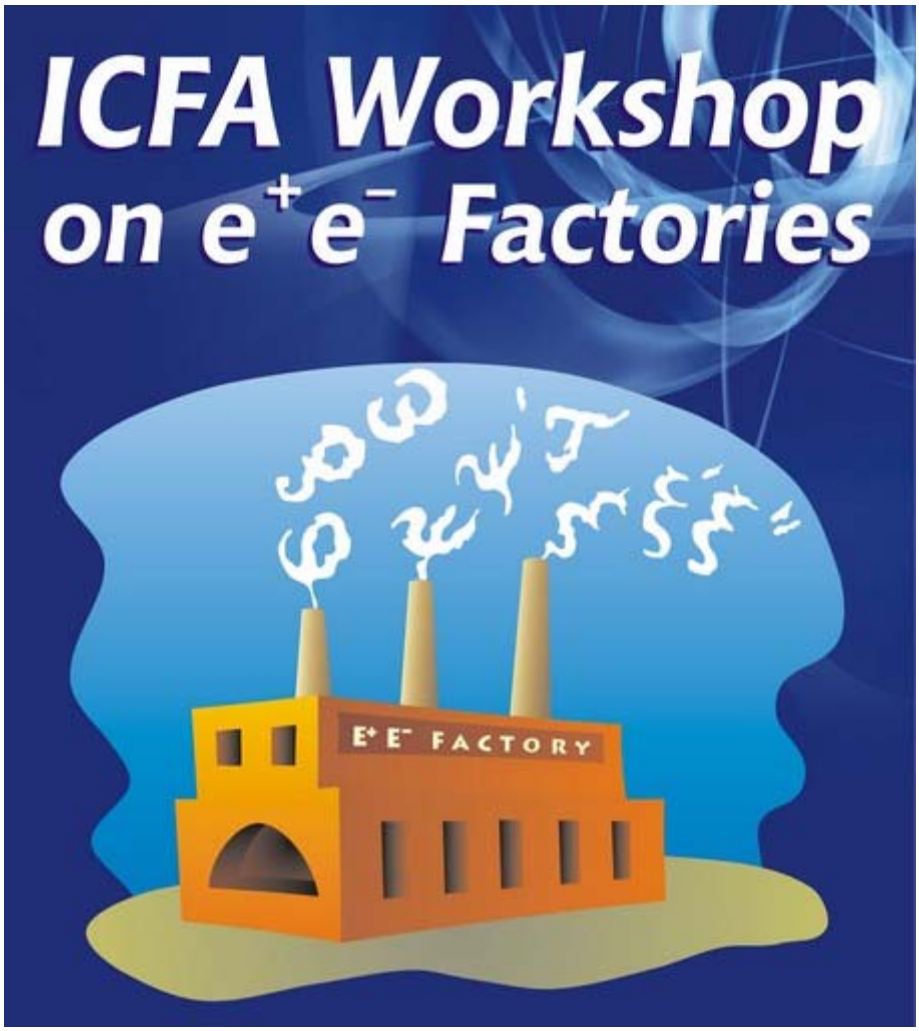

Contributions to the Proceedings

14 – 16 April, 2008

Budker Institute of Nuclear Physics,
Novosibirsk, Russia

AN OVERVIEW OF THE BEPCII PROJECT

C. Zhang for the BEPCII Team, IHEP, CAS
P.O.Box 918, Beijing 100049, China

Abstract

The BEPCII, as a natural extension of the BEPC (Beijing Electron-Positron Collider), is a double ring e-e$^+$ collider and a synchrotron radiation (SR) source with its outer ring, or SR ring. As an e-e$^+$ collider, the BEPCII operates in the beam energy region of 1-2.1 GeV with design luminosity of 1×10^{33}cm^{-2}s^{-1} at 1.89 GeV. As a light source, the SR ring operates at 2.5 GeV and 250 mA. The project started construction in the beginning of 2004. The upgrade of the injector linac completed in late 2004. The BEPC ring dismount started in July 2005. Installation of the storage ring components completed in October 2007. The commissioning is in progress. In the meantime, the BESIII detector was constructed, assembled and tested in the off-line position beside the interaction region (IR). This paper provides an overview of the BEPCII project.

GENERAL DESCRIPTION

The BEPCII serves the purposes of both high energy physics experiments and synchrotron radiation applications. The details of the BEPCII design can be found in its design report [1]. The goals of the BEPCII are shown in Table 1.

Table 1: The design goals of the BEPCII

Beam energy	1-2.1 GeV
Optimum energy	1.89 GeV
Luminosity	1×10^{33} cm^{-2}s^{-1} @189 GeV
Linac injector	Full energy inj.: 1.55-1.89 GeV Positron inj. rate ≥50 mA/min
Dedicated SR	250 mA @ 2.5 GeV

Serving as a collider, the BEPCII will operate in the beam energy region of 1.0-2.1 GeV so that its physical potential in τ-charm range is preserved. The design of the BEPCII aims at a high luminosity. The luminosity of an e$^+$-e collider is expressed as

$$L(\mathrm{cm}^{-2}\mathrm{s}^{-1}) = 2.17\times10^{34}(1+r)\xi_y \frac{E(GeV)k_b I_b(\mathrm{A})}{\beta_y^*(\mathrm{cm})},$$

where $r=\sigma_y^*/\sigma_x^*$ is the beam aspect ratio at the interaction point (IP), ξ_y the vertical beam-beam parameter, β_y^* the vertical β-function at IP, k_b bunch number in each beam and I_b the bunch current. The strategy for the BEPCII to reach the design luminosity is to apply multi-bunch collisions (k_b=93) with two rings and micro-β at IP with short bunches whose length is compatible to the β_y^* value. A multi-coil superconducting magnet is used on each side of the southern IP. The layout and installed double-ring accelerator units in the BEPCII tunnel are shown in Fig. 1.

The inner ring and the outer ring cross each other in the northern and southern IP's. The horizontal crossing angle between e$^+$ and e beams at the southern IP, where the detector locates, is 11×2 mrad to meet the requirement of sufficient separation but no significant degradation to the luminosity. In the northern crossing region, e$^+$ and e beams cross horizontally and a vertical bump is used for beam separation, so that the optics of the two rings remains symmetric. For the dedicated synchrotron radiation operation of the BEPCII, electron beams circulate in the outer ring with a pair of horizontal bending coils in SC magnets and in the northern IP a bypass is designed to connect two halves of the outer ring. The machine physics issues are discussed in Ref. [2].

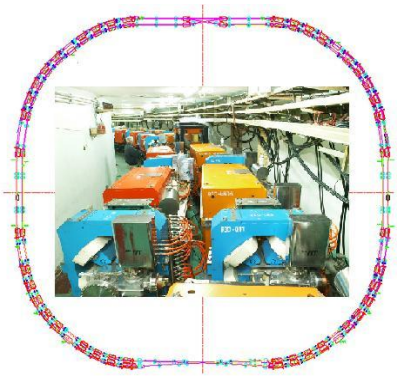

Figure 1: Layout and installed double-ring units.

The milestones of the BEPCII are as follows:

January 2004	Construction started
May 4, 2004	Dismount of 8 linac sections started
Dec. 1, 2004	Linac delivered e beams for BEPC
July 4, 2005	BEPC ring dismount started
March 2, 2006	BEPCII ring installation started
Nov. 13, 2006	Commissioning with conventional IR magnets started
Oct. 24, 2007	Commissioning with superconducting IR magnets started
Jan. 29, 2008	2×500 mA e$^+$e collision realized with luminosity higher than 1×10^{32}cm^{-2}s^{-1}

THE BEPCII ACCELERATORS

INJECTOR LINAC

The BEPC injector is a 202-meter electron/positron linac with 16 RF power sources and 56 S-band RF structures. The BEPCII requires the injector in two aspects. One is the full energy of e$^+$ and e beams injected into the storage rings, i.e. $E_{\mathrm{inj}} \geq 1.89$ GeV; the other is e$^+$ injection rate ≥ 50 mA/min. To realize the full energy top-off injection up to 1.89 GeV, the 30MW klystrons are replaced with the new 45-50 MW ones and the modulators upgraded with new pulse transformer oil tank assembly, PFN's, thyratrons, charging choke and DC power supplies. In order to

compensate the RF phase drift due to various factors, an RF phasing system is developed.

The technical measures taken for increasing positron intensity in the BEPCII injector can be summarised as following: to increase the e^- beam current on e^+ target from 2.5A to 6A, the repetition rate from 12.5Hz to 50Hz, the bombarding energy for e^+ from 140MeV to 240MeV; to develop a new positron source to increase the yield from 1.4% to 2.7%, and to apply two-bunch injection scheme. Though the pulse length reduced from 2.5 ns to 1ns, the total gain factor of the e^+ intensity can be about 20 times higher than the BEPC. The new developed positron source is pictured in the Fig. 2.

Figure 2: The new developed positron source.

All the new hardware subsystems, including the electron gun, the 40MeV pre-injector, the 200MeV booster section and the positron source of the linac were installed in the summer 2004 after dismounting the old devices. Figure 3 shows the BEPCII injector linac.

Figure 3: The BEPCII injector linac.

It took less than one month to start up the machine and process the new systems before the linac provided electron beams for the dedicated SR operation of the BEPC storage ring starting from the beginning of the December 2004. The commissioning of the linac for e^+ beam has been carried out during the machine studies. The first e^+ beam of 50 mA was obtained at the linac end on March 19, 2005. The e beam current output from the gun is ~10A, and ~6A at the positron converter target which is the same as simulation. All of the 16 RF power sources were rebuilt, and stably work at 50pps. The new control and beam instrumentation systems make the machine commissioning and operation more convenient. The performance of the linac is listed in Table 2, showing that its design specification is reached.

Table 2: The results of the linac commissioning

	Unit		Measured	Design
Energy	GeV		1.89	1.89
Beam current	mA	e^+	63	37
		e	>510	500
Emittance	mm·mr	e^+	0.35	0.4
		e	0.1	0.1
Energy spread	%	e^+	0.30	0.5
		e	0.37	0.5
Repetition rate	Hz		50	50
Pulse length	ns		1.0	1.0
e^+ injection rate	mA/min.		50~80	>50

THE STORAGE RINGS

The BEPCII storage rings consist of two rings, i.e. the e^+ ring and the e ring. The two outer halves of the e^+ and e rings are used for the dedicated SR operation. Table 3 lists the main parameters of the BEPCII storage rings.

Table 3: Main Parameters of the BEPCII storage rings

Parameters	Unit	Collision	SR
Energy	GeV	1.89	2.5
Circumference	m	237.53	241.13
RF frequency	MHz	499.8	499.8
RF voltage	MV	1.5	1.5~3.0
Beam emittance	nm·rad	144	120
Bunch number		93	200-400
Beam current per ring	A	0.91	0.25
Injection energy	GeV	1.89	1.89
β-function at IP	m	1/0.015	–
Crossing angle	mrad	11× 2	–
Beam-beam Parameter		0.04	–
Luminosity	$cm^{-2}s^{-1}$	1.0×10^{33}	–

RF system

Two SC cavities are installed in the BEPCII with one cavity in each ring to provide RF voltage of 1.5 MV/ring. Each cavity is powered with a 250 kW klystron. The horizontal high power test shows the Q values of 5.4×10^8 and 9.6×10^8 at V_{rf}=2 MV for the west and east cavities respectively, higher than the design values of 5×10^8 at 2 MV. Figure 4 pictures the cavity in installation.

Figure 4: A superconducting cavity in installation.

Magnets and power supplies

The BEPCII will reuse 44 BEPC bends and 28 quads. In total 267 new magnets, including 48 bends, 89 quads, 72 sextupoles, 4 skew quads and 54 dipole correctors, need to be produced. Most magnets were fabricated in the IHEP workshop. The magnets were measured with both rotating coils and stretched wire. The results are in agreement with each other within 10^{-3}. Figure 5 pictures a quadrupole magnet in measurement with a rotating coil. There are 1 electric and 4 permanent wigglers in the storage rings serving as SR wavelength shifters. Among the 4 permanent wigglers, three are out-vacuum and one in-vacuum.

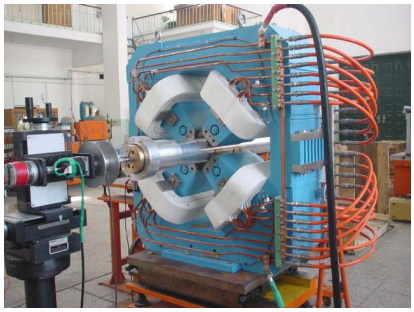

Figure 5: A quadrupole magnet in measurement.

To provide required flexibility for BEPCII operation with various modes, each arc quadruple is excited by an independent power supply. There are all together 345 power supplies in the storage rings. The power supplies have been installed, connected to the magnets and tested. Their current stability is better than 1×10^{-4}.

Vacuum System

The BEPCII imposes two challenges to the vacuum system, one is the vacuum pressure, and the other is the impedance. The designed dynamic vacuum pressure are 8×10^{-9} Torr in the arc and 5×10^{-10} Torr in the IR. Antechambers are chosen for the arc of both e^+ and e rings. For the e^+ ring, the inner surface of the beam pipe is coated with TiN in order to reduce the secondary electron yield (SEY). Measurement results show that the maximum SEY is 1.6-1.9 after the coating, seen in Fig. 6.

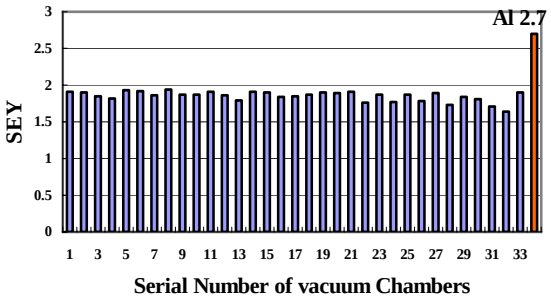

Figure 6: Measured SEY of TiN-coated chambers.

IR and SC Insertion Magnets

The IR has to accommodate competing and conflicting requirements from the accelerator and the detector. Many types of equipment including magnets, beam diagnostic instruments, masks, vacuum pumps, and the BESIII detector must co-exist in a crowded space. A special pair of superconducting insertion magnets (SIM's) is placed in the IR. Each SIM consists of a main and a skew quadrupoles, 3 compensation solenoids and 2 dipole coils, for squeezing the □-functionat IP, compensating the detector solenoid and to serve as the bridge connecting outer ring for SR operation, respectively. The SIM's were installed into IR in Oct. 2007. Some special warm bore magnets in IR such as septum bending magnet and two-in-one quadrupoles have been manufactured, tested and installed. Figure 7 shows two SIM's and some warm magnets in the IR.

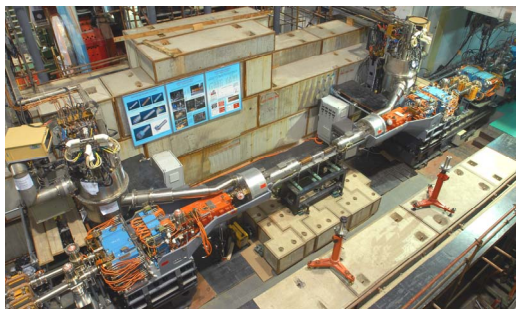

Figure 7: SIM's and some warm magnets installed in IR.

Instrumentation and Control

The instrumentation system consists of 136 beam position monitors (BPM's), 2 DCCT's, 2 bunch current monitors and 2 synchrotron radiation monitors. Transverse bunch-by-bunch feedback systems are equipped in order to damp coupled bunch instabilities. The control system is based on the EPICS environment, providing a friendly man-machine interface for operators. The instrumentation and control systems have been examined during the commissioning.

Cryogenics system

The BEPCII cryogenics system is composed of four sub-systems: the central cryogenic plant and three satellite cryogenic systems for the RF cavities, the SIM magnets, and the SSM detector solenoid. Two 500W refrigerators are equipped to cool the SC devices to 4.5K, one for the cavities and another for the magnets. The cavity side cryogenics has been in normal operation since mid-2006, while the magnet part since mid-2007 after problems of control Dewar, valve boxes and current leads were fixed.

Commissioning and Operation

The operation of the BEPC completed on July 4, 2005, and then dismount of the old ring started. The storage ring installation was completed in early November 2006 except the cryogenics of the magnets. It was decided to install conventional magnets in the IR to start storage ring commissioning (Phase 1) and SR operation. In the meantime, improvement of the cryogenics system and measurement of the SC magnets was carried out at the off-line position. The Phase 2 commissioning and SR operation with SIM's in the IR was started late Oct. 2007. By the

end of the Jan. 2008, 2×500mA e^+-e^-beam collision was realized and the luminosity measured with zero-degree γ detector was higher than $1\times10^{32}cm^{-2}s^{-1}$. Details of the commissioning are presented in another paper of these proceedings [3].

BESIII DETECTOR

Design Consideration

A high quality detector with advanced technology comparable to BEPCII needs to be built in order to reach the physics goal of the project. Therefore a modern detector, the BESIII, is designed to meet the following requirements:

- Very good photon energy resolution, good angle resolution for photon measurement.
- Accurate 4-momenta measurement of low charged particles.
- Good hadron identification capabilities.
- A modern data acquisition system and the front-end electronics system based on the pipeline technique.

The choice of the detector components is based on physics requirements, existing experience, budgetary, schedule and etc. Figure 8 shows the schematics of the BESIII detector, which consists of main drift chamber (MDC), CsI crystal electromagnetic calorimeter (EMC), time of flight (TOF) counters, μ counters, SC solenoid magnet and beryllium beam pipe. Table 4 gives main parameters of the BESIII detector.

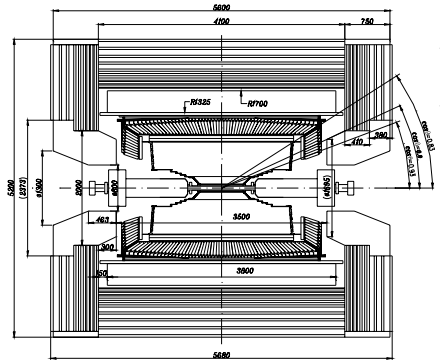

Figure 8: Schematic drawing of the BESIII detector.

Table 4: Main parameters of the BESIII detector

Sub-system	BESIII
MDC	σ_{xy} = 130μm
	$\Delta P/P$=0.5% @ 1GeV
	$\sigma_{dE/dx}$= (6-7) %
EMC	$\Delta E/E$=2.5%@1GeV
TOF detector	σ_T=100 ps (barrel), 110 ps (endcap)
μ counters	9 layers
Magnet	Superconducting, B=1.0 Tesla

Construction

On March 27, 2008, the BESIII beryllium beam pipe was successfully installed inside the MDC, which marks the full completion of the BESIII detector construction. In the past 4 years, all sub-detectors, the MDC, barrel and endcap TOF, barrel and endcap EMC, μ counters were produced, assembled and tested with DAQ, trigger and slow control systems. The SC magnet was constructed, tested and field measured at 1 Tesla and 0.9 Tesla. The software and physics preparation are in good shape. Figure 9 pictures the barrel EMC in installation.

Figure 9: Installation of the Barrel EMC.

On Feb. 14, 2008, the BESIII realized cosmic ray data acquisition (see Fig. 10) after all the sub-detectors were put into place, which indicated that BESIII had successfully finished initial tuning.

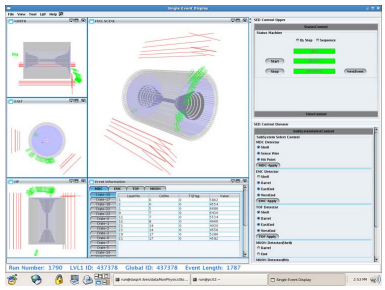

Figure 10: BESIII cosmic ray data acquisition.

Machine -Detector Interface

The interface between the BEPCII accelerator and the BESIII detector is intensively studied. With injection optimisation, the dose rate gets acceptable for pulling the BESIII detector into the IR. More collimators will be installed in the storage rings to reduce background during data acquisition. Some interlocks are introduced. Shielding and radiation background monitors will be installed in the detector. The details are given in Ref. [4].

PLAN AND SCHEDULE

The BESIII detector is scheduled to roll in the IR of the BEPCII in mid-April, 2008. The collider will be operated together with BESIII detector (Phase 3 commissioning) after the IR is reinstalled early June. It is expected that the luminosity would be high enough for the BESIII detector to start experiment by the end of 2008.

REFERENCES

[1] BEPCII Group, BEPCII Design Report, IHEP-Proceedings, Aug. 2001.
[2] Q.Qin, et al, these Proceedings, April 2008.
[3] J.Q.Wang, et al, these Proceedings, April 2008.
[4] D.P.Jin, et al., these Proceedings, April 2008.

THE SECOND PHASE COMMISSIONING OF BEPCII

J.Q. Wang, L. Ma and C. Zhang for the BEPCII Commissioning Team, IHEP, CAS
P.O. Box 918, Beijing 100049, China.

Abstract

BEPCII is the upgrade project of Beijing Electron-Positron Collider (BEPC), which will operate in the beam energy region of 1-2.1 GeV with the design luminosity of $1\times10^{33}cm^{-2}s^{-1}$ at 1.89 GeV. From Nov. 2006 to Aug. 2007, the phase one beam commissioning of BEPCII storage rings was carried out with the so called backup scheme which adopted conventional magnets in the IR instead of the superconducting insertion magnets (SIM). After the SIM was installed into the interaction region, the second phase commissioning began in Oct. 2007. The tuning method for high luminosity but low background has been extensively studied, and the beam current reached more than 1/2 of the design of 0.91 A, with the luminosity higher than $1 \times 10^{32}cm^{-2}s^{-1}$, which is 10 times of BEPC. In addition, beam was delivered to SR users for about 1 month at 2.5GeV with maximum current over 250mA. This paper describes the progress on beam commissioning, the main results achieved and issues related to high current and high luminosity.

INTRODUCTION

The BEPCII is the upgrade project of BEPC, serving continuously the dual purpose of high energy physics experiments and synchrotron radiation applications. The design goals and its construction is described in Ref. [1,2]. As an e^+-e^- collider, it consists of an electron ring (BER) and positron ring (BPR), respectively. The two rings cross each other at the southern interaction point (IP), where the dector is located, with a horizontal crossing angle of 11mrad×2. A pair of superconducting insertion magnets (SIM) are used to squeeze the β function at the IP, compensating the detector solenoid and to serve as the bridge connecting two outer half rings for SR operation, respectively. For the dedicated synchrotron radiation mode, electron beam circulates in the ring made up of two outer half rings. 5 wigglers were installed in the outer rings to generate more strong SR.

In accordance to the progress of construction, as well as to meet the demand from the SR users community, the beam commissioning of BEPCII is carried out in 3 phases: Phase 1, with the backup scheme which adopted the conventional magnets in the IR instead of SIM; Phase 2, with SIM in the IR; Phase 3, joint commissioning with detector.

The phase 1 commissioning was from Nov. 13, 2006 to Aug. 3, 2007. In this phase, 100mA by 100mA beam collision was achieved with β_y^*=5cm, while the estimated luminosity reached the level of BEPC. Two rounds of synchrotron radiation operation were arranged during the period. The beam performance and commissioning results have been reported on the APAC07 [3] and PAC07[4].

After the superconducting magnets SIM's and new vacuum chambers were installed into the IR in summer of 2007. The second phase commissioning was carried out from October 24, 2007 to Mar. 28, 2008. The main milestones of this phase of commissioning are listed in the following:

Oct. 25, the electron beam was stored

Oct. 31, the positron beam was stored

Nov. 18, the first e^+ e^- collision realized at β_y^*=1.5cm

Jan. 29, 2×500mA e^+ e^- collision realized with luminosity higher than $1\times10^{32}cm^{-2}s^{-1}$

In this phase, the dedicated SR mode was run for about one month, with peak beam current of 250mA. The beam lifetime reached to 10hrs at 200mA while the gap of the in-vacuum wiggler 4W2 was set to 18mm.

The following sections will mainly introduce the second phase commissioning for the collision mode, including the beam performance, the luminosity tuning and some issues relating to high beam current.

BEAM CURRENT GROWTH

The second phase commissioning of BER and BPR started in Oct. 2007. Since the difference on the storage ring between the first and second phases is only on the final focus quadrupoles, it took only one day to get beam stored in BER and BPR respectively.

To keep the vacuum pressure of the superconducting cavities well below the threshold set for the RF window protection, the rate to increase the beam currents in both rings was deliberately restrained to 10mA per day. However, when the beam current in BER exceeded 100mA,

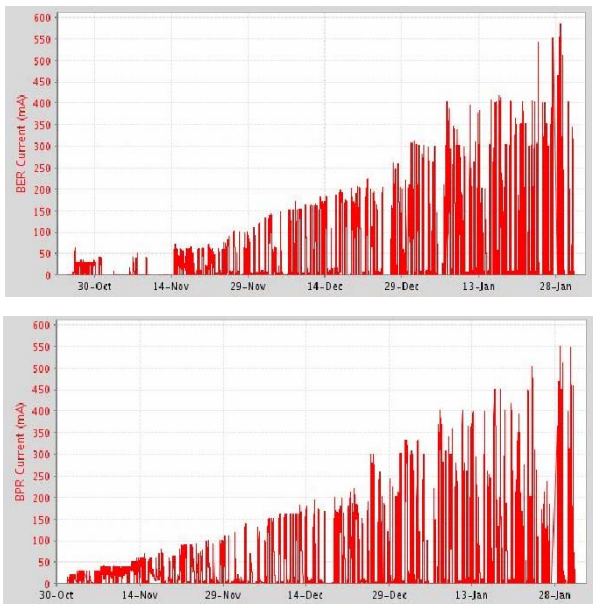

Figure 1: Current growth during the period of commissioning, BER (upper) and BPR (down)

#wangjq@ihep.ac.cn

the SC cavity (SCC) tripped often due to its arc interlock of window and following vacuum pressure raised quickly.. Similar condition happened in BPR when the current is over 200mA. To overcome the problem, a DC bias voltage was used on the power coupler of the SC cavity to suppress the multipacting effect. This worked very effectively and the vacuum condition significantly improved. Then the beam current of both rings was able to be improved steadily. Transverse feedback system was employed for smooth injection and stable operation at high beam current. The growths of the beam current in the BER and BPR are shown in Fig. 1.

BEAM PERFORMANCE

Optics and orbit

Then closed orbit and optics correction was done based on the response matrix and its analysis using LOCO (Linear Optics from Closed Orbits) method [5]. As the result, the measured beam optics functions are in good agreement with theoretical prediction with discrepancy within ±10% at most quadrupoles [6]. Table 2 summarizes the main parameters achieved for BER and BPR during this commissioning period.

Table 1: The main parameters of the BER and BPR

Parameters	Design	Achieved	
		BER	BPR
Energy (GeV)	1.89	1.89	1.89
Beam curr. (mA)	910	550	550
Bunch curr. (mA)	9.8	>10	>10
Bunch number	93	93	93
RF voltage	1.5	1.6	1.6
Tunes (ν_x/ν_y)	6.54 /5.59	6.544 /5.599	6.540 /5.596
$*\nu_s$ @ V_{RF}= 1.5MV	0.033	0.032	0.032
β_x^*/β_y^* (m)	1.0 /0.015	~1.0 /0.016	~1.0 0.016
Inject. Rate (mA/min)	200 e^- 50 e^+	>200	>50

$*\nu_s$ is extrapolated from the measurement at RF voltage of 1.69 MV for BER and 1.61MV for BPR, respectively.

LOCO analysis indicated that the quadrupole strengths are mostly lower than the design set within 1~2%. One contribution to this systemic component was from the short distance between the quadrupole and its adjacent sextupole. Another may from the fringe filed effect. Other origin of these errors is still pursued.

Injection

Efforts were mainly paid to improve the injection rate of positron beam. After the optimization of energy set and the orbit in the transport line, the injection rate was improved to more than 50mA/min, which is the designed goal. Occasionally, two neighbouring bunches were injected simultaneously, that may due to the unwanted micro bunches from the linac. This will be eliminated after the subharmonic bunching system is installed later. A wire scanner is being studied to get better match on the optics between linac and storage ring to increase the stability of the injection efficiency.

The two kickers are used for injection, thus the betatron phase advance between the two kickers is designed as 180 degree to form a local bump during injection. However, to reduce the residual orbit oscillation of the stored beam during injection, it's tricky to set the right timing and amplitude of the two kickers. This was done using the Libra BPM system [7]. The residual oscillations of the stored beam is measured and minimized while scanning the time delay and amplitude of each kicker in steps. Thanks to the sameness between the waveforms of the two kickers, after the time delay and amplitude of the two kickers was optimized for the injecting bunch, the residual orbit oscillation of all the other bunches during injection can be reduced to around 0.1mm, corresponding to about $0.1\sigma_x$, as shown in Fig 2. This made it possible to inject beam during collision.

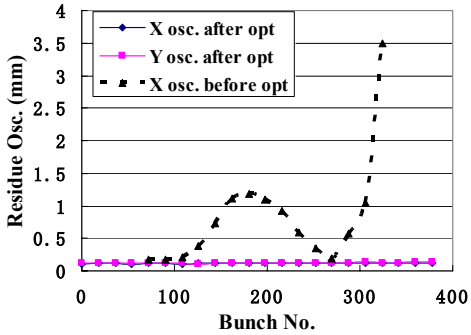

Figure 2: The residual oscillation of all bunches before (dashed line) and after (solid) the kickers optimized.

In most cases, one beam can be injected smoothly in collision with the other beam when the bunch current is below 7mA. But above 7mA/bunch, the injection of the second beam in collision becomes difficult with slow injection rate and beam loss monitors show significant dose. A horizontal separation at IP was helpful to get smooth injection. However, when the bunch current is high, say more than 7mA, it sometime leads to partial loss of one beam during the process to bring the two beams into collision. To investigate a better ways for smooth injection and stable collision with high bunch current is still under way.

Instabilities & feedback

The single bunch beam dynamics as well as collective effects is described in detail in ref. [8]. An analog bunch-by-bunch transverse feedback (TFB) system has been adopted to cure the instabilities [9].

In longitudinal, since SC cavity is adopted, the beam behaves fairly stable. However, synchrotron oscillation sideband was sometime observed along with beam current increase, but it seemed not caused by the beam instability, but by some noise in the LLRF loop. After the LLRF

properly tuned, the beam is much stable in longitudinal direction up to 550mA with 99 bunches in both rings.

In transverse, coupled bunch instability was observed in both BER and BPR. In BER, vertical sidebands near the rf frequency was observed on the spectrum analyser. These may be due to resistive wall. In BPR, a broadband distribution of vertical sideband spectrum has been observed, which can be attribute to the electron cloud effect. With the TFB carefully tuned, the sidebands of couple bunch instabilities in both BER and BPR can be well suppressed, as shown in Fig. 3.

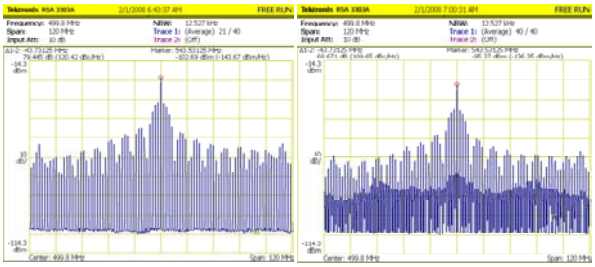

Figure 3: TFB turn on (left) and turn off (right)

Besides, streak camera was used to observe the vertical beam size blow up due to ECI, and there was not obvious grow up of the bunch size at the tail of the bunch train. As prevention to further ECI, solenoid has been winded on the vacuum chamber and can be put into use when needed.

Beam lifetime

The beam lifetime of single bunch is mainly limited by Touschek effect, and it behaves similarly versus bunch current in BER and BPR. The limitation of beam lifetime at high current operation seems dominant by the vacuum. Particularly, the vacuum pressure in BPR is about 70% higher than BER [10], this may lead to the shorter beam lifetime of BPR. Since there is slight blow up of beam size, the beam lifetime did not get worse during beam-beam collision.

However, the beam lifetime in both rings are shorter than expected from calculation, systematic studies are needed in the future.

LUMININOSITY TUNING

Single bunch collision

The two single bunches in each ring were brought to collision at the IP by Beam-Beam Scan (BBS). In phase one, beam-beam tune shift were measured and used to optimize the beam parameters for high luminosity. In phase two, a luminosity monitor (LUM) based on the detection of zero degree γ from radiative bhabha process was installed. It can distinguish the luminosity bunch by bunch and is fast enough to be used in the tuning procedures. Thus the beam parameters such as tune, coupling and local optics at IP were optimized to maximize the specific luminosity given by the LUM. The specific luminosity is defined as the luminosity divided by the number of bunches and also the product of bunch current of the two beams.

According to the beam-beam simulation the factional part of the transverse tunes were chosen near (6.54/5.59) for both rings. To get the best luminosity, tunes of each ring were scanned around the region. Then the tunes for BER and BPR were set near (6.54, 5.64) with two rings differed by about 0.005.

Optimization is also on the x-y coupling or beam size. This was done by adjusting the local vertical orbit in one sextupole in the arc. It's found that 1% coupling gives the best specific luminosity.

The vertical dispersion at IP was measured to be less than 10mm, and the contribution to the beam size at IP can be neglected. The local optical functions at the IP such as coupling and β_y^* waist were also adjusted to optimize the luminosity.

With the above beam parameters optimized, the maximum bunch current achieved in stable collision with high luminosity is 11mA by 11mA, which is higher than the design of 9.8mA.

Multi-bunch collision

For multi-bunch collision, it is important to have uniformly filled bunches. This has been configured in the injection control programme based on the event timing system. An algorithm has been developed to select the bucket with current below the limit set for each bunch according to the DCCT or Bunch Current Monitor (BCM), and then refill it with the rule of the smallest the first, thus, to get a uniform filling, as shown in Fig. 4.

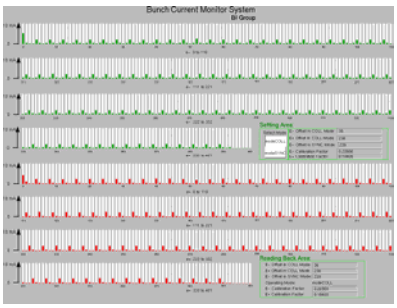

Figure 4: Display of uniform filling with BCM on 300mA×300mA multi-bunch collision.

Multi-bunch collision were practiced in two ways, one with relative high bunch current but small number of bunch, say above 7mA/bunch, the other is with moderate bunch current, but 93 bunches as designed. At same total beam current, the former case has the higher luminosity. But as mentioned before, the injection and collision process is not so stable. Thus, the best luminosity achieved was with 93 bunches at total beam current of 500mA, which is higher than $1\times10^{32}cm^{-2}s^{-1}$ with zero degree γ-detector, 10 times of BEPC.

The specific luminosity in multi-bunch case with high current seems lower than that with single bunch, shown in Fig. 5 [11]. One possible reason is the coupled bunch oscillation at high current. An indication is that when sometime the transverse feedback was better tuned, particularly at Y-direction, the luminosity could improve significantly.

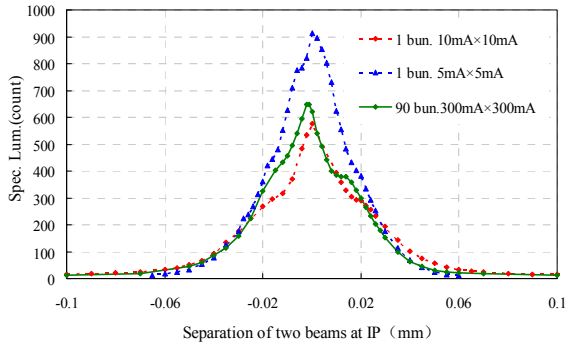

Figure 5: Spec. lum. of single(dashed) and multi-bunch (solid) vs. the vertical separation of two beams at IP.

Parasitic operation with wiggler

It is expected that SR user experiment can be carried out simultaneously during physics running. In the case with one wiggler 1W2 imposed, after the beam optics correction, the degradation of luminosity can be mitigated. Though the study is very preliminary, it proves in principle the feasibility of parasitic operation for SR use.

BACKGROUND

Experimental studies have been carried out to study the radiation dose around IP as well as the way to reduce the background. The main conclusion is that with the injection optimization the dose rate in the IR gets acceptable for the BESIII detector which is being pulled into the IR, and with collimators and masks, the background in the detector during its data acquiring could be well controlled. The details are introduced in ref. [12].

HIGH CURRENT ISSUES

Along with beam intensity growth, particularly when it is higher than 300mA, the heating effect due to SR and HOM may appear. Thus, more than 1000 thermal couplers were stick to the vacuum chamber, and the temperature at each location was displayed as bars in colour according to its dangerousness as green, yellow and red, respectively.

In most case, the temperature rise was due to the SR power increase. After the flux of cooling water adjusted, the heating was mitigated. However, some HOM heating appeared in the DCCT and the in-vacuum permanent wiggler 4W2, with the temperature rise shows the feature of sensitive to the bunch current.

For DCCT, though the RF shielding of copper layer to bridge the image current re-routing on the ceramic gap was adopted, its capacity seems not big enough for some low frequency part of the image current. Some capacitors will be connected to improve the RF shield.

For the 4W2, to prevent the magnet poles being over heated due to HOM, which may lead to demagnetization, a movable beam pipe designed to shield the HOM, was put into the right place. It functioned as expected and the temperature rise dropped to acceptable level even the beam current went up to more than 500mA, and no demagnetization observed.

Besides HOM heating, the orbit position measured by some BPM appeared sensitive to the beam current. This may attribute to the transverse wake field.

Nonlinear increase of vacuum pressure versus beam current was observed in BPR, as shown in Fig. 6. The threshold depends on the filling pattern. This may due to beam induced multipacting inside the beam pipe and can be one cause of the higher vacuum pressure in BPR. Solenoid winding may be helpful to ease the problem.

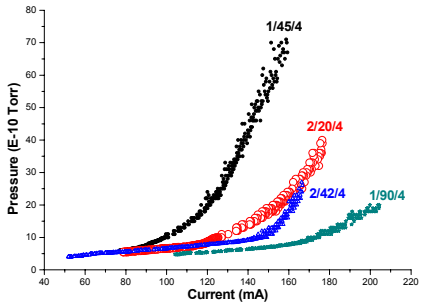

Figure 6: Nonlinear vacuum pressure versus beam current, with filling pattern marked on each curve.

SUMMARY

The optimization methods to achieve high current as well as high luminosity have been practice systematically. The beam current has reached more than 1/2 of design with no disastrous instabilities, and most devices performed stably as expected. However, there are still lot of issues for further studies such as to improve the specific luminosity at high beam current, to understand the beam loss mechanism, and so on.

The detector is being moved into the IR this spring, and the third phase commissioning is scheduled in early June. To improve the luminosity while control the background acceptable for data taking is still challenging.

ACKNOWLEDGEMENT

The authors thank all the members of the BEPCII team for the supporting commissioning. Colleagues from BNL, DESY, KEK, SLAC provided much help on the SIM, cryogenic system, SRF system etc. Thanks also go to the BEPCII IMAC members.

REFERENCES

[1] BEPCII Group, BEPCII Design Report, Aug. 2001.
[2] C. Zhang, these proceedings.
[3] C. Zhang et al, Proc. of APAC'07, India, Jan. 2007.
[4] J. Q. Wang et al, Proc. of PAC'07, U.S.A, July. 2007.
[5] J. Safranek et al, Proc. of EPAC'02, France, 2002.
[6] Y.Y. Wei et al, these proceedings.
[7] H.Z. Ma et al, internal report, Mar. 2008.
[8] Q. Qin et al, these proceedings.
[9] J.H. Yue et al, these proceedings.
[10] Q. Xiao et al, internal report, Mar. 2008.
[11] C.H. Yu et al, internal report, Mar. 2008.
[12] D.P. Jin et al, these proceedings.

BEAM DYNAMICS STUDIES IN THE BEPCII STORAGE RINGS*

Q. Qin#, N. Huang, W.B. Liu, Y.D. Liu, Y.M. Peng, J. Qiu, D. Wang, X.H. Wang, N. Wang, J.Q. Wang, Y.Y. Wei, X.M. Wen, J. Xing, G. Xu, C.H. Yu, C. Zhang, Y. Zhang, Z. Zhao, D.M. Zhou,
IHEP, CAS, P.O. Box 918-9, Beijing 100049, P.R. China

Abstract

As an upgrade project of the Beijing Electron Positron Collider (BEPCII), the commissioning of the storage rings for both collision and synchrotron radiation modes started in Nov. 2006. Besides the normal commissioning on luminosity and beam performance, beam dynamics studies are being carried on as well. Some results on beam parameters determination, single and multi-bunch effect, and beam instabilities of two rings are given in this paper.

INTRODUCTION

The upgrade project of the Beijing Electron Positron Collider (BEPC), BEPCII, is composed of a linac, two transport lines for both positron and electron beams, and two storage rings in parallel to accommodate e- and e+ beams, respectively. The two halves of the outer rings are connected as a synchrotron radiation ring with 14 beam lines extracted from 5 wigglers and 9 bending magnets. The layout and other details of the three rings of BEPCII can be found in [1, 2] in this proceedings.

In this paper, we mainly discuss the beam dynamics study in the collision rings, say, BER and BPR for e- and e+ beam, respectively. Some main nominal parameters of the lattice are listed in Table 1.

Table 1: Main parameters of the BEPCII collision rings

Beam energy	GeV	1.89
Circumference	m	237.53
Beam current	A	0.91
Bunch current / Bunch No.	mA	9.8 / 93
Natural bunch length	mm	13.6
RF frequency	MHz	499.8
Harmonic number		396
Emittance (x/y)	nm.rad	144/2.2
β at IP (x/y)	m	1.0/0.015
Crossing angle	mrad	±11
Tune (x/y/s)		6.54/5.59/0.034
Momentum compaction		0.0237
Energy spread		5.16×10^{-4}
Natural chromaticity (x/y)		−10.8/−20.8
Luminosity	$cm^{-2}s^{-1}$	1×10^{33}

Figure 1 shows the Twiss functions of the interaction region, the RF region and the whole ring. There're 10 dipoles in each arc of a ring and a quasi-FODO structure with two missing dipoles are applied, in order to have a big emittance and a high beam current.

In the second section, we will discuss the determination of the beam main parameters. Single and multi-bunch beam effects will be introduced in section 3. Some instabilities were observed and showed in section 4. At last, a summary will be given.

*Work supported by National Foundation of Natural Sciences contract 10725525

#qinq@ihep.ac.cn

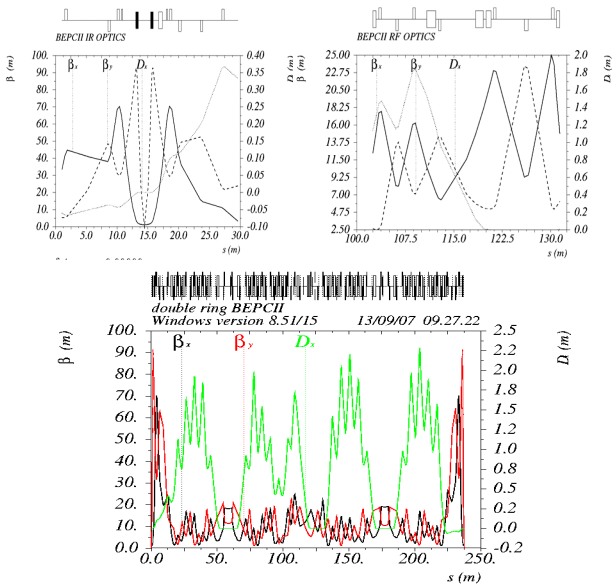

Figure 1: Twiss functions in the IR (up-left), the RF region (up-right) and the whole ring (down) of BER/BPR.

DETERMATION OF BEAM PARAMTERS

β Functions and Transverse Tunes

The beta functions along the two rings are measured before and after the optics corrections with the LOCO [3] based on the measured response matrices. Tune modulation method is applied to measure the beta functions in all the locations of quadrupoles. Figure 2 shows the measured and nominal beta functions after the optics corrections for BER as an example. The relative errors between the nominal and measured beta functions are less then 10% averagely.

The beta functions at the IP are measured with the same

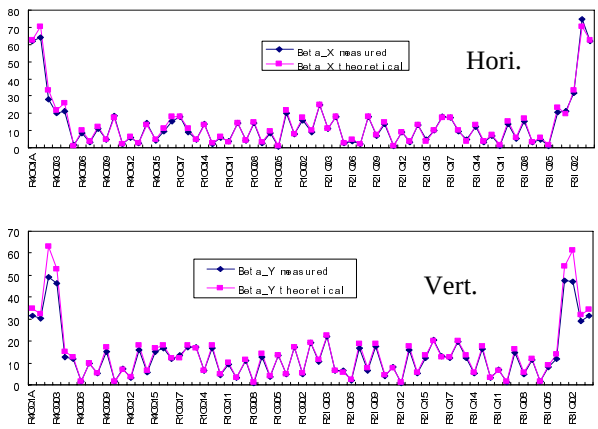

Figure 2: Comparison between measured and nominal β functions in BER after optics correction.

method, but the thick lens model is taken into account as we calculate the average beta at the edge of the first quad near the IP. Since the superconducting quads (SCQ) near the IP off-centrally bend the beam in horizontal, the contribution from this effect is also considered. The average β function of a quad can be expressed as [4]

$$\bar{\beta}_{x,y} = \pm\frac{2}{\Delta kl}\left[\cot(2\pi\nu_{x,y})(1-\cos(2\pi\Delta\nu_{x,y}))+\sin(2\pi\Delta\nu_{x,y})\right], \quad (1)$$

where Δkl means the change of the integral strength of a quad, and $\Delta\nu$ the corresponding change of tunes. If the SCQ bends the beam with an angle of θ, and its bending radius is ρ, we can easily get

$$\bar{\beta}_{x} = \pm\frac{2}{\left(\Delta kl+\frac{\theta}{\rho}\right)}\left[\cot(2\pi\nu_{x})(1-\cos(2\pi\Delta\nu_{x}))+\sin(2\pi\Delta\nu_{x})\right]. \quad (2)$$

The thick lens model [5] of a quad gives us the following formulae to calculate the β functions at the IP, i.e., $\beta_{x,y}^*$ as

$$\begin{aligned}\bar{\beta}_{y} &= \{\frac{L_0\sin^2(k_0l)}{k_0^2l}+\frac{k_0l-\sin(k_0l)\cos(k_0l)}{2k_0^3l}+\frac{L_0^2[k_0l+\sin(k_0l)\cos(k_0l)]}{2k_0l}\}\cdot\frac{1}{\beta_y^*}\\ &+\frac{k_0l+\sin(k_0l)\cos(k_0l)}{2k_0l}\cdot\beta_y^* \qquad (3)\\ &= C_1\cdot\frac{1}{\beta_y^*}+C_2\cdot\beta_y^*,\end{aligned}$$

and

$$\begin{aligned}\bar{\beta}_{x} &= \{\frac{L_0\sinh^2(k_0l)}{k_0^2l}-\frac{k_0l-\sinh(k_0l)\cosh(k_0l)}{2k_0^3l}+\frac{L_0^2[k_0l+\sinh(k_0l)\cosh(k_0l)]}{2k_0l}\}\cdot\frac{1}{\beta_x^*}\\ &+\frac{k_0l+\sinh(k_0l)\cosh(k_0l)}{2k_0l}\cdot\beta_x^* \qquad (4)\\ &= D_1\cdot\frac{1}{\beta_x^*}+D_2\cdot\beta_x^*.\end{aligned}$$

Here, k_0l is the nominal integral strength of quad, L_0 is the drift length closest to the IP, and *C*s and *D*s are connected with $\beta_{x,y}^*$ as

$$\begin{aligned}\beta_y^* &= \frac{\bar{\beta}_y-\sqrt{\bar{\beta}_y^2-4C_1C_2}}{2C_2}\\ \beta_x^* &= \frac{\bar{\beta}_x-\sqrt{\bar{\beta}_x^2-4D_1D_2}}{2D_2}.\end{aligned} \quad (5)$$

Thus, we can get the $\beta_{x,y}^*$ with the measured average $\bar{\beta}_{x,y}$ of the SCQs near the IP. The results are listed in Table 2. By anti-symmetrically changing the strengths of SCQs near the IP, the waist of β can be found and thus the $\beta_{x,y}^*$ could be deduced too. The method using LIBERA BPM system to measure the $\beta_{x,y}^*$ is being developed.

Table 2: Measured $\bar{\beta}_{x,y}$ of the SCQs and the IP

	$\bar{\beta}_x$ (m)	$\bar{\beta}_y$ (m)
SCQW-1*	1.293	60.87
SCQE-1	3.661	60.60
IP-1	0.983	0.0171
SCQW-2	2.202	62.45
SCQE-2	3.658	62.12
IP-2	0.986	0.0167

* 1 and 2 mean the times of measurement

As listed in [2], the measured tunes are close to the nominal values, since the optics is corrected well.

Dispersion Function

The dispersion functions around the rings are measured with the changing of orbits due to the changing of RF frequency. The results are showed in [3]. From the measured dispersion of the BPMs close to the IP, we can deduce the dispersions at the IP, which are 1 or 2 cm in horizontal and several mm in vertical.

Chromaticity and Optimized RF Frequency

Corrected and natural chromaticities were measured systematically at the first stage of the BEPCII commissioning, in which the SCQs were replaced by the normal conducting magnets. Table 3 shows the results of the chromaticity measurement.

Table 3: Corrected and natural chromaticity measurement

Nomi. ξ_x/ξ_y	Meas. ξ_x/ξ_y	Nomi. ξ_x/ξ_y	Meas. ξ_x/ξ_y
-5.0/-5.0	-5.33/-5.02	-1.0/-1.0	-1.28/-0.82
-3.0/-3.0	-3.19/-2.46	+1.0/+1.0	+1.05/+0.95
-2.0/-2.0	-2.33/-0.89	+5.0/+5.0	+4.50/+3.28
Naturalξ_{x0}/ξ_{y0}	-11.7/-10.4	Meas. ξ_{x0}/ξ_{y0}	-10.33/-10.07

By changing the RF frequency at different chromaticity values, we measured the corresponding transverse tunes, and thus found the central beam path in the sextupoles and the optimized RF frequency, shown in Fig. 3. In the BER, it is 499.802 MHz as that given in Fig. 3.

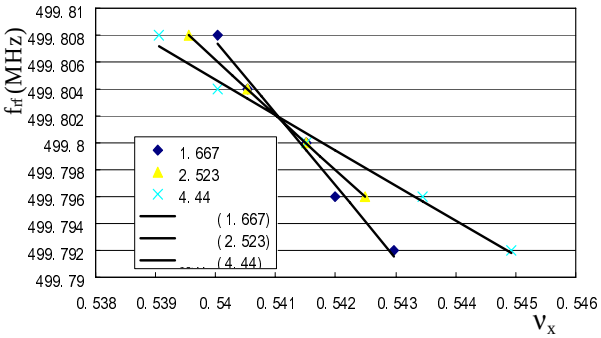

Figure 3: Optimized RF frequency measurement.

Transverse Coupling

The details of the transverse coupling adjustment and measurement are given in [3].

SINGLE BEAM DYNAMICS

Bunch Lengthening

In colliders, bunch lengthening is the main single bunch instability and limits the enhancement of luminosity. After fixing the operation lattice for collision, we measure the bunch lengthening in both rings with streak camera. In the measurement, we use single bunch for each beam without any collision. The momentum compaction is calculated from the measured synchrotron tune and the RF voltage, which was calibrated by the power of cavities. The bunch length is measured when the single bunch current is changed with the fixed RF voltage. The bunch length is fitted with the distribution of bi-Gaussian as that used in the BEPC before [6]. Static image was measured

and reduced from the measured bunch lengths. Figure 4 shows the bunch lengthening as a function of current in the BER and BPR, respectively.

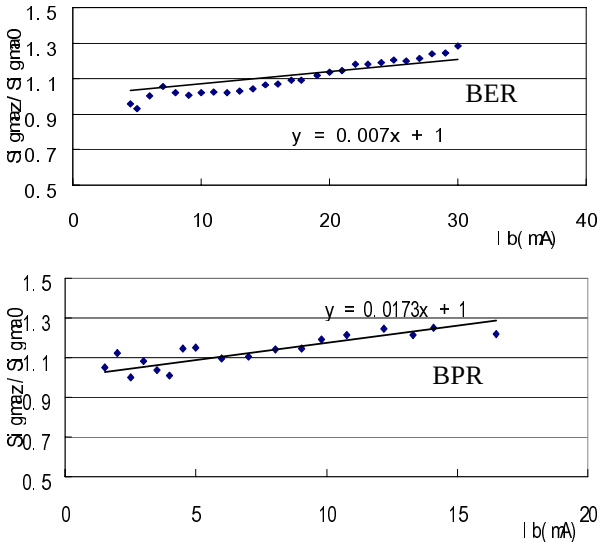

Figure 4: Bunch lengthening vs. bunch current.

From the bunch lengthening, we can get the inductance of the BER and BPR as L = 32.1 nH and L = 118 nH, respectively, which also correspond to $|Z/n|_0$ = 0.25 Ω and $|Z/n|_0$ = 0.94 Ω. Since the bunch lengthens at low current due to potential well distortion, it can be expressed as [7]

$$\frac{\sigma_l}{\sigma_{l0}} \approx 1 + \frac{e\alpha_p I_b \omega_0 L}{8\sqrt{\pi}\nu_s^2 E}\left(\frac{R}{\sigma_{l0}}\right)^3, \qquad (6)$$

where σ_l and σ_{l0} are the bunch length at current I_b and the natural bunch length, respectively, α_p the momentum compaction, ω_0 the angular revolutionary frequency, L the inductance, R the average radius of ring, ν_s the longitudinal tune, and E the beam energy. With the calculated L from the bunch lengthening measurement, we can get $\sigma_l/\sigma_{l0} \approx 0.0053I_b+1$ for the BER and $\sigma_l/\sigma_{l0} \approx 0.01855I_b+1$ for the BPR, respectively, which are similar with the fitting results shown in Fig. 4.

Tune Variation as a Function of Bunch Current

The effective impedance can also be estimated from the tune variation due to the changing of bunch current with the following expressions [8]:

$$\frac{d\nu_\perp}{dI} = \frac{R}{4\sqrt{\pi}(E/e)\sigma_l}\overline{\beta}_\perp Z_{\perp,eff}\ , \qquad (7)$$

where $\overline{\beta}_\perp$ is the average β function around the ring. The tune variation in each ring is got when the bunch current decreases without the other beam existing. Figure 5 shows the results of the measurement. All the measurements are done with single bunch case, and the tunes are measured with the FFT done by the signals taken from the single pass BPM system. With the eq. (6) and $|Z/n|_0 = b^2 Z_{\perp,eff}/2R$, the estimated low frequency longitudinal impedances of the BER and BPR are $|Z/n|_0$ = 1.29 Ω and $|Z/n|_0$ = 1.10 Ω, respectively. The errors of fitting impedance are less than ±3% after the data filter.

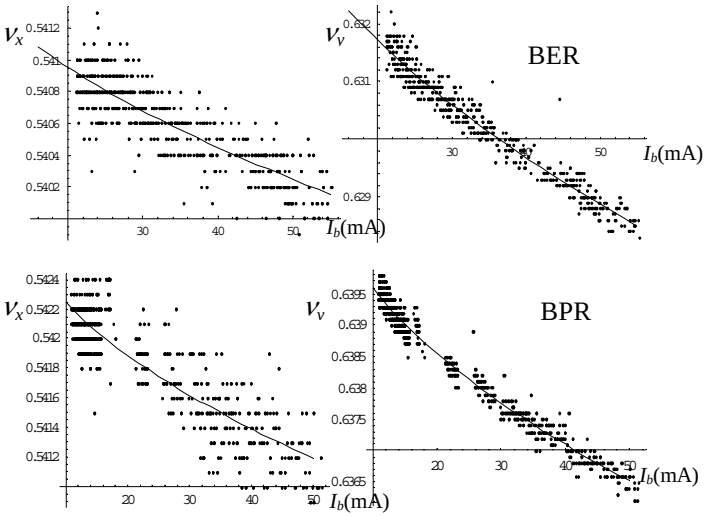

Figure 5: Tune variation as a function of bunch current.

Beam Lifetime

The single bunch beam lifetimes in the BER and BPR are measured for several times under different machine conditions, as shown in Fig. 6. The RF voltage is kept higher than 1.5 MV for enough longitudinal Touschek lifetime during the observations.

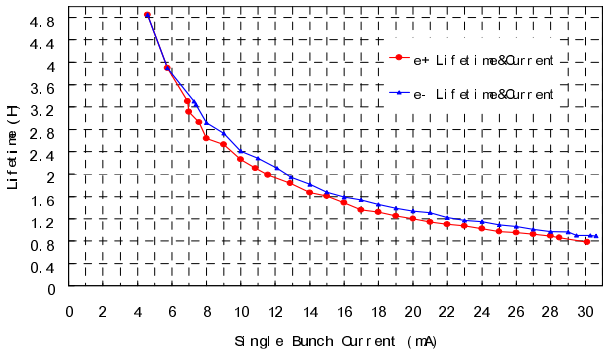

Figure 6: Single bunch beam lifetime observation

From Fig. 6, we can found that at low currents, the lifetime of e- and e+ beam in BER and BPR approaches the same value, which means the Touschek lifetime of the single bunch beam in BER and BPR are the same. By extrapolating the lifetime curve, we get the Touschek lifetime in both rings is about 10 hrs@1mA, which is far from the design value of 7.1 hrs@9.8mA.

With the vacuum pressure given in the rings, the beam-gas lifetime can be estimated. The residual gas consists of about 70% CO and 30% H_2 in the BPR, and 30% CO and 70% H_2 in the BER. At the bunch current of 1mA, the beam-gas lifetime of e+ beam is calculated as 146hrs with the average vacuum pressure is 0.178 nTorr. So the total calculated lifetime of e+ beam is ~43 hrs, which is larger than 10 hrs we observed.

The beam lifetime of multi-bunch case is also observed with different beam currents and vacuum pressure. Figure 7 depicts the average vacuum pressure under different beam current in both rings. Taking an example of 500mA *500mA in collision for both beams, we have the average vacuum pressure of 3.58 nTorr in BPR and 1.79 nTorr in

BER. The various beam lifetimes calculated in both rings and the observed lifetimes are listed in Table 4.

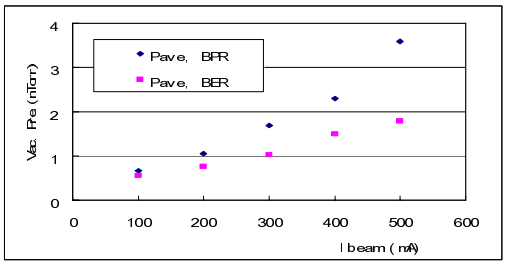

Figure 7: Average vacuum pressure at different beam. current of BER and BPR with same bunch numbers

From Table 4, we can see that the e+ beam lifetime agrees very well to the observed one, while the e- beam doesn't. The reason should be the vacuum is not as good as expected, even at the very low beam current. It is believed that if the vacuum improved, the lifetime at very low bunch current should be longer, which was thought as the Touschek lifetime, and the total beam lifetime would be longer if the Touschek lifetime increased.

Table 4: Calculated and observed (obsd.) beam lifetime

	<*p*> (nTorr)	b-g (hr)	Tous. (hr)	b-b (hr)	Total (hr)	obsd. (hr)
BER	1.79	33	2.0	6.0	1.44	2.94
BPR	3.58	7.3	2.0	6.0	1.24	1.12

BEAM INSTABILITY

As we discussed previously, bunch lengthening is the main instability of single bunch case in our machine. The electron cloud instability (ECI) becomes the main multi-bunch instability in the positively charged ring, especially the high current factory-like machines. The beam blow-up due to the electron cloud (EC) will cause the reduction of luminosity and the coupled bunch instability will limit the beam current. The ECI was also observed clearly in the BEPCII e+ ring, though the beam current is not as high as other machines. Figure 8 shows the beam spectra we got from both BER and BPR. In Fig. 8, the beam current I_B = 40 mA in both rings with the same bunch pattern. We can easily find that there're more sidebands in BPR than that in BER, which is one of the main evidence of ECI.

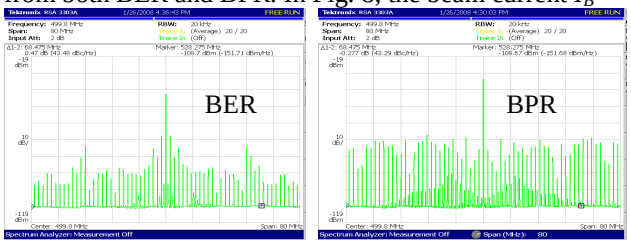

Figure 8: Spectrum distribution of both rings with same I_B.

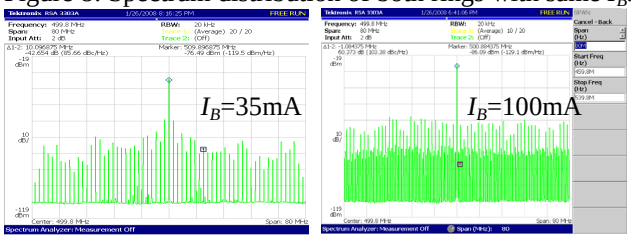

Figure 9: Spectrum in BPR (N_b = 99, uniform filling).

Keeping the same bunch pattern but changing the bunch current, we can find the threshold beam current of ECI for different bunch numbers, as the example shown in Fig. 9. Table 5 summarizes the threshold we got in the experiment. It seems the threshold current of ECI is low, which is only about two times higher than that in BEPC.

Table 5: Threshold beam current of ECI@different N_b&S_b

N_b	S_b (RF bucket)	I_b (mA)	I_{th} (mA)
48	8	~1.0	~50
99	4	~0.35	~35
198	2	~0.15	~30

The mode distributions got from sidebands analysis are shown in Fig. 10, where we can easily find the difference between the BER and BPR.

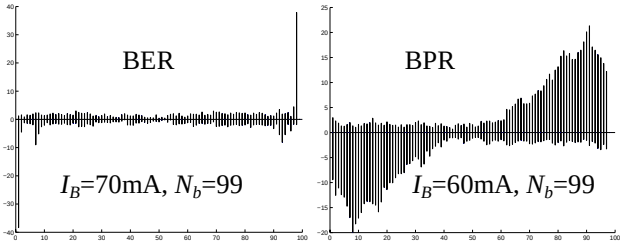

Figure 10: Mode distribution between BER and BPR.

The blow-up of vertical bunch size was also observed with streak camera. We don't find clear blow-up vertically at different bunch pattern and beam current. More studies are needed.

SUMMARY

The BEPCII rings reach their main design parameters after the optics correction in the commissioning. Twiss functions are measured along the rings, and close to the nominal values. The transverse coupling can be adjusted locally with 3 or 4 bumps in sextupoles. Single bunch effects reveal the impedance related issues, and the low frequency longitudinal impedances of the two rings are got from bunch lengthening and tune variation with bunch current. The measured Touschek beam lifetime is far from the calculated one, and thus the total beam lifetime does not agree well enough to the observed one. It could be explained somewhat that the vacuum is not as good as expected right now. ECI has been observed in the e+ ring of BEPCII. The spectra and mode distribution are studied under different bunch patter and current. The threshold current of ECI with 99 uniform filling bunches is about 35 mA. Further studies on beam phenomena are needed.

REFERENCES

[1] C. Zhang, this proceedings, April 2008.
[2] J.Q. Wang, this proceedings, April 2008.
[3] Y.Y. Wei, et al, this proceedings, April 2008.
[4] F. Zimmermann, SLAC-PUB-7844, June 1998.
[5] D.M. Zhou, IHEP-AC-BEPCII/2007-31, 2007.
[6] Q. Qin, et al, NIM A 463 (2001) 77-85.
[7] B. Zotter, CERN 85-19, 1985.
[8] S. A. Heifets and S.A. Kheifets, Rev. Mod. Phys. 63, 631 (1991).

PEP-II STATUS*

M. Sullivan†, K. Bertsche, M. Browne, Y. Cai, W. Cheng, W. Colocho, F.-J. Decker, M. Donald, S. Ecklund, R. Erickson, A. S. Fisher, J. Fox, S. Heifets, T. Himel, R. Iverson, A. Kulikov, A. Novokhatski, V. Pacak, M. Pivi, C. Rivetta, M. Ross, P. Schuh, J. Seeman, K. Sonnad, M. Stanek, P. Tenenbaum, D. Teytelman, J. Turner, M. Weaver, D. Van Winkle, U. Wienands, W. Wittmer, M. Woodley, Y. Yan, G. Yocky, SLAC, Menlo Park, CA 94025, W. Kozanecki, CEA/Saclay, France; M. Biagini, INFN, Frascati, Italy.

Abstract

PEP-II and BaBar have just finished run 7, the last run of the SLAC B-factory. PEP-II was one of the few high-current e+e- colliding accelerators and holds the present world record for stored electrons and stored positrons. It has stored 2.07 A of electrons, nearly 3 times the design current of 0.75 A and it has stored 3.21 A of positrons, 1.5 times more than the design current of 2.14 A. High-current beams require careful design of several systems. The feedback systems that control instabilities, the RF system stability loops, and especially the vacuum systems have to handle the higher power demands. We present here some of the accomplishments of the PEP-II accelerator and some of the problems we encountered while running high-current beams.

PEP-II DESIGN

The PEP-II is an asymmetric-energy double storage ring e+e- accelerator [1]. The rings are housed in a 2.2 km long tunnel with the low-energy ring (LER) above the high-energy ring (HER). The LER has eight RF cavities driven by 4 klystrons and the HER has 11 klystrons driving 28 RF cavities. Each ring contains two transverse bunch-by-bunch feedback systems (X and Y) and one longitudinal bunch-by-bunch feedback system. The beams collided head-on in the middle of the BaBar detector. The head-on collision is achieved through the use of powerful horizontal bending magnets made of permanent magnet (PM) material. The 0.5 m long magnets are positioned 0.21 m from the Interaction Point (IP). Both beams travel through a shared quadrupole, the next magnetic element outboard of the IP. This magnet is also built from PM material [2]. These two magnets the dipole and the quadrupole are inside the 1.5T solenoidal field of the BaBar detector. Table 1 lists some of the design parameters of PEP-II and figure 1 shows the tunnel layout. Figure 2 is an anamorphic layout of the IP showing the beam trajectories as they enter and exit the detector.

RUN 7

Throughout the history of PEP-II the beam energies have been constant and set to deliver luminosity at the peak of the upsilon 4S resonance (10.580 GeV E_{cm}). The

Table 1: Design and actual values of PEP-II parameters

	Design	Actual
Parameter	HER/LER	HER/LER
Beam Energy (GeV)	8.97/3.12	8.0-10.1/3.12
Beam Current (A)	0.75/2.14	2.07/3.21
β_x* (cm)	50	30-105
β_y* (mm)	15-25	9-10
Number of bunches	1658	1722
Ion gap (%)	5	1.6
Crossing angle(mrad)	0	<0.05
Horizontal ξ_x	0.03/0.03	0.113/0.027
Vertical ξ_y	0.03/0.03	0.062/0.047

Figure 1. Tunnel layout of the two beam lines. The LER is above the HER.

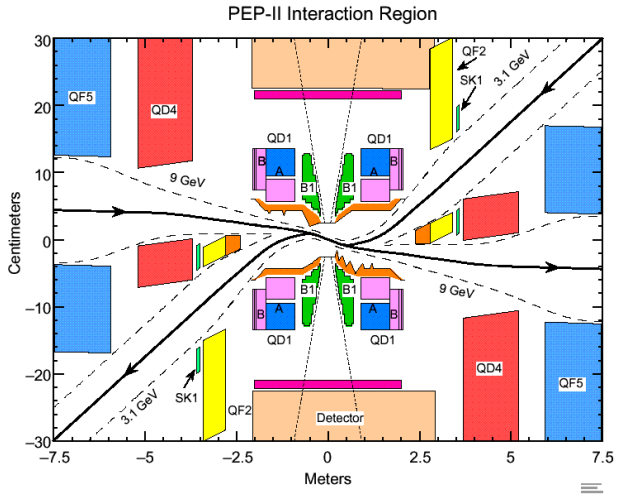

Figure 2. Layout of the beam trajectories at the IP. Note the change in vertical scale. The magnets labeled B1 and QD1 are permanent magnets.

*Supported by US DOE contract DE-AC02-76SF00515.
†sullivan@slac.stanford.edu

only change to any beam energy was to lower the HER by 68 MeV in order to collect off resonance data for the detector. This occurred about 10% of the time.

Run 7 was initially planned to be a similar run to the previous 6 runs. However, near the very beginning of the run we discovered that this run was going to be shortened and decided to move the accelerator E_{cm} to the upsilon 3S resonance (10.355 GeV). We did this by lowering the HER beam energy down by 377 MeV. After a little over two months of running at the 3S the E_{cm} was lowered again down to the 2S resonance (10.023 GeV) for the month of March. The very end of March and the first week of April were used to scan the E_{cm} from the 4S resonance to 11.200 GeV. All of the E_{cm} changes were done by adjusting the HER beam energy. It is very difficult to adjust the LER beam energy due to the fact that the final focus quadrupole for the LER is a permanent magnet and can not be changed.

ACHIEVEMENTS

Table 2 lists some of the luminosity accomplishments of PEP-II and the BaBar detector. As already mentioned, PEP-II has stored multiple ampere currents in both storage rings. In addition, luminosity achievements have all far exceeded the design goals.

Table 2: Some luminosity records of PEP-II

	Design	Record
Peak Luminosity ($cm^{-2}s^{-1}$)	3×10^{33}	12×10^{33}
Average daily lum./month (pb^{-1})	135	649
Luminosity/month (fb^{-1})	4	19.7
Best 24 hrs (pb^{-1})	135	911
Best 12 months (fb^{-1})	30	115

Figures 3-5 show plots of luminosity performance for PEP-II.

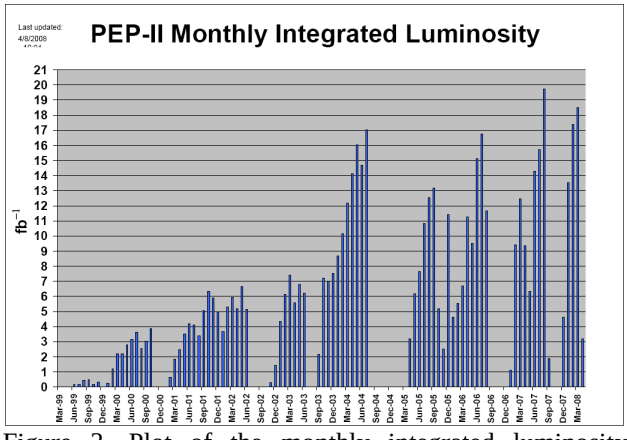

Figure 3. Plot of the monthly integrated luminosity delivered by PEP-II. There is a large increase in performance during the run 4 in 2004. This was the result of employing a continuous top up mode called "trickle-charge". The improved stability of the machine with fixed beam currents greatly improved efficiency. In addition, luminosity tuning could now be optimized for a single beam current thereby improving peak performance [3].

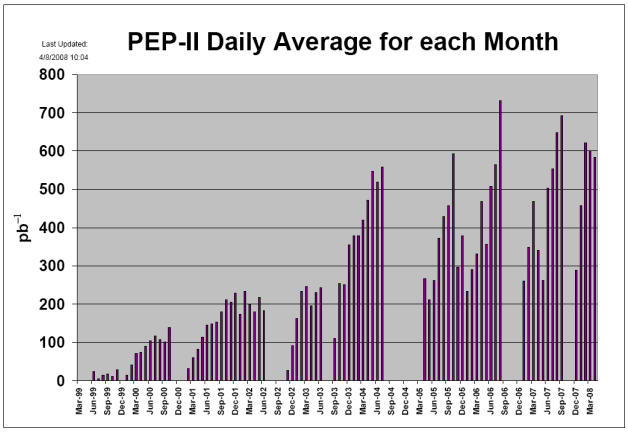

Figure 4. Plot of the average luminosity delivered each day for each month. Note that Aug. 2006, Sep. 2007 and Apr. 2008 were partial months. Aug. 2006 had 18 days of running, Sep. 2007 had 4 days and Apr 2008 had 7 days so the average is over fewer days. 135 pb^{-1}/day is the design performance level. Discounting the partial months, Feb. and Mar. of 2008 are the second and third best months after the month of Aug. 2007.

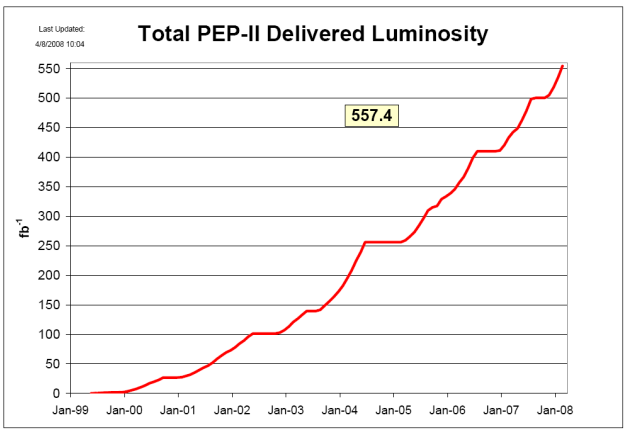

Figure 5. Plot of the total delivered integrated luminosity.

HIGH BEAM CURRENTS

As the beam currents of the two rings gradually increased over the years of running, we have found and fixed several weaknesses in the various subsystems of PEP-II. We will address several of these issues here but this will by no means be an exhaustive list.

Feedback systems

The single ring transverse stability threshold for the HER is about 100 mA. The transverse stability threshold for the LER is about 250 mA. Added stability is attained in the transverse planes through the beam-beam damping from the collision. This improved the margin for the bunch-by-bunch transverse feedback systems and in general the transverse systems worked quite well. Improved digital delay lines for these systems improved feedback loop stability. We also exchanged the initial Al transverse kicker electrodes for ones made from molybdenum [4].

The bunch-by-bunch longitudinal feedback systems had a few more high current related issues and they also had system upgrades [5]. The cable size and vacuum feed throughs from the beam kicker structure was increased in order to improve reliability and power transmitting capacity. For the LER, we installed a Frascati-style cavity kicker to handle the power loads from the higher LER beam current. This LER installation also included absorptive filters and RF circulators [6].

RF systems

The klystrons producing the RF to maintain the energy of the beams were controlled by a series of feedback loops. This entire low-level RF system (LLRF) was upgraded several times as power levels rose due to increases in the beam currents [7]. The last run of PEP-II had very little RF system troubles, mainly due to the reduced beam energy of the HER which greatly decreased the load on the RF system. Although we raised the HER energy to values never seen before at the end of the run, the system behaved very well.

Vacuum

Overall the vacuum systems of both rings performed very well [8]. PEP-II has accumulated over 60,000 A-hrs in the LER and over 40,000 A-hrs in the HER. These are undoubtedly the highest integrated beam currents achieved by any storage ring to date. The base pressure of the HER is 0.1 nTorr and the dynamic pressure is 1 nTorr/A. The base pressure of the LER is 0.1 nTorr and the dynamic pressure is 0.5 nTorr/A.

During the latter half of run 6 (spring-summer 2007) and near the end of run 7 (April 2008) we developed a problem with some of our HER distributed ion pumps (DIPs). These pumps are located in the large dipole magnets of the HER and use the dipole magnetic field as the pumping field. A subset of these pumps started to spontaneously outgas either with a slow rise in pressure or with a sudden increase in pressure and then a sudden drop in pressure. Some of these events would generate enough gas to make the HER beam go unstable. These events are not completely understood and the only cure was to turn off the pumps that were outgassing. One interesting note is that these pumps did not cause much trouble during run 7 until we raised the HER beam energy well above the value used for the 4S resonance. This increased the dipole magnetic field that these pumps use.

SR heating

In general, except for one issue which we discuss below, synchrotron radiation (SR) heating from the high-current beams was well controlled. There were a few initial issues in each ring that had to be fixed: a compound bending angle in the LER was not adequately shielded, some masking for SR in the HER was inadequately cooled, and the HER chamber for the high-power radiation fans from the interaction point (IP) dipoles had to be redesigned. As beam currents increased, a few vacuum components had to be replaced for units able to intercept higher levels of SR power.

We did have one problem that was the result of heated vacuum chambers from SR. The 5.5 m long HER dipole chambers were designed to intercept SR power from a beam with 3A of current at 9 GeV. Although well cooled, the dipole chambers still expand (or flex) when SR power strikes the chamber wall. This flexure was taken up by a bellows section on one end of the chamber and by a zero length bellows or flex flange at the other end of the chamber. The zero length bellows had a RF seal to maintain chamber wall continuity across the gap. However, we found that the chamber flexure was large enough to cause the RF fingers in this seal to become over-crushed allowing a gap to form. This gap allowed higher order mode (HOM) power to penetrate behind the RF seal and heat up vacuum components. In addition, the gap permitted arcing at the seal boundary. This problem was uncovered during the summer shutdown in 2006. Initially we thought there were perhaps a handful of RF seals that had failed. We replaced the ones we had found. During run 6 we found out that at least 50% of these shields had failed and we made plans during the shutdown to replace as many as we could. We ended up replacing all of the seals after finding that more than 95% had failed [9]. Figure 6 is a picture of one of the failed RF seals.

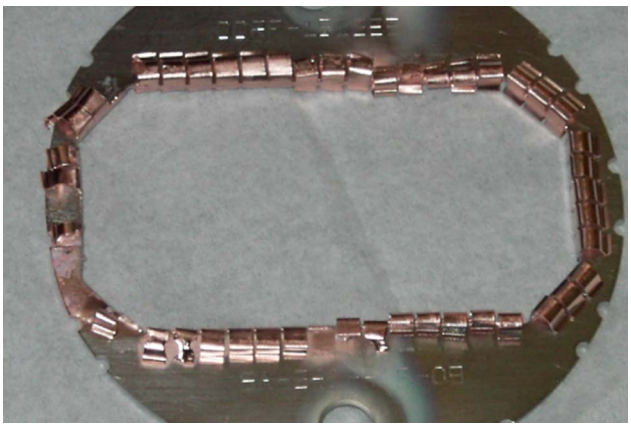

Figure 6. Picture of a damaged HER flex flange RF seal. HOM power getting behind the GlidCop (dispersion strengthened Cu) fingers heated up the stainless steel frame to the melting point of Cu (left side of picture). In addition, one can see signs of arcing where there is Cu deposition on the stainless steel frame top and bottom. The right hand side of the picture shows undamaged fingers.

High order mode (HOM) heating

HOM heating of various vacuum components probably had the largest impact on machine performance. Most of these issues were in the LER storage ring which had the higher beam current. We had to remove (and ended up not replacing) two out of four elliptically shaped vacuum valves located around the IP that persistently overheated due to HOM power getting past the RF screen. The other

two valves of identical design and similar locations never caused any problems.

Upstream of the interaction region (IR), we have massive pumping from non-evaporative getter pumps (NEGs). The NEG wafers are stacked for capacity and the RF screens between the NEG pumps and the beam turned out to be too thin. As the LER beam current increased, some of the HOM power started to leak through these weak screens and be absorbed by the NEG material. The NEG would then heat up and start to outgas causing intolerable backgrounds for the detector. Roughly 10-15% of the total pumping in this area was affected. The NEG material was removed from those chambers with the thinnest screens during the summer downtime in 2004.

In the beginning of run 5 (Dec. 2005), we had two problems with arcing vacuum components. These events had a signature that showed up as a sudden beam instability followed, in most cases, by vacuum activity. This would cause a beam loss. One of the problems was found to be an RF flange gasket that was sticking into the vacuum chamber near the LER RF cavities [9]. The other was near the detector and was difficult to track down but eventually ended up being a problem with a flange RF seal not working properly [10,11].

In May 2006 we tried to shorten the LER bunch by increasing the LER RF total gap voltage and discovered that the beam position monitor (BPM) buttons would absorb too much HOM power and get hot enough for the top buttons to fall off. If the button fell onto the bottom button that button would all of a sudden receive an enormous amount of power and end up melting the ceramic in the feed through causing a vacuum leak. We ended up replacing or removing the BPM buttons in the entire LER. The replacements had smaller sized buttons and, in addition, the button and feed through were one piece of metal; a technology not readily available when PEP-II was built.

Another HOM heating issue was a particular feed through for a titanium sublimation pump (TSP) in the LER. We found a burned connector to the pump filaments and ended up not being able to use this pump. In the same area, we also had a single bellows section that was getting very hot. No other place in the LER had these problems (there are at least 190 other similar places). This was finally tracked down to the presence of a fixed collimator about 10 m upstream of the pump and bellows. The collimator was able to convert longitudinal modes into transverse HOMs and this transverse RF was getting into the bellows and into the pump connector. Installing a HOM absorber in the antechamber of the beam pipe greatly reduced the HOM power in this area [12].

SUMMARY

The PEP-II accelerator has surpassed all of its design goals. PEP-II can be called one of the most successful accelerators in the history of this field. Many doubted PEP-II would ever reach the design goals (3×10^{33} $cm^{-2}s^{-1}$ and 135 pb^{-1}/day). The BaBar detector has amassed one of the largest data samples in the history of e+e- colliding accelerators.

The high-current beams of both storage rings have pushed accelerator technology into new territory and have brought an increased awareness of the importance of HOM heating effects. Future high-current accelerators will have to pay close attention to the effects of HOM heating in all subsystems sensitive to this process.

ACCNOWLEDGEMENTS

We would like to acknowledge all of the people who, working together, designed, built and ran the PEP-II accelerator. The outstanding performance of PEP-II is a testament to the dedication of all of the support groups who maintained, repaired and upgraded the accelerator.

REFERENCES

[1] "PEP-II an Asymmetric *B* Factory", Conceptual Design Report, CALT-68-1869, LBL-PUB-5379, SLAC-418, UCRL-ID-114055, UC-IIRPA-93-01, June 1993.

[2] M. Sullivan, *et. al.*, "Results from a Prototype Permanent Magnet Dipole-Quadrupole Hybrid for the PEP-II B-Factory", Proceedings of PAC97, 1997, pg. 3330.

[3] J. L. Turner, *et. al.*, "Trickle-charge: a New Operational Mode for PEP-II", Proceedings of EPAC04, 2004, MOPLT146, pg. 881.

[4] U. Wienands, *et. al.*, "High-temperature Kicker Electrodes for High-beam-current Operation of PEP-II", Proceedings of EPAC04, 2004, THPLT163, pg. 2843.

[5] J. D. Fox, *et. al.*, "Development and Testing of a Low Group-delay Woofer Channel for PEP-II", Proceedings of EPAC04, 2004, THPLT155, pg. 2822.

[6] P. A. McIntosh, *et. al.*, "An Over-damped Cavity Longitudinal Kicker for the PEP-II LER", Proceedings of PAC03, 2003, pg. 1341.

[7] P. A. McIntosh, *et. al.*, "PEP-II RF System Operation and Performance", Proceedings of EPAC04, 2004, TUPKF062, pg. 1087.

[8] U. Wienands, "Vacuum Performance and Beam Lifetime in the PEP-II Storage Rings", Proceedings of PAC01, 2001, pg. 597.

[9] U. Wienands, *et. al.*, "Tracking Down a Fast Instability in the PEP-II LER", Proceedings of EPAC06, 2006, MOPLS051, pg. 658.

[10] M. Sullivan, *et. al.*, "Anomalous High Radiation Beam Aborts in the PEP-II B-factory", Proceedings of EPAC06, 2006, MOPLS049, pg. 652.

[11] A. Novokhatski, *et. al.*, "Modeling of the Sparks in Q2-bellowsof the PEP-II SLAC B-factory", Proceedings of PAC07, 2007, MOPLS051, pg. 658.

[12] A. Novokhatski, *et. al.*, "Damping the High Order Modes in the Pumping Chamber of the PEP-II Low Energy Ring", Proceedings of EPAC04 ,2004, pg. 854.

KEKB Status

Y. Funakoshi, T. Agho, K. Akai, K. Ebihara, K. Egawa, A. Enomoto, J. Flanagan, H. Fukuma, K. Furukawa, T. Furuya, J. Haba, S. Hiramatsu, T. Ieiri, N. Iida, H. Ikeda, T. Kageyama, S. Kamada, T. Kamitani, S. Kato, M. Kikuchi, E. Kikutani, H. Koiso, M. Masuzawa, T. Mimashi, A. Morita, T. T. Nakamura, K. Nakanishi, H. Nakayama, M. Nishiwaki, Y. Ogawa, K. Ohmi, Y. Ohnishi, N. Ohuchi, K. Oide, M. Ono, M. Shimada, M. Suetake, Y. Suetsugu, T. Sugimura, T. Suwada, M. Tawada, M. Tejima, M. Tobiyama, N. Tokuda, S. Uehara, S. Uno, N. Yamamoto, Y. Yamamoto, Y. Yano, K. Yokoyama, Ma. Yoshida, Mi. Yoshida, S. Yoshimoto, F. Zimmermann*
KEK, 1-1 Oho, Tsukuba, Ibaraki 305-0801, Japan

Abstract

The KEKB status is described focusing on the beam operation with crab crossing. This report deals mainly with the beam dynamics issues with crab crossing. There is a large discrepancy between the beam-beam simulation and the experiment at the high bunch currents. We discuss causes of this discrepancy in detail.

INTRODUCTION

The crab cavities were installed at KEKB during the winter shutdown in FY 2006. A dedicated machine time from the mid. of Feb. to the end of June 2007 was devoted to the commissioning of the crab cavity system and the machine study with crab crossing. We focus on the beam dynamics issues with crab crossing in this report. Performance of the crab cavities as a hardware system is reported elsewhere [1].

KEKB B-FACTORY

KEKB B-Factory [2] has been operating at KEK since 1999 for the e+e- collision experiment mainly at the $\Upsilon(4S)$ resonance. KEKB is composed of the low energy positron ring (LER) at 3.5 GeV, the high energy electron ring (HER) at 8 GeV, and an injector linac. Two beams collide at the physics detector named "Belle". The machine parameters are listed in Table 1. The highest luminosity, $1.72 \times 10^{34}\mathrm{cm}^{-2}\mathrm{s}^{-1}$, was achieved in Nov. 2006. The peak luminosity is higher than the design by 70 % mainly due to smaller β_{y}^{*} (6 mm vs. 10 mm), horizontal betatron tune closer to a half integer (LER:0.505 / HER:0.511 vs. 0.52), and higher stored current in the HER (1.35 A vs. 1.1 A). The daily integrated luminosity is as twice high as the design due to Continuous Injection Mode as well as acceleration of 2 bunches per an rf pulse at the linac. The electron cloud in the LER, which was much severer than was thought in the design phase, has been mitigated up to 1.8 A with 3.5 bucket spacing by solenoid windings of 2,200 m. Figure 1 shows the history of KEKB before the installation of the crab cavities.

* visiting from CERN, Switzerland

Table 1: KEKB Machine Parameters.

	May 2008		**Nov. 2006**		
	LER	HER	LER	HER	
Energy	3.5	8.0	3.5	8.0	GeV
Circum.	3016		3016		m
ϕ_{cross}	crab crossing		± 11		mrad
$\mathrm{I}_{\mathrm{beam}}$	1619	854	1662	1340	mA
$N_{bunches}$	1584		1387		
$\mathrm{I}_{\mathrm{bunch}}$	1.02	0.539	1.20	0.965	mA
ε_x	15	24	18	24	nm
β_x^*	90	90	59	56	cm
β_y^*	5.9	5.9	6.5	5.9	mm
σ_y^*	1.1	1,1	1.9	1.9	μm
V_c	8.0	13.0	8.0	15.0	MV
ν_x	.505	.509	.505	.509	
ν_y	.567	.596	.534	.565	
ν_s	-.0240	-.0204	-.0246	-.0226	
ξ_x	.099	.119	.117	.070	
ξ_y	.097	.092	.105	.056	
Lifetime	94	158	110	180	min.
Lumi.	16.10		17.12		/nb/s
Lum/day	1.232		1.232		/fb

CRAB CROSSING

One of the main design features of KEKB is the horizontal crossing angle of 22 mrad, at the interaction point (IP). Although there are a lot of merits in the crossing angle scheme, the beam-beam performance may degrade. The design of KEKB predicted that the vertical beam-beam parameter ξ_{y} is as high as 0.05 if betatron tunes are properly chosen, and actually KEKB has already achieved $\xi_{\mathrm{y}} \sim 0.056$. Thus the beam-beam issues associated with the crossing angle was not critical if ξ_{y} is lower than 0.05 or so. The crab crossing scheme, proposed by R. Palmer[3], was an idea to recover the head-on collision with the crossing angle. It has been also shown that the synchro-betatron coupling terms originating from the crossing angle are canceled by crab crossing[4]. The crab crossing scheme has been considered in the design of KEKB from the beginning as a backup measure against the crossing angle. Once, crab

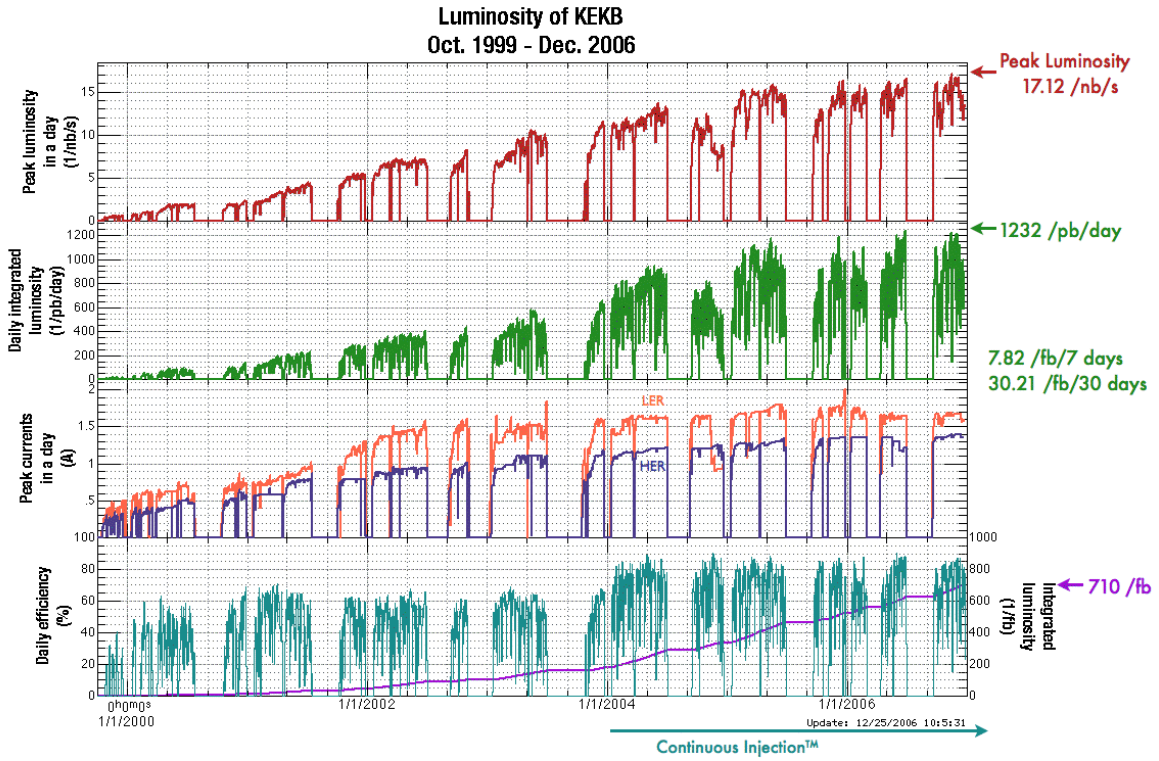

Figure 1: History of KEKB before installation of crab cavities.

crossing seemed non-urgent issue because KEKB achieved $\xi_y > 0.05$ at the early stage of the operation (in 2003). However, recently an interesting beam-beam simulation results appeared[5], predicting that the head-on or crab crossing provides higher $\xi_y > 0.1$. Figure 2 shows the comparison of ξ_y for the head-on (crab crossing) and the crossing angle with a strong-strong beam-beam simulation. Then the development of the crab cavities has been revitalized.

The original design of KEKB had two cavities for each ring, on both side of the IP, so that the crab kick excited by the first cavity is absorbed by another one. The new single crab cavity scheme extends the region with crab orbit until both cavities eventually merge to each other in a particular location in the ring. Then it needs only one cavity per ring. The layout is shown in Figure 3. In the case of KEKB, this scheme not only saved the cost of the cavities, but made it possible to use the existing cryogenic system at Nikko for the superconducting accelerating cavities also for the crab cavities. The beam optics was modified for the crab cavities to provide necessary magnitude of the beta functions at the cavities and the proper phase between the cavities and the IP. A number of quadrupoles have switched the polarity and became to have independent power supplies.

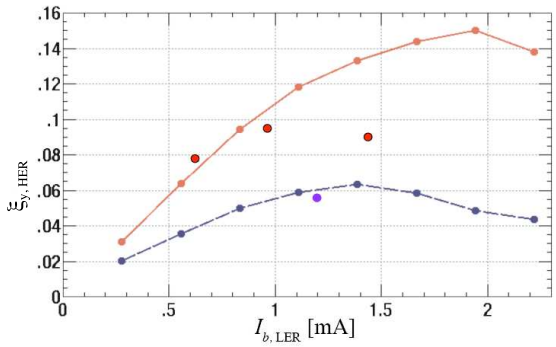

Figure 2: Predicted beam-beam parameters by the strong-strong beam-beam simulations with the crossing angle of $\pm 11\mathrm{mrad}$ (purple) and the head-on(crab crossing) (red). Some experimental data are also shown with closed circles.

MACHINE STUDY AND PHYSICS RUN WITH CRAB CROSSING

Figure 4 shows a history of KEKB after the installation of the crab cavities. A dedicated beam study of the crab cavities and crab crossing started on 14th Feb. 2007 and finished at the end of June 2007. The beam study began with very small beam currents, since tolerance of the crab cavities against the beam power was unknown. Also conditioning of the cavities by using the beams was needed like usual accelerating cavities. A warm-up of the system up to the room temperature was needed at the end of April 2007 to recover from frequent trips. In most cases, the beam study was done with relatively small beam currents typically 100mA (LER) and 50mA (HER), since the most important purpose of the beam study is to prove that we can achieve such a high beam-beam parameter with crab crossing as the beam-beam simulation predicts. A high beam current operation of the crab cavities was also tried for different two purposes. Firstly, we hoped to confirm that a

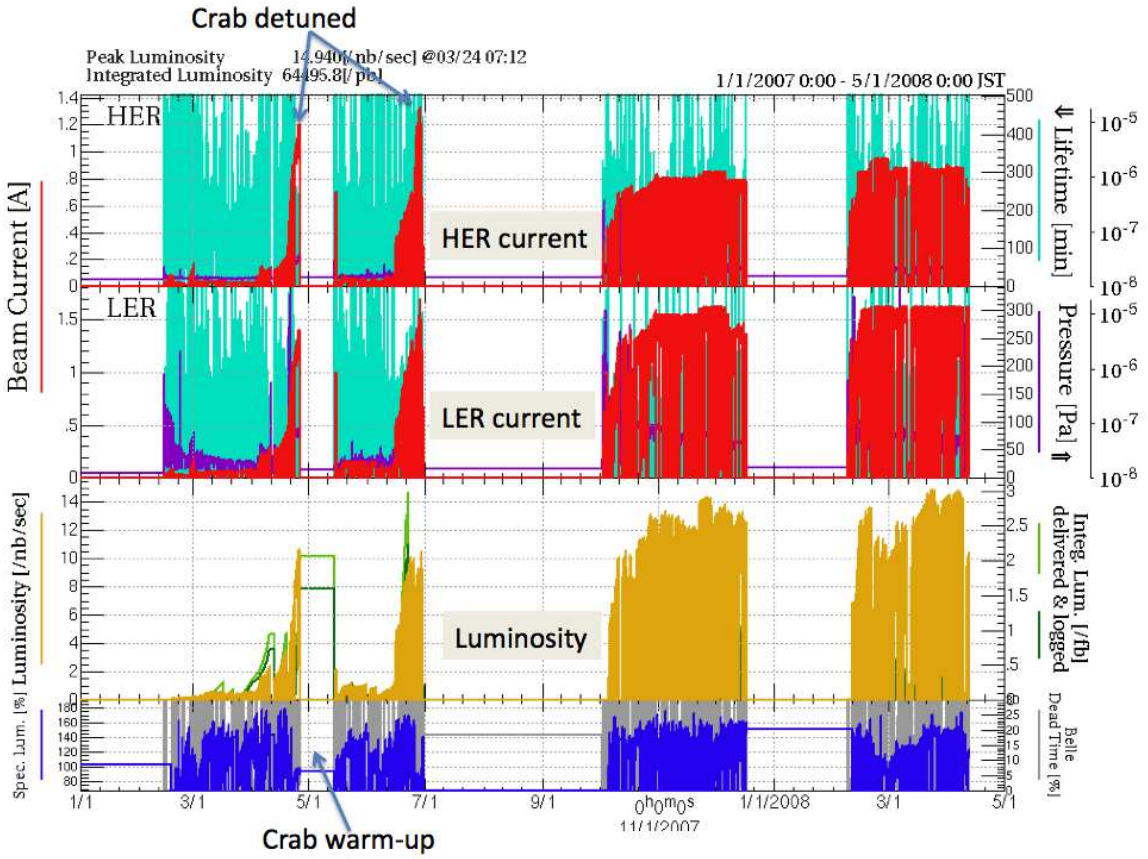

Figure 4: History of KEKB before installation of crab cavities.

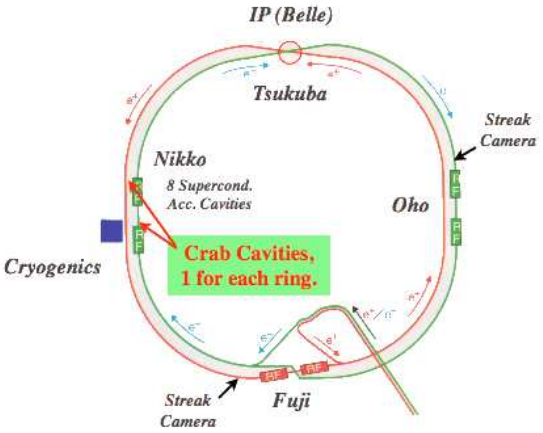

Figure 3: Layout of the crab cavities in the KEKB rings.

high luminosity is actually achieved with the crab on. In the high beam current operation, the peak luminosity exceeded $1 \times 10^{34}\mathrm{cm}^{-2}\mathrm{s}^{-1}$, which is the design luminosity of KEKB. Secondary, we confirmed that the nominal beam currents before the installation of the crab cavities can be stored with the crab cavities detuned. This means that we can return the situation before carb installation by detuning them in case that the crabs are serious obstacles for the high luminosity. In the autumn run in 2007 following the beam study, the physics operation was done with the crab cavity on. Until now, we have been operating KEKB with the crab cavities on. So far, the highest luminosity with crab crossing is $1.61 \times 10^{34}\mathrm{cm}^{-2}\mathrm{s}^{-1}$. This value is somewhat lower than before the crab installation. However, the value was achieved with much lower beam currents, particularly for the HER beam. A comparison of machine parameters before and after the crab installation is also shown in Table 1.

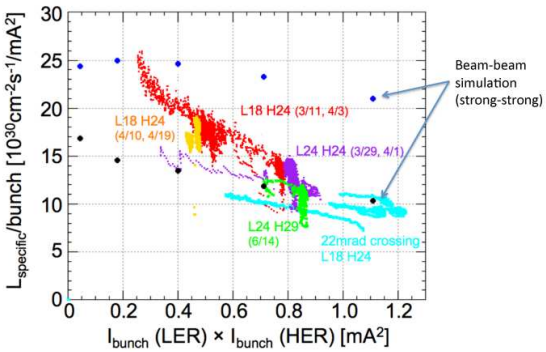

Figure 5: Beam current dependence of specific luminosity.

Beam-beam performance with crab crossing

To evaluate beam-beam performance, two parameters are used in this report, *i.e.* the specific luminosity and the

beam-beam parameters. Figure 5 shows the specific luminosity as function of the bunch current product. Here, the specific luminosity is defined as the luminosity divided by a number of bunches and the bunch current product. In the figure, the points in thin-blue are data of the 22mrad crossing angle. The others are those with crab crossing. Different colors correspond to different combinations of the LER and HER horizontal emittances. In the 22mrad crossing angle operation, a combination of 18nm(LER) and 24nm(HER) was used. In the crab beam study, other combinations of 24nm(LER)/24nm(HER), 24nm(LER)/29nm(HER) were also tried in addition to the conventional combination of 18nm/24nm. The specific luminosity is inversely proportional to the beam cross section at the IP and it is constant, if the beam sizes are constant with different beam currents. In reality, however, the specific luminosity shows a very rapid decline as the bunch current product increases, indicating a rapid (vertical) beam blowup due to the beam-beam effect. In the figure, also shown is the specific luminosity predicted by the beam-beam simulation. Both predictions with and without crab crossing are shown. As seen in the figure, the experimental data are consistent with the simulation in case of the 22mrad crossing angle. On the other hand, in case of crab crossing, the experimental values are much lower than the predictions particularly at the high bunch currents, although at the low bunch currents there is a good agreement between them. This low specific luminosity at high bunch currents is a serious problem and has not been solved until now, although a large amount of efforts have been devoted to the study on this problem. We will mention these efforts in the following. Another serious problem with crab crossing is that the bunch current product is limited at around $0.85\mathrm{mA}^2$ due to decreases of beam lifetime. This problem is also serious, since the design value of the SuperKEKB is $1.53\mathrm{mA}^2$. This beam current limitation is not predicted by the beam-beam simulation.

In Figure 1, some experimental values of the vertical beam-beam parameter are shown together with the beam-beam simulation. As seen in the figure, the experiment value of the 22mrad crossing angle is consistent with the simulation. In case of crab crossing, however, the experimental value is much lower than the simulation at the high bunch currents, although there is a good agreement at the low bunch currents. The maximum vertical beam-beam parameter with crab crossing exceeds 0.093. This value is very high in a usual sense and indicates the potential superiority of crab crossing.

POSSIBLE CAUSES OF LUMINOSITY RESTRICTION

We have been struggling with the problem of the low specific luminosity at the high bunch currents. These efforts are summarized in this section.

Too wide tuning parameter space? In case of the high luminosity machine like KEKB, various kinds of machine tuning are important and without them the achievable luminosity is very low. At KEKB, most of magnets are standardized typically every two weeks. After this, the magnets are set at the values which brought good performance. This gives a basis of machine tuning. The next step is optics corrections on the global x-y coupling and the global dispersions, the beta-beatings. These corrections are very important and give a start point of the following tuning. In the routine luminosity tuning of KEKB, we make tuning on many parameters such as the orbital offsets at the IP and the crossing angles in both horizontal and vertical directions, the local x-y coupling at the IP, the horizontal and vertical dispersion at the IP and their slopes, the vertical waist points at the IP, the crab voltages, the x-y coupling parameters at the crab cavities, the betatron tunes and so on. In the conventional method of tuning at KEKB, most of these parameters (except for the parameters optimized by observing their own observable) are scanned one by one just observing the luminosity and the beam sizes. One possibility of the low specific luminosity is that we have not yet reached an optimum parameter set due to too wide parameter space. As a more efficient method of parameter search, we introduced in autumn 2007 the downhill simplex method for twelve parameters of the x-y coupling parameters at the IP and the vertical dispersions at the IP and their slopes. These twelve parameters can be searched at the same time in this method. We have been using this method since then. However, even with this method an achievable specific luminosity has not been improved, although the speed of the parameter search seems to be rather improved.

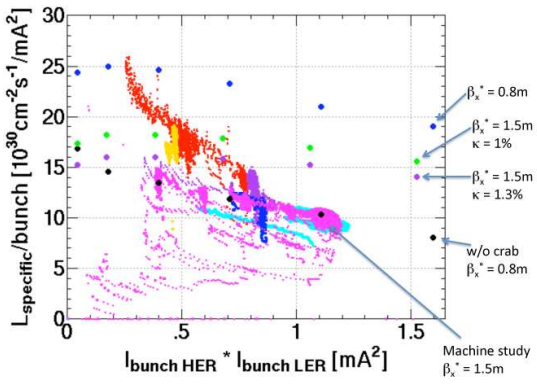

Figure 6: Beam current dependence of specific luminosity with different horizontal beta functions at the IP.

Beam lifetime issue Another possibility of the cause of the low specific luminosity is short beam lifetime. In the luminosity tuning, we sometimes encounter the situation that we can not set parameters giving a higher luminosity due to poor beam lifetime. Of these parameters, the most typical one is the horizontal beam offset at the

IP. On the other hand, we observe that the beam lifetime becomes short as the bunch currents increase. Due to this beam lifetime degradation, to what extent we can approach the optimum set of parameters for the luminosity could depend on the bunch currents. This is a possible scenario that beam lifetime limits the specific luminosity. As for the process which affects beam lifetime depending on the bunch current, there are some possibilities, *i.e.* the beam-beam tail, the degradation of dynamic aperture due to the beam-beam effect and so on. Recently, we found another process which might be responsible for the lifetime decrease. This is the dynamic beam-beam effects; *i.e.* the dynamic beta effect and the dynamic emittance effect. Since the horizontal tune of KEKB is very close to the half integer (typically .506), the effects are very large. The horizontal beta function at the IP (β_x^*) shrinks from 0.9m to 0.2m and the horizontal emittance (ε_x) is enlarged from 18nm to 55nm with ν_x of .506 and the unperturbed beam-beam parameter (ξ_{x0}) of 0.09. The change of the beta function at the IP means a large beta beat all around the ring. In this situation, we found that the horizontal beam sizes at around the crab cavity in both rings are very large (typically 7mm) at the high bunch currents and the physical aperture there is only around 5 σ_x. Therefore, there is a possibility that the physical aperture around the crab cavities affects the beam lifetime seriously. This possibility was confirmed by an orbit bump study. Then, we decided to change the optics to widen effective physical aperture around the crab cavities. For this purpose, the horizontal beta function at the IP was enlarged from 0.8m to 1.5m for both rings. As a result, the horizontal beta function at the crab cavities could be decreased, since the condition of crab crossing requires that the product of the horizontal beta functions at the IP and at the crab cavity should be preserved. With this optics, we investigated the specific luminosity. If the discrepancy of the specific luminosity between the experiment and the simulation shown in Figure 5 comes from the beam lifetime issue, this discrepancy can be decreased with the optics change. The experimental result is shown in Figure 6. The specific luminosity with $\beta_{\rm x}^* = 1.5{\rm m}$ is shown in the magenta color. The values of the beam-beam simulation are also plotted with two different values of the global x-y coupling. A remarkable thing with this new optics is that the maximum bunch current with this new optics is that the maximum bunch current with crab crossing was increased. It seems that the cause of this bunch current limitation is physical aperture around the crab cavities associated with the dynamic beam-beam effects. However, the tendency that the specific luminosity agrees with the simulation at the low bunch currents and disagrees at the high bunch currents still exists even with this new optics. Therefore, we can not conclude that the beam lifetime issue creates the steeper slope of the specific luminosity than the beam-beam simulation.

Other possibilities There are some other possibilities which may cause the discrepancy between the experiment and the simulation, *i.e.* the synchro-betatron resonance, the vertical crabbing motion, some unknown noise, a cross-talk of the beam-beam effects and the lattice non-linearity and so on. These effects are not implemented in the strong-strong beam-beam simulation.

In the course of KEKB operation, it turned out that the synchro-betatron resonance of ($2\nu_{\rm x} + \nu_{\rm s} = {\rm integer}$) or ($2\nu_{\rm x} + 2\nu_{\rm s} = {\rm integer}$) affects the KEKB performance seriously. Nature of the resonance lines was studied in details during the machine study on crab crossing last year. We found that the resonances affect (1) single-beam lifetime, (2) single-beam beam sizes (both in horizontal and vertical directions), (3) two-beam lifetime and (4) two-beam beam sizes (both in horizontal and vertical directions) and the effects are beam current dependent. The effects lower the luminosity directly or indirectly through the beam-size blowup, the beam current limitation due to poor beam lifetime or smaller variable range of the tunes. The strength of the resonance lines can be weaken by choosing properly a set of sextupole magnets. KEKB adopted the non-interleaved sextupole scheme to minimize non-linearily of the sextupoles. LER and HER have 54 pairs and 52 pairs of sexupoles, respectively. With so many degree of freedom in the number of the sextupoles, optimization of sextupole setting is not an easy task even with present computing power. The candidates of sextupole setting are found in computer. Usually dynamic aperture and an anomalous emittance growth [6] are optimized on the synchro-betatron resonance. Recently, in KEKB an efficient method of optimization has been developed by using Temperature Parallel Simulated Annealing (TPSA) method [7]. Usually a setting of sextupoles which gives good performance in computer does not necessarily bring good performance in the real machine and most of candidates of the sextupole setting do not give satisfactory performance. When we change a linear optics, usually we need to try many candidates of settings until we finally obtain a setting with sufficient performance. The single-beam beam size and the beam lifetime are criteria for sextupole performance. Or as an easier method of the estimation of sextuple performance, a beam loss is observed when the the horizontal tune is jumped down across the resonance line. The resonance line in HER is stronger than that in LER, since we do not have a local chromaticity correction in HER. In usual operation, we can operate the machine with the horizontal tune below the resonance line in case of LER, while we can not lower the horizontal tune of HER below the resonance line. The beam-beam simulation predicts a higher luminosity with the lower horizontal tune in HER. To weaken the strength of the resonance line in HER, we tried to change the sign of α(momentum compaction factor). Since the ν_s is negative with the positive α, the resonance is a sum resonance ($2\nu_{\rm x} + \nu_{\rm s} = {\rm integer}$). By changing the sign of α, we can change it to a difference resonance ($2\nu_{\rm x} - \nu_{\rm s} = {\rm integer}$). The trial was made in June 2007. The trial was successful and we could lower the horizontal tune below the resonance. However, when we tried the negative α in LER,

unexpectedly large synchrotron oscillation due to the microwave instability occurred. Due to this oscillation, we gave up the trial of the negative α optics.

The vertical crab at the IP could degrade the luminosity. It can be created by some errors related to the crab kick such as a mis-alingnment of the crab cavity and the local x-y coupling at the crab cavity. The x-y coupling parameters at the crab cavities give a tuning knob to adjust the vertical crab at the IP. By tuning them, we can eliminate the vertical crab at the IP even if it is created by other sources such as a mis-alignment of accelerating cavities. So far, however, tuning of these parameters is not so effective to raise the luminosity.

The beam-beam simulation predicts a significant luminosity degradation if there is a fast noise to the beams. Possible noises which may induce such a loss may come from the phase error of the crab cavities themselves and the transverse bunch-by-bunch feedback system. As for the phase error of the crab cavities, the measured error was less them 0.01 degree for fast noise ($\succeq 100\mathrm{Hz}$) and 0.1 degree for slow noise ($\preceq 100\mathrm{Hz}$). The measured phase error is much smaller than the allowed values given by the beam-beam simulation. As for the feedback system, in the operation of the crossing angle of $\pm 11\mathrm{mrad}$, we once found that the luminosity decreases with a higher feedback gain. Only the LER vertical gain affects the luminosity. We found that the luminosity degrades by about 15 % with a 3 dB higher feedback gain than the usual value. Although the reason why the feedback gain affects the luminosity has not been understood yet, there is a possibility that some noise from the system affects the luminosity. In the present beam operation, we use a very low feedback gain in the LER vertical direction. Although there remains some oscillation in the single beam mode with this gain, the oscillation is damped by the Landau damping in case of the two beam operation. With an even lower gain, there is no luminosity gain.

The disagreement between the beam-beam simulation and the experiment at the high bunch current is also being investigated on the simulation side. The strong-strong beam-beam simulation, which predicted the high specific luminosity, does not include some effects. For example, the lattice non-linearity is not considered in the strong-strong simulation. Generally speaking the cross talk between the beam-beam effects and the lattice non-linearity plays some role in the beam-beam performance. To study this effect, a weak-strong simulation which includes a full lattice was done [8]. However, we found no significant degradation of the specific luminosity at the high bunch current so for.

Another possibility of a cause of the disagreement which we considered is an unexpectedly large vertical emittance. The beam-beam simulation showed that the attainable luminosity depends largely on the single beam vertical emittance. If the actual vertical emittance is much larger than the assumed value, it could create the disagreement. We carefully checked the calibration of the beam size measurement system. We found some errors in the calibration of the HER beam size measurement system and the actual vertical emittance was somewhat smaller than was considered. The latest values of the global x-y coupling of both beam are around 1.3 %. This value is within our consideration.

SUMMARY

The crab cavities which were installed at KEKB in the end of FY 2006 have been working much more stably than the initial expectation. They are presently being used in the usual physics run. It seems that the success of the development of the crab cavity is very important, since the crab cavity may have applications to other machines such as SR facilities or an upgrade of LHC. The crab cavities at KEKB, however, have not yet realized their potential capability in the sense that the specific luminosity is much lower than the prediction of the beam-beam simulation at the high bunch currents. In spite of a large amount of effort to solve this problem, we have not yet found the cause of this problem. Since the design of SuperKEB counts the luminosity gain by crab crossing, finding the cause is very important task for us.

REFERENCES

[1] K. Nakanishi *et al.*, in these proceedings.

[2] KEKB B-Factory Design Report, KEK-Report-95-7, June 1995.

[3] R. B. Palmer, SLAC PUB-4707 (1988); In Proc. DPF Summer Study Snowmass 88, Snowmass, CO, 1988, ed. S. Jensen. Singapore: World Sci. (1988), p.613.

[4] K. Oide and K. Yokoya, Phys.Rev.A40:315 (1989).

[5] K. Ohmi et al, Proc. of EPAC06, 616 (2006).

[6] K. Oide and H. Koiso, Phys.Rev. E49, 4474 (1994).

[7] A. Morita *et al.*, Proc. of PAC07 (2007).

[8] K. Ohmi, in these proceedings.

UPGRADE PLAN OF KEKB

Y. Ohnishi*, KEK, Oho 1-1, Tsukuba, Ibaraki, 305-0801, Japan
For the KEKB upgrade team

Abstract

The KEKB accelerator has been achieved the luminosity larger than the design value, 10^{34}, and it is finding a way to an upgrade plan of KEKB. The target of the upgrade is a high luminosity that increases by a factor 10 to 30 from the present luminosity. In this report, a strategy and a design of the upgraded KEKB are presented.

INTRODUCTION

Roadmap of KEK, the near-term future program of KEK, has been presented in January, 2008[1]. In the framework of the KEK's roadmap, the KEKB will be shutdown in 2009 and upgraded to achieve a higher luminosity by a factor 30 and more than the present KEKB. The preliminary target luminosity is 5×10^{35} cm^{-2}s^{-1} at the upgraded KEKB.

Recently, crab cavities have been developed and installed in KEKB. The crab cavity realizes an effective head-on collision, although it is a finite-angle crossing of 22 mrad at IP. The head-on collision can resolve a coupling of x and z directions of a particle motion within a colliding bunch. When a horizontal betatron tune is closer to the half integer, a particle motion in the y direction becomes symmetric for x and $-x$ positions of the particle that is a turn-by-turn position. This half-integer tune technique can resolve a coupling of x and y directions. Consequently, the three-dimensional motions becomes the one-dimensional motion when the crab crossing and the half-integer tune technique are adopted as a collision scheme. A beam-beam interaction is a nonlinear force and generates chaotic phenomena in general. However, particles result in a tracking simulation of a circular collider, for instance several thousand turns, are confined within a near-integral surface(KAM) in the phase space. The particle trajectories do not diverge in the case of the one-dimensional motions with the beam-beam interaction, though a "chaos" appears as increasing the beam-beam force. On the other hand, the nonlinear force with multi-dimensional system makes the beam blow-up. If the system becomes one-dimensional and avoids bad resonances, the beam-beam parameter can be increased with increasing beam currents. Therefore, the crab crossing scheme can improve the luminosity much higher than the geometrical gain of the overlap region[2]

The schedule for the KEKB upgrade is restricted in the KEK's roadmap and it is very tight. The baseline is a high current scheme(HC)[3] for the KEKB upgrade. On the other hand, extremely low emittance and low beta function at IP(LELB) with a large Piwinski angle has been proposed at the SuperB project[4, 5]. The LELB scheme can make bunch length longer then the HC scheme and can realize a high luminosity at relatively lower beam currents. A crab waist scheme[6] will be adopted to the LELB scheme at SuperB and can mitigate bad betatron coupling resonances. The crab waist scheme utilizes a sextupole pair which is located at a betatron phase advance of $n\pi$ in the horizontal and $(n/2)\pi$ in the vertical plane from IP. The crab waist can improve the luminosity by a factor of two approximately than that without the crab sextupoles. The crab waist scheme has been tested in DAΦNE at Frascati[7]. We consider the LELB scheme and the crab waist as an alternative scheme when a feasibility of the crab waist will be proved at the real machine.

HIGH CURRENT SCHEME

The machine parameters of the KEKB upgrade are shown in Table 1. The beam energy with the boost factor

Table 1: Machine parameters.

	LER	**HER**	**unit**
E	3.5	8	GeV
I_b	9.4	4.1	A
N	1.18×10^{11}	5.13×10^{10}	
n_b	5018		
ε_x	12		nm
$\varepsilon_y/\varepsilon_x$	0.5		%
β_x^*	20		cm
β_y^*	3		mm
σ_z	3		mm
θ_x	30→0		mrad
ξ_x	0.272		
ξ_y	0.295		
R_L	0.86		
R_{ξ_x}	0.98		
R_{ξ_y}	1.11		
L	5.5×10^{35}		cm^{-2}s^{-1}

is determined by physics requirements so as to be sensitive against both of a new physics such as $B \to \tau\nu$ and time dependent CP violations, for instance $B \to \phi K^0$, $J/\Psi K^0$, in principle. From a point of view to reduce a power consumption, we also should consider to optimize the beam energy for each ring with keeping the center of mass energy. Since a bending radius of the HER dipole magnet is much longer than those of LER, the power loss due to a synchrotron radiation(SR) is less dependent on the beam energies in KEKB. The relation between the SR power and

* yukiyoshi.onishi@kek.jp

the luminosity is expressed by

$$P_{rad} = U_0 I = \frac{2T_0 EI}{\tau_x} \propto \frac{L}{\tau_x}, \quad (1)$$

where U_0 is a energy loss per one turn, T_0 is a revolution time, and τ_x is a transverse damping time. The longer damping time with keeping the luminosity can save the power consumption, however, shorter damping time is preferable to achieve the higher luminosity. In spite of this, we will choose give up wigglers in LER to make the same damping time in HER rather than changing the beam energy to reduce the power consumption. To compensate the different damping time between LER and HER, the emittance in HER is adjusted to realize a equilibrium condition of colliding bunches.

The emittance is 12 nm which is almost the minimum value determined by the present magnet configuration in the arc section. This low emittance improve the luminosity by 30 % compared with 24 nm. The beta function at IP is 20 cm in the horizontal and 3 mm in the vertical plane, respectively. The bunch length at a zero current is also 3 mm to make hour-glass effect small as much as possible. The horizontal crossing angle at IP is 30 mrad, however, an effective head-on crossing can be realized to adopt crab cavities.

In order to carry out the KEKB upgrade, the facility has to be shut down for three years. The beam pipes of both rings have to be replaced by new ante-chambers to achieve the extremely higher beam currents. In addition, the beam optics in the vicinity of the interaction point will be modified to squeeze the beta function at IP. We have designed the new QCS final focusing magnet with the compensation solenoid and special quadrupole magnets in the interaction region(IR) so as to realize the strong focusing. A positron damping ring is necessary to accomplish the increase of the beam current and the strong focusing at IP. The positron damping ring provides good-quality and high-intensity positrons to the LER ring.

After the modification and the replacement of components in KEKB, the beam operation will be resumed. During the operation, an upgrade and reinforcement of the RF system, the cooling and the electric facilities are carried out. We also continue to develop new crab cavities that can be operated at the high beam current of 10 A. After completion of the upgrade, the luminosity of 5.5×10^{35} cm^{-2}s^{-1} will be achieved. This luminosity estimation is obtained from a strong-strong beam-beam simulation[8]. Figure 1 shows the expected peak and integrated luminosity, beam currents as a function of a fiscal year.

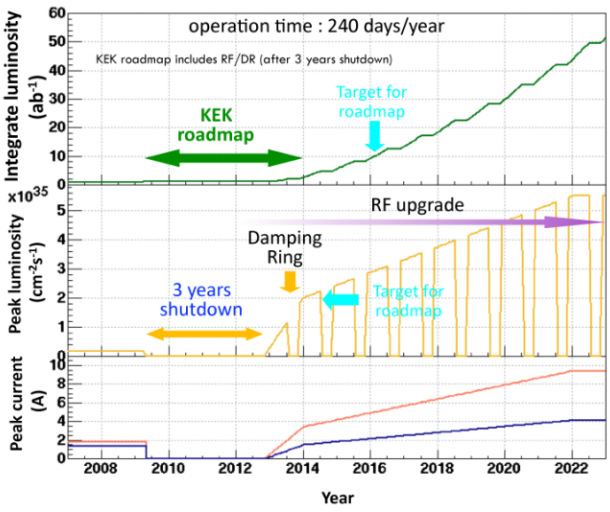

Figure 1: Projected luminosity.

OPTICS

The magnet configuration for the upgrade is based on KEKB. The same arc lattice of 2.5π non-interleaved sextupole scheme is used. A flexibility of the lattice is large and a emittance and a momentum compaction can be adjusted independently. When the arc emittance is chosen to be 12 nm, a range of the momentum compaction is $0 < \alpha_p < 7 \times 10^{-4}$ in LER and $1 \times 10^{-4} < \alpha_p < 8\times^{-4}$ in HER, respectively. The lattice parameters are shown in Table 2.

Table 2: Lattice parameters.

	LER	HER	unit
ε_x	12		nm
β_x^*	20		cm
β_y^*	3		mm
σ_z	3		mm
V_c (RF)	12	17.4	MW
α_p	1.9×10^{-4}	1.4×10^{-4}	
ν_s	-0.0231	-0.0157	

Further low emittance, 2.2 nm can be achieved in only LER when the dipole magnets are replaced with 4 m long magnets. The length of the present magnet is 0.9 m. The emittance becomes the similar level to that of SuperB. Therefore, a partial super-bunch collision scheme can be possible in the upgrade.

Another advantage of this lattice is that a nonlinear kick due to a sextupole magnet for on-momentum particles can be compensated by another sextupole magnet which is a relation of $-I'$ transformation while a chromatic effect can be collected. Therefore, a larger transverse dynamic aperture can be expected in the lattice by optimizing a magnetic field strength of sextupoles. On the other hand, these sextupoles are utilized to correct optics such as x-y couplings, dispersion functions, beta functions in a positive way. In order to generate a quadrupole and/or skew element, sextupole movers to provide a beam offset and/or an auxiliary coil additional to a main coil of the sextupole magnet are used.

Figure 2 shows a dynamic aperture in LER. There are 54(52 in HER) families of sextupoles in LER. With opti-

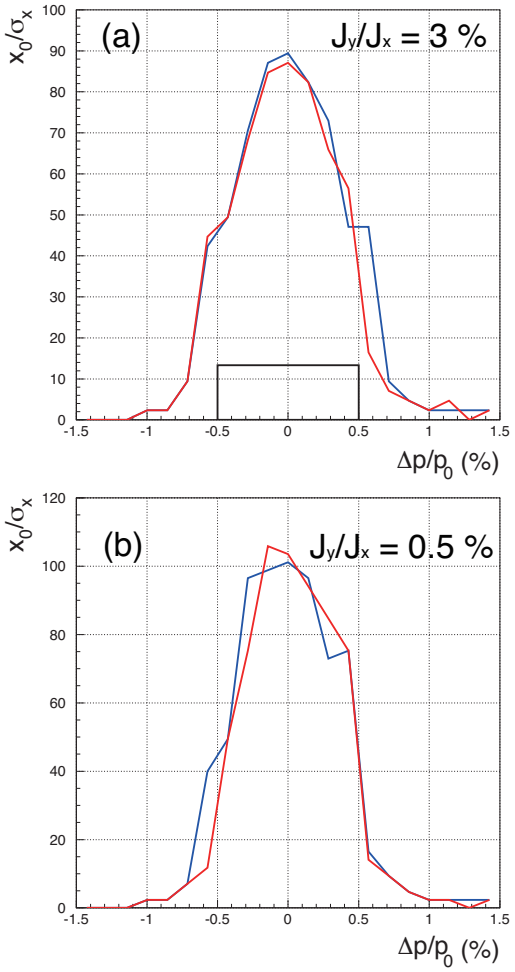

Figure 2: (a) Dynamic aperture for the injected beam in LER. Rectangle shows the requirement for the injection aperture (hard edge of 2σ of the injected beam). (b) Dynamic aperture for the storage beam in LER. The ratio of the initial action variable is the same as the coupling parameter of the ring. Blue line indicates no machine error, red line indicates optics corrections for the machine error.

mizing sextupole magnets, the dynamic aperture is investigated by using a particle-tracking simulation in SAD[9]. In the tracking simulations, a misalignment(vertical) of the beam-line is assumed as a machine error. For instance, the maximum discrepancy of the tunnel level from the reference point is -14 mm. These deformation of the beam-line away from the flat surface affects the optics although a closed orbit distortion is corrected. Consequently, the coupling($\varepsilon_y/\varepsilon_x$) deteriorates to be 0.75 % due to the machine error and the luminosity will be degraded. In order to improve a lattice performance, optics corrections such as x-y couplings, dispersion, and beta functions are performed. The optics correction can reduce the coupling parameter less than 0.1 % which comes from the beam-line distortion.

A positron damping ring is assumed for the injection in LER. In Fig. 2(a), the rectangle shows the requirement from the injected beam and the initial ratio of the vertical action variable to the horizontal is 3 % that is determined by emittances and an injection error. The dynamic aperture satisfies the injection requirement. For the storage beam, Touschek lifetime at 9.4 A and 0.5 % coupling is estimated to be 17 min which comes from the off-momentum dynamic aperture. However, Touschek lifetime becomes to be about 150 min which is longer than the luminosity lifetime of 81 min since a beam size changes due to a dynamic effect and a blow-up from a beam-beam interaction.

IR DESIGN

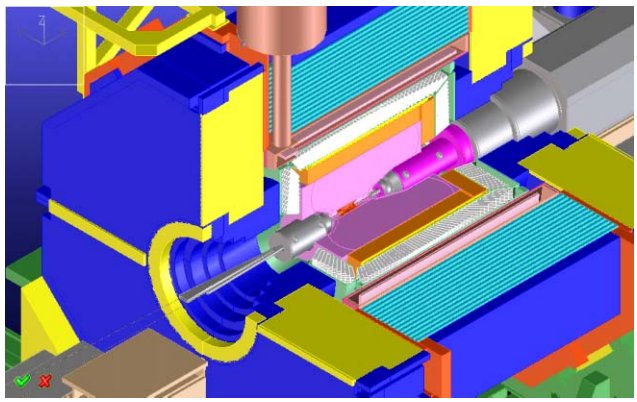

Figure 3: Interaction region.

The final focus quadrupole magnets are placed as close as possible to IP to reduce chromatic effects and the maximum beta function in the vicinity of IP. Figure 3 shows a cut view of the QCS magnet and the detector. The layout of the IR magnets is shown in Fig. 4. The solenoid field of the detector is compensated with anti-solenoids on each side of IP. The integrated field of the solenoids should be

$$\int B_z ds = 0. \quad (2)$$

The remaining x-y couplings and dispersion functions are corrected to be zero at IP and localized in IR by using skew quadrupole magnets and horizontal and vertical dipole magnets in IR. The crossing angle of 30 mrad is adopted to separate two beams in IR. A local chromaticity correction is adopted in LER. We also consider the local chromaticity correction for HER to keep a larger dynamic aperture.

A physical aperture and synchrotron radiation(SR) fans are estimated by a beam size that includes a dynamic emittance and a dynamic beta due to a beam-beam interaction. The dynamic effect depends on a betatron tune and a beam-beam parameter. We assume that the horizontal betatron tune(fractional part) is 0.505 and the horizontal beam-beam parameter is 0.27 as the nominal values. The horizontal beta function becomes the maximum value at QC2 that is the horizontal focusing magnet at the closest to IP. When $5\sigma_x$ beam size at QC2 is required, 100 mm for the nominal beta function of 20 cm at IP and 75 mm for 40 cm are

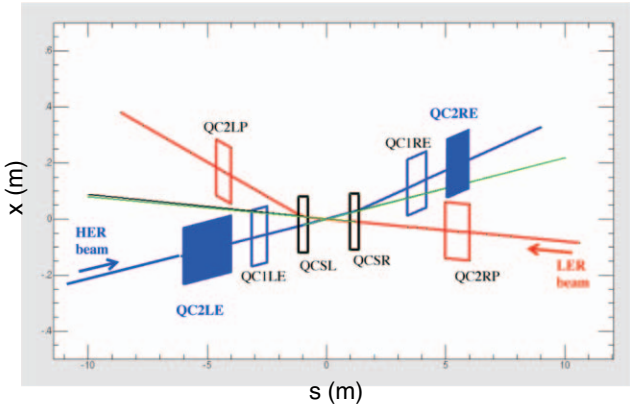

Figure 4: QCS and special IR magnets.

needed as the physical aperture. We also consider SR fans with $3\sigma_x$ beam size. A spread of the SR fan is large in QC2(L) that locates the left side of IP. Introducing a offset of QCS from the design orbit, it makes the SR fan small significantly. Further, the larger horizontal beta function makes the SR fan small. If there is unexpected difficulties to handle the SR fan, we might choose 40 cm as the nominal horizontal beta function at IP. In this case, the luminosity deteriorates by about 20 %.

VACUUM SYSTEM

Copper beam pipes with ante-chambers[10] are adopted for the arc section. Benefits of the ante-chamber are a low SR power density, a low photoelectrons around a positron beam, and a low beam impedance. Figure 5 shows a schematic view of the ante-chamber. The ante-chamber consists of a beam chamber and a SR chamber. The nominal radius of the beam chamber is 45 mm and the height of the SR chamber is 15 mm. A NEG pump is installed in a channel which is the same structure of the SR chamber at the opposite side. The NEG channel is separated by a slit for a RF shield from the beam chamber. Cooling channels are attached at both side of the SR chamber and the NEG chamber.

Figure 5: Ante-chamber.

New bellows are adopted to connect beam pipes for each other. We call this new component a comb-type bellows. The features of the comb-type bellows are a low beam impedance and a high thermal strength. Figure 6 shows a temperature of bellows as a function of the beam current. The temperature of the comb-type bellows is lower than a conventional finger-type bellows by a factor of two. The comb-type bellows can be adopted to a complex shape such as the ante-chamber. However, an accurate alignment of the beam pipes is needed since there is a less flexibility.

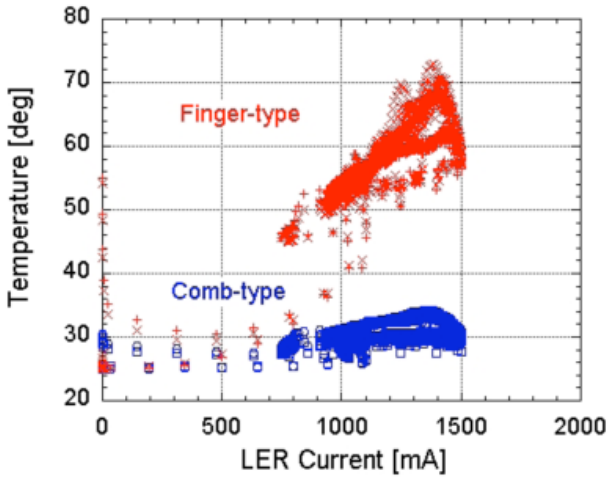

Figure 6: Temperature of bellows.

The high current and the short bunch length imply not only an intense SR power and a higher HOM heating but also an instability due to a coherent synchrotron radiation(CSR). In order to handle CSR, a smaller radius of the beam pipe is effective to suppress the instability. Therefore, we also consider the ante-chamber with a radius of 25 mm. For the small aperture of the beam pipe, the impedance and the pumping availability should be evaluated. We still continue the CSR calculation that is complicated due to an interference of the other impedance of the ring. If the small aperture of the beam pipe is not available due to some difficulties, we will choose longer bunch length of 4 mm. In the case of 4 mm bunch length, the CSR instability can be suppressed significantly and the luminosity will deteriorate by 16 % that is obtained from computer simulations.

CRAB CAVITY

The new crab cavity that can be adopted for the 10 A beam current has been developed for the KEKB upgrade. We consider two candidates for the crab cavity. One is a coaxial type, the other is a wave-guide type crab cavity. The different structures are used for the lower order mode(LOM) damping. Figure 7 shows a schematic view of the crab cavity The detail description can be found in elsewhere[11]. One or two crab cavities are installed for each ring to provide the appropriate crab kick. In the crab crossing scheme, these cavities are located at Nikko section where the superconducting acceleration cavities(SCC) are

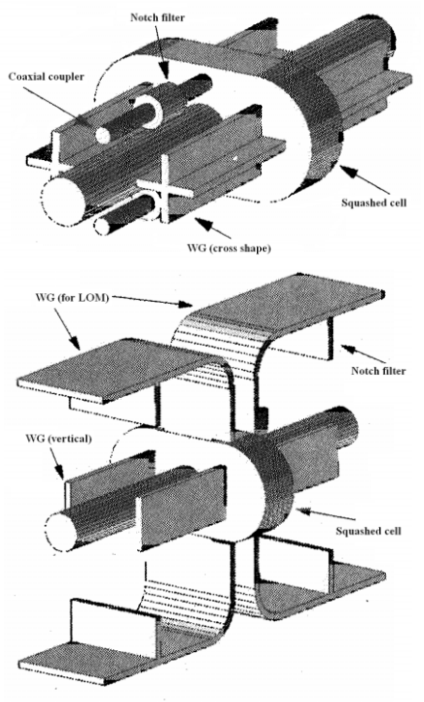

Figure 7: Upper: coaxial type, lower: wave guide type crab cavity.

also located in HER. Therefore, this scheme is similar to the present KEKB and the crabbing mode is not localized in the IR.

SUMMARY

The target luminosity of the KEKB upgrade is 5×10^{35} $cm^{-2}s^{-1}$ or higher for the KEKB upgrade. The baseline is the high current scheme. The design of the vacuum system is almost completed except for the IR chamber. Proto-type of the ante-chamber and the comb-type bellows, and so on have been tested at the present KEKB. However, the CSR evaluation has not done yet. In the IR design, there are still things to be fixed, especially, cure of the SR fan and the design of the beam pipes.

The items of the KEKB upgrade and the luminosity gain are shown in Table 3. During the 3 years shutdown, the replacement of the beam pipe and the modification of the IR will be done at least. Then, the damping ring will be installed and the beam current will be increased gradually. However, the upgrade scenario is strongly dependent on the budget accepted by the Japanese government and international collaborations interested in the flavor physics.

Table 3: Items for the KEKB upgrade.

Item	Gain	Purpose
beam pipe	1.5	HC, short σ_z, EC
IR	1.5	squeeze β^*
low ε_x & ν_x $\rightarrow$0.5	1.3	mitigate nonlinear effects
crab crossing	2	mitigate nonlinear effects
RF/infrastructure	3	HC
DR/e^+ source	1.5	low β^*, injection
charge switch	?	EC, lower e^+ current

REFERENCES

[1] See http://www.kek.jp/intra-e/Introduction/column/.

[2] K. Ohmi, et al., Proceeding of PAC2005, May 2005.

[3] KEK Report 2004-4, June 2004.

[4] INFN/AE-07/2, SLAC-R-856, LAL 07-15, Match 2007.

[5] M. Biagini, ICFA workshop on e^+e^- Factories'08, April 2008.

[6] P. Raimondi, et al., Presented at 3rd Workshop on Super Flavor Factory based on Linear Collider Technology (Super B III), June 2006.

[7] C. Milardi, ICFA workshop on e^+e^- Factories'08, April 2008.

[8] K. Ohmi, ICFA workshop on e^+e^- Factories'08, April 2008.

[9] SAD code is developed at KEK.
See http://acc-physics.kek.jp/SAD/.

[10] Y. Suetsugu, et al., KEK Proceedings 2004-1ZA, 2004.

[11] K. Akai, et al., Proceeding of PAC2005, May 2005.

OVERVIEW OF BEAM DYNAMICS STUDIES AT DAΦNE

M. Zobov, INFN Laboratori Nazionali di Frascati, Frascati, Italy
for DAΦNE Collaboration Team*

Abstract

Since several years the DAΦNE Team has been discussing ideas and performing experimental activities aimed at the collider luminosity increase. In this paper we briefly describe the proposed ideas and discuss results of the most relevant beam dynamics experimental studies that have been carried at DAΦNE. We also introduce the concept of crab waist collisions that is the base of the undergoing DAΦNE upgrade.

INTRODUCTION

DAΦNE is an electron-positron collider working at the c.m. energy of the Φ resonance (1.02 GeV) to produce a high rate of K mesons [1]. The collider complex consists of two independent rings having two common Interaction Regions (IR) and an injection system composed of a full energy linear accelerator, a damping/accumulator ring and transfer lines. Figure 1 shows a view of the DAΦNE accelerator complex while some of the main collider parameters are listed in Table 1.

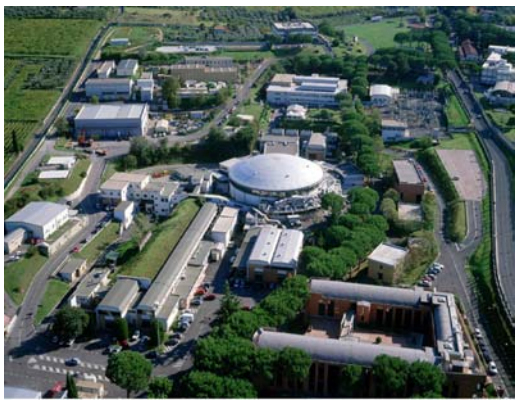

Fig. 1 View of DAΦNE accelerator complex.

Since 2000 DAΦNE has been delivering luminosity to three experiments, KLOE [2], FINUDA [3] and DEAR [4]. The KLOE experimental detector surrounded by a superconducting solenoid has been used for a wide variety of physics measurements with emphasis on the kaon decays, and most notably on the issue of CP violation. The second magnetic detector FINUDA is devoted to the study of hypernuclear physics. The small non-magnetic experiment DEAR has been used for the study of the properties of kaonic atoms.

In 2007 DAΦNE was shut down for the SIDDHARTA experiment installation [5] and for relevant collider modifications aimed at testing the novel idea of crab waist collisions [6, 7, 8]. DAΦNE operations with the crab waist scheme started in the very end of 2007 and the first results of the new scheme implementation are reported in [9] at this Workshop.

Table 1: DAΦNE main parameters (KLOE run)

Energy [GeV]	0.51
Trajectory length [m]	97.69
RF frequency [MHz]	368.26
Harmonic number	120
Damping time, τ_E/τ_x [ms]	17.8/36.0
Bunch length [cm]	1-3
Number of colliding bunches	111
Beta functions β_x/β_y [m]	1.6/0.017
Emittance, ε_x [mm·mrad] (KLOE)	0.34
Coupling [%]	0.2-0.3
Max. tune shifts	0.03/0.04
Max. beam current e-/e+ [A]	2.5/1.4

COLLIDER PERFORMANCE

Since the beginning of the experimental data taking runs in 2000 DAΦNE has been continuosly improving its performances in terms of luminosity, lifetime and backgrounds. Fig.2 shows the daily peak luminosity for KLOE, DEAR and FINUDA runs.

The DEAR experiment was performed in less than 5 months in 2002-2003, collecting about 100 pb^{-1}, with a peak luminosity of $0.7x10^{32}$ $cm^{-2}s^{-1}$. The KLOE experimental program has been completed in 2006, acquiring more than 2 fb^{-1} on the peak of the Φ resonance, more than 0.25 fb^{-1} off-resonance and performing a high statistics resonance scan. The best peak luminosity obtained during this run was $1.5x10^{32}$ $cm^{-2}s^{-1}$, with a maximum daily integrated luminosity of about 10 pb^{-1}. The second run of FINUDA, which collected 0.96 fb^{-1}, started in October 2006. During this run a peak luminosity of $1.6x10^{32}$ $cm^{-2}s^{-1}$ has been achieved, while a maximum daily integrated luminosity similar to that in the KLOE run has been obtained with lower beam currents, lower number of bunches and higher beta functions at the collision point.

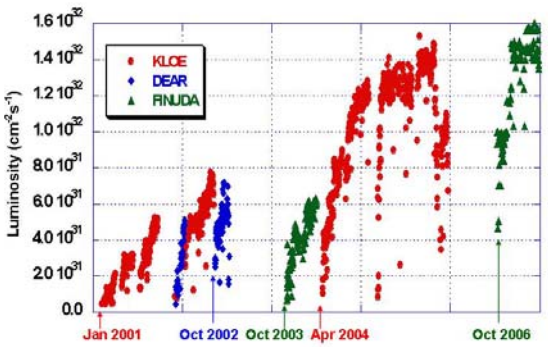

Figure 2. DAΦNE peak luminosity for KLOE (red), DEAR (blue) and FINUDA (green).

The steady luminosity progress shown in Fig. 2 was achieved by the optimization of the machine parameters and hardware changes implemented during long shut downs in 2003 and in 2006. In the following we overview only some of the main beam dynamics issues that have been studied at DAΦNE and helped to improve the collider performance.

SINGLE BUNCH DYNAMICS

We have not detected any destructive single bunch instability. Indeed, we have managed to store bunch currents that are by a factor 10 higher than those required in typical operating conditions. So the main efforts in single bunch dynamics optimization were aimed at bunch lengthening reduction and single bunch vertical size blow up elimination.

Nowdays analytical estimates (see, for example, [10, 11]) and existing 2D and 3D numerical codes have proven their reliability in RF design and vacuum chamber's coupling impedance optimization. Careful vacuum chamber design and detailed impedance calculations allow to predict bunch behaviour in modern storage rings [12]. A good agreement between bunch lengthening simulations and measurements was found for all the three rings of the DAΦNE accelerator complex, the accumulator [13] and the electron and positron main rings [14, 15]. In particular, for the main rings it was possible not only to calculate correctly the bunch lengthening effect and the bunch charge distribution, but also to predict in advance the bunch shape oscillation instability. This quadrupole mode instability was clearly observed in experimental measurements [16].

Achieving higher luminosity required shorter bunch length, i.e. a reduction of the beam coupling impedance responsible for the bunch lengthening in the main rings. This was particularly important for the electron ring where the impedance was by about a factor 2 higher due to the ion clearing electrodes (see Fig. 3).

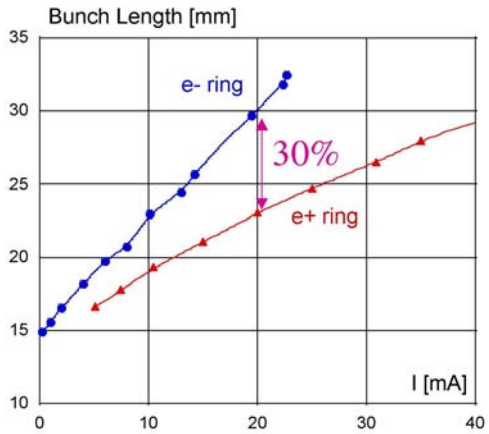

Fig. 3 Bunch length in the electron (blue) and positron (red) rings as a function of bunch current (measured at V_{RF}=120 kV, α_c = 0.017).

Another harmful effect related to the impedance was the vertical beam size blow up. As can be seen in Fig. 4, the blow up was stronger for higher RF voltages and higher bunch currents and it had a threshold behavior. Dedicated measurements have shown that the blow up threshold was strongly correlated with the longitudinal microwave instability threshold.

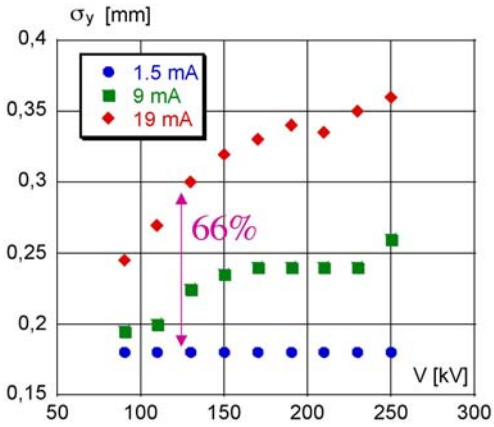

Fig. 4 Vertical beam size measured by the synchrotron light monitor as a function of RF voltage for three different bunch currents.

For the reasons above, it has been decided to decrease the electron ring coupling impedance by extracting the long ion clearing electrodes from the wiggler sections [17]. The electrodes removal is estimated to decrease the impedance by a factor 2. Its effects are:

- electron bunches are by about 25-30% shorter in typical operating conditions (see Fig. 5);
- the quadrupole instability threshold has been pushed beyond the operating bunch currents;
- no vertical beam size blow up has been observed for the whole range of operating bunch currents and RF voltages.

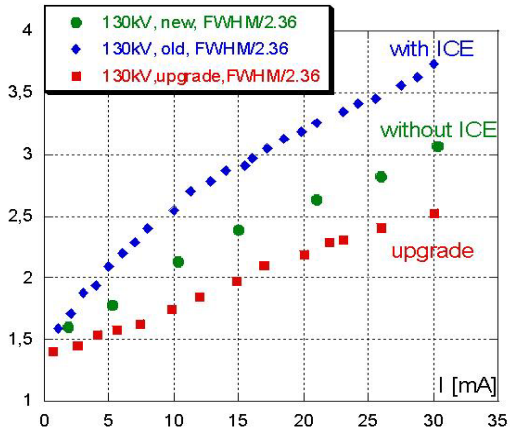

Fig. 5 Bunch lengthening (cm) in the DAΦNE electron ring at V_{RF} = 130 kV, α_c = 0.019 (blue – original vacuum chamber, green – after clearing electrode removal, red – upgraded vacuum chamber)

This helped to increase the specific luminosity by approximately 50% during the last FINUDA run [18]. During the upgrade for the crab waist experiment the DAΦNE vacuum chamber was substantially modified (see [19]). In particular, the design of both interaction regions was greatly simplified. Now the IR chambers are just two straight intersecting tubes with very smooth tapers. Besides, new low impedance injection kickers and new shielded bellows were installed in the rings. These modifications have reduced further the beam coupling impedance and decreased bunch lengthening, as one can see in Fig. 5.

MULTIBUNCH DYNAMICS

Since the very beginning of the DAΦNE project multibunch instabilities were recognized as one of the most harmful potential dangers. For this reason the vacuum chamber was designed taking care of HOM damping and shifting the HOM frequencies far from revolution harmonics in order to avoid excessive power losses. New designs and novel ideas were adopted for almost all principal vacuum chamber components: RF cavities [20, 21], shielded bellows [22], longitudinal feedback kickers [23], BPMs [24], DC current monitors, injection kickers, transverse feedback kickers and others [25]. For example, longitudinal feedback kickers based on the DAΦNE kicker design are routinely used in more than 10 operating colliders and synchrotron radiation sources.

However, these measures were not sufficient to eliminate completely any multibunch instability and powerful feedback systems also were developed to damp the residual unstable multibunch oscillations.

During DAΦNE operation two multibunch instabilities were limiting collider performance: the longitudinal quadrupole instability in the electron ring and the strong horizontal instability in the positron one.

The multibunch longitudinal quadrupole instability was essentially the same as the single bunch quadrupole mode, but much stronger in multibunch operation. For some time this kind of instability was limiting the electron beam current at a level of 700-800 mA due to the current saturation at injection and was leading to luminosity loss in beam-beam collisions of unstable bunches. The instability was kept under control by a proper feedback tuning providing different longitudinal kicks for the bunch heads and bunch tails [16]. Later, due to the impedance reduction after ion clearing electrodes removal the instability has been completely suppressed for the whole range of operating beam currents.

Instead the positron beam horizontal instability still remains one of the most stringent collider performance limitations. Indeed, the maximum positron stored current is significantly lower than the electron one. The instability has many typical features of electron cloud instability:

- Large positive tune shift
- Anomalous pressure rise
- Very fast growth rate (several μs)
- Bunch pattern dependence (see Fig. 6)
- Some evidence of beam scrubbing
- Others

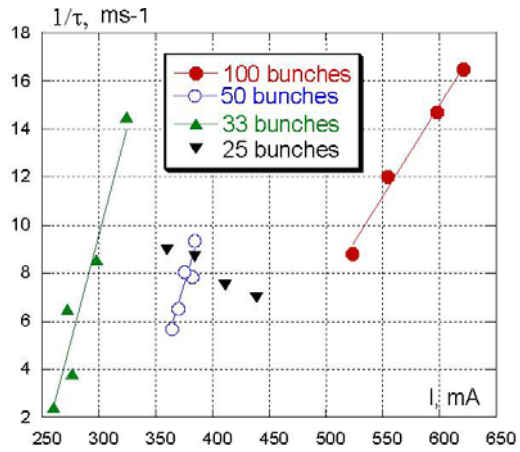

Fig. 6. Positron beam instability decrements as a function of beam current for different bunch patterns.

Several measures helped to keep the instability under control to store reasonable positron beam currents in collision (>1 A). These are:

- Implementation of powerful transverse feedback systems providing damping times as fast as few μsec [26].
- Careful injection optimization necessary to minimize perturbation of the already stored beam. It has been achieved by reducing the injection kicker pulse length and by fine injection bump adjustment.
- During the current DAΦNE run for SIDDHARTA experiment several solenoids have been wound around the vacuum chambers of interaction regions and straight sections. This yielded some reduction of anomalous pressure rise and has also been beneficial to the increase of the vertical instability threshold.
- A modest effect of beam scrubbing has been observed on a long time scale.

Further improvements are expected after installation of additional solenoids. Besides, the feasibility of vacuum chamber titanium coating is under discussion.

BEAM-BEAM COLLISIONS

For lepton colliders with low transverse impedance the existing beam-beam simulation codes predict rather well beam-beam behaviour of colliding bunches: beam blow up, beam-beam lifetime, good working point areas etc. In order to simulate beam-beam effects in DAΦNE the LIFETRAC [27] code has been successfully used.

Fig. 7 shows the luminosity tune scan plot provided by LIFETRAC where the brighter red colours correspond to higher luminosity. The superimposed solid line arrow shows how the DAΦNE tunes changed with time, while the stars indicate the electron and positron ring tune during the FINUDA run. Following the code predictions, optimizing dynamic aperture and going closer to the

integer tunes we have gradually improved both the peak luminosity and beam-beam lifetime.

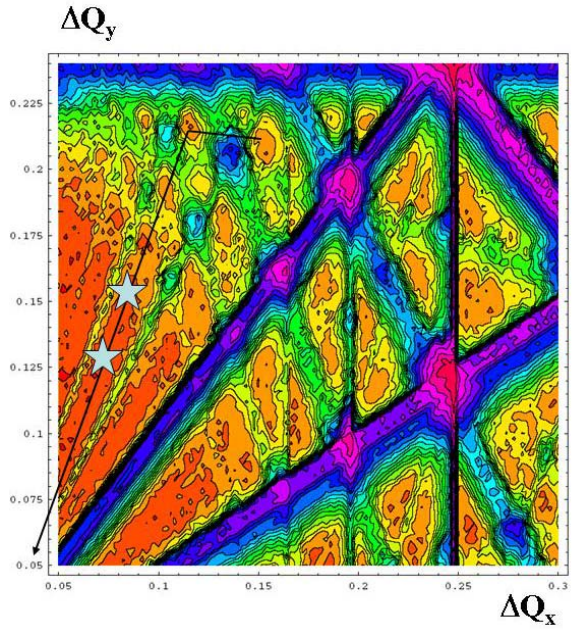

Fig. 7 Luminosity numerical tune scan.

At an early stage of beam-beam studies it was predicted that the crosstalk between lattice nonlinearities and beam-beam interaction could dramatically deteriorate the collider performance [28]. This effect becomes particularly strong in multibunch operation. It has been shown numerically that in order to cope with this effect it is necessary to reduce the nonlinear tune dependence on oscillation amplitude as much as possible.

For this purpose three octupoles have been installed in each ring. They have proven to be very effective in increasing the dynamic aperture and in compensating the cubic nonlinearity of the lattice. The octupoles have become essential in multibunch collisions of consecutive bunches to prevent strong lifetime reduction at the maximum beam currents [29].

Long-range beam-beam interactions (parasitic crossings) were another source of luminosity degradation in the DAΦNE original configuration before the collider upgrade for crab waist collisions. Due to drastic lifetime reduction the parasitic crossings put a limit on the maximum storable currents and, as a consequence, on the achievable peak and integrated luminosity. In order to mitigate this problem, numerical and experimental studies of the parasitic crossings compensation by current-carrying wires have been done [29, 30]. During the operation for the KLOE experiment two such wires have been installed at both ends of the interaction region, outside the vacuum chamber. They produced a relevant improvement in the lifetime of the "weak" beam (positrons) at the maximum current of the "strong" one (electron) without luminosity loss (see Fig. 8), in agreement with the numerical predictions.

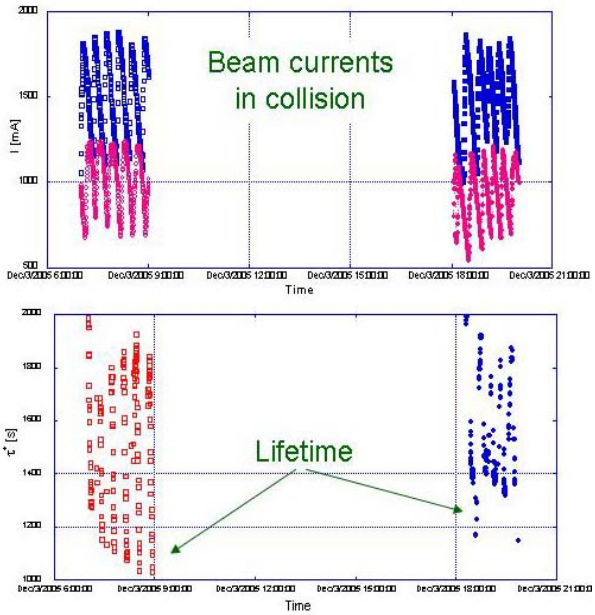

Fig. 8 Beam currents and positron beam lifetime with current-carrying wire off (left) and on (right).

DAΦNE UPGRADE ACTIVITIES

Since several years the DAΦNE team has been discussing proposals and ideas aimed at increasing the luminosity of the collider. Some of them are listed below:

- "All wiggler" structure to decrease the damping time
- Negative momentum compaction factor [31]
- PC compensation with current-carrying wires [30]
- Collisions under a very high crossing angle [32]
- Strong RF focusing [33, 34]
- Crabbed waist collisions [7, 35].

Collisions in a negative momentum compaction lattice and PC compensation with the wires have been tested experimentally at DAΦNE while 3 different proposals for DAΦNE upgrade, DANAE [36], strong RF focusing collider [37] and crab waist upgrade [35], have been published.

After many discussions the DAΦNE team decided, and the LNF Scientific Committee approved, testing the large crossing angle and crab waist compensation scheme at DAΦNE since:

- A high luminosity gain is expected
- Does not require large hardware modifications
- Fits the DAΦNE schedule: the modifications are being done during the planned shut down for the FINUDA detector roll-out and SIDDHARTA detector installation
- The cost of the modifications is moderate
- If the test is successful the crabbed waist scheme can be adopted for the SuperB factory design [38].

The Φ-factory has been upgraded in the second half of 2007 to implement the crab waist collision scheme [19]. Commissioning of the modified collider started in November 2007. Details of the DAΦNE hardware upgrade and the first obtained results are described

elsewhere at this Workshop [9]. Below we discuss the crab waist collision concept from beam dynamics point of view.

Crab Waist Concept

The Crab Waist scheme of beam-beam collisions can substantially increase collider luminosity since it combines several potentially advantageous ideas. Let us consider two bunches with the vertical σ_y, horizontal σ_x and longitudinal σ_z sizes colliding under a horizontal crossing angle θ (as shown in Fig. 9a). Then, the CW principle can be explained, somewhat artificially, in the three basic steps.

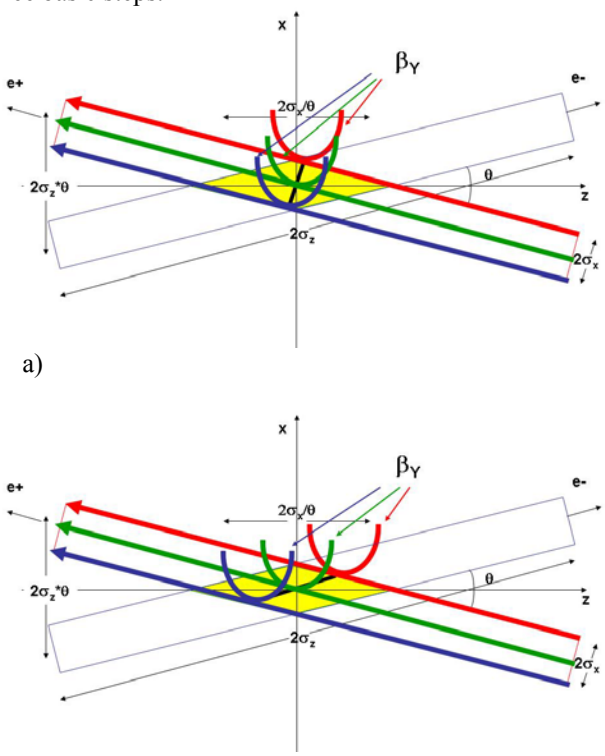

a)

b)

Fig. 9 Crab Waist collision scheme
((a) – crab sextupoles off; (b) – crab sextupoles on)

The first one is large Piwinski angle. For collisions under a crossing angle θ the luminosity L and the horizontal and vertical tune shifts ξ_x and ξ_y scale as (see, for example, [39]):

$$L \propto \frac{N\xi_y}{\beta_y^*} \propto \frac{1}{\sqrt{\beta_y^*}}; \quad \xi_y \propto \frac{N\sqrt{\beta_y^*}}{\sigma_z\theta}; \quad \xi_x \propto \frac{N}{(\sigma_z\theta)^2}$$

Here the Piwinski angle is defined as:

$$\phi = \frac{\sigma_z}{\sigma_x} tg\left(\frac{\theta}{2}\right) \approx \frac{\sigma_z}{\sigma_x}\frac{\theta}{2}$$

with N being the number of particles per bunch. Here we consider the case of flat beams, small horizontal crossing angle $\theta << 1$ and large Piwinski angle $\phi >> 1$.

The idea of colliding with a large Piwinski angle is not new (see, for example, [40]). It has been also proposed for hadron colliders [41, 42] to increase the bunch length and the crossing angle. In such a case, if it were possible to increase N proportionally to $\sigma_z\theta$, the vertical tune shift ξ_y would remain constant, while the luminosity would grow proportionally to $\sigma_z\theta$. Moreover, the horizontal tune shift ξ_x drops like $1/\sigma_z\theta$. However, differently from [41, 42], in the crab waist scheme described here the Piwinski angle is increased by decreasing the horizontal beam size and increasing the crossing angle. In this way we can gain in luminosity as well, and the horizontal tune shift decreases due the larger crossing angle. But the most important effect is that the overlap area of the colliding bunches is reduced, since it is proportional to σ_x/θ (see Fig. 9).

Then, as the second step, the vertical beta function β_y can be made comparable to the overlap region length (i.e. much smaller than the bunch length):

$$\beta_y^* \approx \frac{\sigma_x}{\theta} << \sigma_z$$

We get several advantages in this case:

- Small spot size at the IP, i.e. higher luminosity L.
- Reduction of the vertical tune shift ξ_y.
- Suppression of synchrobetatron resonances [43].
- Reduction of the vertical tune shift with the synchrotron oscillation amplitude [43].

There are additional advantages in such a collision scheme: there is no need to decrease the bunch length to increase the luminosity as proposed in standard upgrade plans for B- and Φ-factories [44, 45, and 36]. This will certainly helps solving the problems of HOM heating, coherent synchrotron radiation of short bunches, excessive power consumption etc. Moreover, parasitic collisions (PC) become negligible since with higher crossing angle and smaller horizontal beam size the beam separation at the PC is large in terms of σ_x.

However, large Piwinski angle itself introduces new beam-beam resonances which may strongly limit the maximum achievable tune shifts (see [46], for example). At this point the crab waist transformation enters the game boosting the luminosity. This is the third step. The transformation is described by the Hamiltonian

$$H = H_0 + \frac{1}{2\theta} x p_y^2$$

Here H_0 is the Hamiltonian describing particle's motion without CW; x the horizontal coordinate, p_y the vertical momentum. Such a transformation produces a rotation of the vertical beta function according to:

$$\beta_y = \beta_y^* + \frac{(s - x/\theta)^2}{\beta_y^*}$$

As shown in Fig. 9b, in this case the beta function waist of one beam is oriented along the central trajectory of the other one.

The crab waist transformation yields a small geometric luminosity gain due to the vertical beta function redistribution along the overlap region. It is estimated to be of the order of several percent [47]. However, the dominating effect comes from the suppression of betatron (and synchrobetatron) resonances arising (in collisions

without CW) through the vertical motion modulation by the horizontal oscillations [7, 8]. In practice the CW vertical beta function rotation is provided by sextupole magnets placed on both sides of the IP in phase with the IP in the horizontal plane and at π/2 in the vertical one (as shown in Fig. 10).

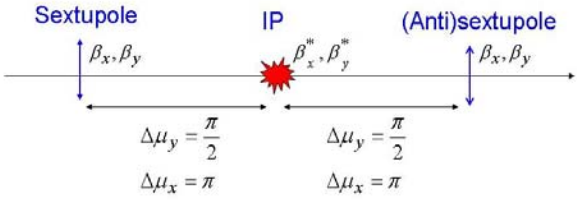

Fig. 10. Crab sextupole locations.

The crab sextupole strength should satisfy the following condition depending on the crossing angle, the beta functions at the IP and the sextupole locations:

$$K = \frac{1}{2\theta}\frac{1}{\beta_y^*\beta_y}\sqrt{\frac{\beta_x^*}{\beta_x}}$$

A detailed discussion on the resonance suppression in crab waist collisions with many numerical examples can be found in [48], while a semi-analytical treatment of this effect is given in [49, 50].

CONCLUSIONS

Since 2000 DAΦNE has been delivering luminosity to three physics experiments, KLOE, FINUDA and DEAR, steadily improving luminosity, lifetime and backgrounds. Beam dynamics studies have been one of the key contributions to the successful collider operation.

During last years the DAΦNE Team has been discussing proposals and ideas for the Φ-factory luminosity increase. Some of them, such as beam-beam collisions with negative momentum compaction factor, parasitic crossings compensation with current-carrying wires and others have been tested experimentally.

After many discussions and thorough analytical and numerical beam dynamics studies it has been decided to implement a novel scheme of crab waist collisions, exploiting the shut down for the SIDDHARTA experiment installation. With this new collision configuration it is expected to reach a luminosity of the order of $5x10^{32}$ $cm^{-2}s^{-1}$.

REFERENCES

[1] G.Vignola et al., Frascati Phys.Ser.4:19-30,1996;
C.Milardi et al., Frascati Phys.Ser.16:75-84,1999;
C.Milardi et al., physics/0408073;
M.Zobov et al., arXiv:0709.3696.
[2] KLOE Coll., Nucl.Instrum.Meth. A482:363-385,2002.
[3] FINUDA Coll., Proc. HYP2000 (Torino, 2000).
[4] DEAR Coll., Phys.Lett. B535:52-58,2002.
[5] SIDDHARTA Coll., Eur.Phys.J. A31:537-539,2007.
[6] P.Raimondi, 2nd SuperB Workshop, Frascati, 2006.
[7] P.Raimondi, D.Shatilov, M.Zobov, physics/0702033.
[8] P.Raimondi et al., arXiv:0802.2667.
[9] C.Milardi et al., this Workshop.
[10] K.Y.Ng, FERMILAB-FN-0673, 1998
[11] L.Palumbo, V.Vaccaro, M.Zobov, physics/0309023.
[12] K.Bane, K.Oide, M.Zobov, SLAB-PUB-11007, 2006
[13] R.Boni et al.,Nucl.Instr.Meth.A418:241-248,1998.
[14] M.Zobov et al., physics/0312072.
[15] B.Spataro, M.Zobov, DAΦNE Note G-64, 2005.
[16] A.Drago et al., PRSTAB 6:052801, 2003.
[17] M.Zobov et al., JINST 2: P08002, 2007.
[18] C.Milardi et al., PAC07, pp.1457-1459, 2007.
[19] C.Milardi et al., arXiv :0803.1450.
[20] S.Bartalucci et al., Part.Accel :48 :213-237,1995.
[21] D.Alesini et al., PRSTAB 7:092001, 2004.
[22] M.Zobov et al.,Nucl.Instr.Meth.A403:185-194,1998.
[23] R.Boni et al.,Part.Accel.52:95-113,1996.
[24] F.Marcellini et al.,Nucl.Instr.Meth.A402:27-35,1998.
[25] M.Zobov et al., Frascati Phys.Ser.10:371-378,1998.
[26] A.Drago, this Workshop.
[27] D.Shatilov, Part.Accel.52:65-93,1996.
[28] M. Zobov, physics/0311129.
[29] C.Milardi et al., arXiv:0803.1544.
[30] C.Milardi et al., physics/0607129.
[31] M.Zobov, physics/0607036.
[32] P.Raimondi, Talk at Alghero Workshop, 2003.
[33] A.Gallo, P.Raimondi, M.Zobov, physics/0309066.
[34] A.Gallo, P.Raimondi, M.Zobov, physics/0404020.
[35] D.Alesini et al, LNF-06/033 (IR), 2006.
[36] DANAE Letter of Intent, see http://www.lnf.infn.it.
[37] C.Biscari et al., EPAC2004, pp. 683-685, 2004.
[38] SuperB CDR, arXiv:0709.0451.
[39] D.Shatilov, M.Zobov, ICFA Beam.Dyn.Newslett.37: 99-109, 2005.
[40] K.Hirata, Phys.Rev.Lett.74:2228-2231,1995.
[41] K.Takayama et al., Phys.Rev.Lett.88:144801,2002.
[42] F.Zimmermann, F.Ruggiero, PRSTAB 5:061001.
[43] D.Pestrikov, Nucl.Instr.Meth. A336 :427-437,1993.
[44] J.Seeman, PAC05, p. 2333.
[45] H.Koiso, PAC05, p. 64.
[46] K.Ohmi et al., PRSTAB 7:104401,2004.
[47] I.Koop, private communications.
[48] D.Shatilov, this Workshop.
[49] K.Ohmi et al., PAC07, pp. 1493-1495, 2007.
[50] K Ohmi, this Workshop.

[*]D.Alesini, D.Babusci, S.Bettoni, M.Biagini, C.Biscari, R.Boni, M.Boscolo, F.Bossi, B.Buonomo, A.Clozza, G.Delle Monache, T.Demma, G.Di Pirro, A.Drago, A.Gallo, A.Ghigo, S.Guiducci, C.Ligi, F.Marcellini, C.Marchetti, G.Mazzitelli, C.Milardi, F.Murtas, L.Pellegrino, M.Preger, L.Quintieri, P.Raimondi, R.Ricci, U.Rotundo, C.Sanelli, M.Serio, F.Sgamma, B.Spataro, A.Stecchi, A.Stella, S.Tomassini, C.Vaccarezza, M.Zobov (LNF, Italy); I.Koop, E.Levichev, S.Nikitin, P.Piminov, D.Shatilov, V.Smaluk (BINP, Russia); J.Fox, D.Teytelman (SLAC, USA); K. Ohmi (KEK, Japan)*

* *Con il contributo del Ministero degli Affari Esteri, Direzione Generale per la Promozione e la Cooperazione Culrturale*

VEPP-2000 ELECTRON-POSITRON COLLIDER COMMISSIONING

Dmitry Berkaev, Alexander Kirpotin, Ivan Koop, Alexander Lysenko, Igor Nesterenko, Evgeny Perevedentsev, Yuri Rogovsky, Alexander Romanov, Petr Shatunov, Dmitry Shwartz, Alexander Skrinsky, Yuri Shatunov, BINP SB RAS, 630090 Novosibirsk, Russia

Abstract

VEPP-2000 electron-positron collider construction has been completed in the Budker INP at the beginning of 2007 year. First beam was captured in a special lattice without final focus solenoids. In this regime all systems of power supplies, machine control and beam diagnostics were calibrated and tuned. In the same mode vacuum chamber treatment by synchrotron radiation was performed with electron beam current up to 150 mA.

The first test of the round beam option was performed at the energy of 508 MeV with the solenoidal field 10 T in two interaction straight sections. Studies of the beam-beam interaction have been done in "weak-strong" and "strong-strong" regimes. Measurements of beam sizes in the both cases have indicated a beam behavior similar to expectations for the round colliding beams.

INTRODUCTION

Budker Institute of Nuclear Physics has started the construction of the VEPP-2000 collider six years ago. At BINP for more than quarter of century the electron-positron collider VEPP-2M has been operated in the energy range of 0.4 ÷1.4 GeV. For a long time its results were the main source of information about hadrons production in this energy range. On the other hand, a whole number of events collected by different experimental groups in the energy span above VEPP-2M (up to 2 GeV) doesn't exceed 10 % of the data accumulated by VEPP-2M. These motivations caused a decision to create instead of VEPP-2M collider a new machine with higher luminosity (up to 10^{32}cm^{-2}s^{-1}) and the beam energy up to 2×1 GeV. For that, it's assumed to construct the new collider in the same experimental hall and use at least at the first stage the existing infrastructure of the accelerators and detectors.

To achieve the final goals (luminosity and energy) under such boundary conditions, the Round Beam Concept was applied in design of the machine optics [1]. The main feature of this concept is rotational symmetry of the kick from the round opposite beam. This is complemented by the $x-z$ symmetry of the betatron transfer matrix between the collisions. Together, it results in particle's angular momentum conservation ($M = xz' - zx' = const$). As a consequence, it yields an enhancement of dynamical stability, even with nonlinear effects from the beam-beam force taken into account.

Computer simulations of the beam-beam interaction in "weak-strong" and "strong-strong" situations confirmed these expectations [2-3].

VEPP-2000 MAGNET STRUCTURE

Magnetic focusing structure of VEPP-2000 [4] has the 2-fold symmetry. It includes two (3 m long) experimental straight sections, two straights (2.5 m) for beams injection and RF cavity and 4 short technical straights with 4 triplets of quadrupole magnets.

The RBC at VEPP-2000 was implemented by placing in the two Interaction Regions symmetrically with respect to collision points two pairs of superconducting solenoids.

The strong solenoid focusing provides equal beta-functions of the horizontal and vertical betatron oscillations. There are two combinations of solenoid polarities ($++\ \ ++$) and ($++\ --$), that rotate the betatron oscillation plane by ± 90 degrees and give alternating horizontal orientation of the normal betatron modes. It results in equal tunes and equal radiation emittances of the betatron oscillations. But the simplest case ($+-\ \ +-$) with an additional small decompensation of solenoid fields also gives round colliding beams and satisfies the RBC requirements.

Superconducting Solenoids

Each solenoid is designed in two sections: main 13 T solenoid 50 cm in length, and 10 cm anti-solenoid (8 T). In part, the main solenoid consist of two identical units each of these has an inner coil wound with Nb_3Sn wire and an outer coil wound with NbTi wire. To feed the solenoid, we use separate power supplies for the outer and inner coils and for the anti-solenoid. All coils are embedded in the iron yoke located in a common LHe cryostat. At this stage the solenoids have been tested in an immersion cryostat and tested. After few quenches the required magnetic field 13 T was achieved.

Dipole Magnets

To achieve the designed energy of 1 GeV in the constrained VEPP-2M complex area, the magnetic field in the bending magnets of 2.4 T is required. An optimization of configuration and dimensions of the coils and the iron core yields this field level with a 10^{-3} non-uniformity in a 4×4 cm^2 gap. A power consumption per one 45 degree dipole magnet amounts to 60 kW. A special rectifier with 10 kA current and total power 1.5 MW has been developed.

Quadrupole, Sextupole, and Steering Magnets

The machine lattice includes 5 families of quadrupole magnets (max. gradient 50 T/m). Each family consists of 4

quads and has a common power supply with the current up to 300 A. The total power consumption is within 60 kW. The chromaticity of solenoid and quadrupole focusing is corrected by two families of sextupoles located in the technical straight section, in between the triplet sections, where the dispersion is high. To widen the dynamic aperture ($\geq 15\ \sigma_{x,z}$), the third sextupole family is applied in the injection and RF cavity straight sections. The closed orbit steering and gradient correction are done with 1-2% correction coils placed in the dipole and quadrupole magnets. current 2×150 mA.

BEAMS INJECTION

Electrons and positrons are injected (in turn) from the booster storage ring BEP with the maximum energy of 900 MeV[5]. The one-turn injection is done horizontally in the median plane of the ring. After a pulsed septum magnet the injected beam is focused while passing a quadrupole doublet and then kicked by a short pulse of a counter-propagating wave of a kicker plate. Two such plates are located along the inner side of the vacuum chambers in the two bending magnets adjacent to the injection drift and serve alternating as the kicker and pre-kicker by the injection of electrons or positrons. The kicker (pre-kicker) is supplied by SOS-diode generators, which produce 70 kV and 10 ns pulses.

Together with the adopted optics of the transfer line, this injection scheme gives a high injection efficiency with either combination of the SC solenoids polarities. This gives us an opportunity to test different variants of round colliding beams, and to have conventional flat colliding beams as well.

VACUUM SYSTEM

High vacuum pumping of the experimental straight sections is performed by an internal wall of the LHe vessel housing the SC solenoids. In other places combined ion-pumping and getter pumping are used to cope with gas desorption from the vacuum pipe irradiated by the synchrotron radiation. Bakeable stainless steal vacuum chamber is equipped with water-cooled radiation cooper absorbers and have to provide vacuum 10^{-6} Pa at the beam current 2×150 mA.

BEAM DIAGNOSTIC

Each vacuum chamber contains (in the middle cross section) a water cooled triangle mirror, which reflects the visible part of the synchrotron radiation from both beams. This light goes outside through a glass window to the optical diagnostic system: beam current (PMT) and beam position and dimensions measurements. CCD-cameras are used as beam position and size recorders in 16 points around the ring. In addition to optical BPMs there are 4 pick-ups in the technical straight section and one current transformer as an absolute current monitor.

RF SYSTEM

The accelerating RF cavity is placed in the drift opposite to the injection straight [6]. It operates on the 14-th revolution frequency harmonic (172.0 MHz.). The accelerating voltage of 100 kV provides a bunch length about 3 cm at the energy of 1 GeV. Energy loss for the synchrotron radiation is 50 keV per turn on the top energy. RF power delivered to the beams equals to 10 kW with colliding beams currents 2×0.1 A The so-called single mode cavity is applied, aiming a stable operation with intense bunches. A HOM damping scheme of the cavity uses two different HOM loads, one is a waveguide load and other is a coaxial load. These HOM modes are being trapped by waveguide load or are being damped in another load.

FIRST BEAM

Before commissioning of VEPP-2000 itself we had to restore the injection part of the accelerator complex. This work started in the early 2006 and was developed step by step following a readiness of corresponding control and supply systems along a chain of transfer lines and accelerators: 3 MeV linac ILU, 250 MeV synchrotron B-3M, buster storage ring BEP. This process reached the VEPP-2000 border near to the end of year.

At the first stage the optics of VEPP-2000 was simplified to the conventional option without solenoids. This "soft" optics (ν_z=1.2; ν_x=2.4) is quite different from the round beam lattice. But a part of the lattice near injection is similar to the project one. The first circulating electron beam was caught at the energy of 140 MeV and soon after at 508 MeV. At the energy of 508 MeV, which was limited at that time by the bending magnets power supply, the whole computer control, beam diagnostic, and steering coils have been tested, tuned and calibrated.

ROUND BEAM

When the beam efficiency transfer achieved 70-80 %, the vacuum chamber treatment by the synchrotron radiation was done with electron beam in both directions. Beam current, while few days training, raised up to 150 mA and the beam lifetime achieved 1000 sec. At that condition, the lifetime of low beam current (about 1mA) exceeds 10 hours.

To start the round beam operation, first of all, we had to align the cooled solenoids. It was done in the same "weak focusing" regime by the CO deviation measurements as a response to the orbit steering coils. Each section of all 4 solenoids has been tested with magnetic field level up to 4 T. So, coordinates of each i-th solenoid section center (x_i, z_i, x_i', z_i') have been obtained from the Orbit Response Matrix analysis (ORM), and necessary mechanical adjustments of the solenoids have been done. After this preliminary alignment the simplest round beam regime ($+-\ \ +-$) was applied with 1 T field in the anti-solenoid and 10 T in the nearest to IP section of the main solenoid. The round beam machine lattice for $\beta^* = 4.5$ cm is shown in Fig. 1.

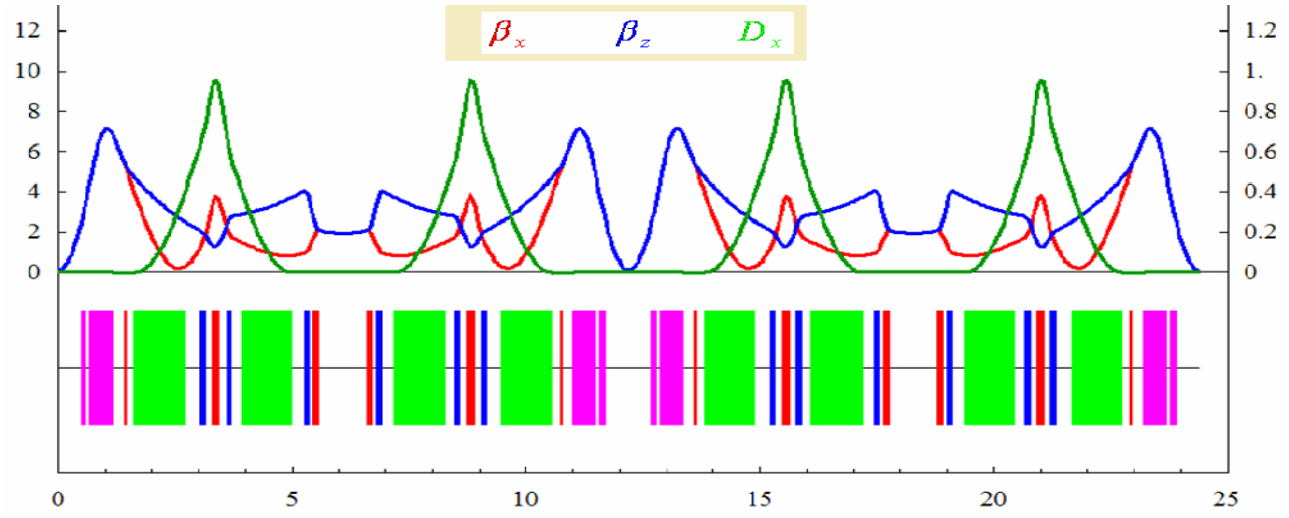

Figure 1: VEPP-2000 lattice (solenoids "on")

The electron beam was successfully injected just after the solenoids "on", with fractional tunes near a half-integer, $\Delta\nu_1 \approx \Delta\nu_2 \approx 0.5$. Later on, few steps of the CO and lattice functions corrections have been done aiming to bring the tunes near to integer. At that, the SVD method was routinely used to minimize a sum of currents in dipole steering coils and deviations in focusing strength of quadrupoles and solenoids from original symmetry. Finally, we get a regime with $\Delta\nu_1 \approx \Delta\nu_2 \approx 0.1 \div 0.15$ and moderate CO deviations ($\Delta x \approx \Delta z \leq \pm 1.5\,mm$) from the axes of quadrupole magnet.

Experimentally we measured horizontal and vertical beam dimensions of the positron beam in other positions. The Fig. 2 presents rms beam dimentions (I^+=3 mA) at three points versus the electron beam current. In point 3 located in the dipole nearest to IP, there is a minimum of β_x (see the Fig. 1). The horizontal rms size behavior at this point.

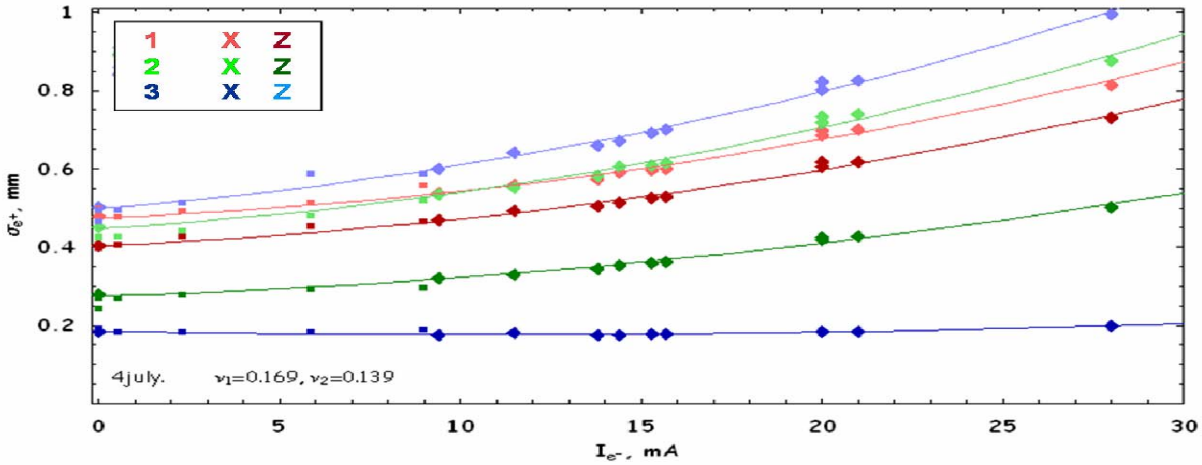

Figure 2: Positron beam rms sizes versus electron current

ROUND COLLIDING BEAM TEST

For the beginning we have studied the round colliding beams in the "weak-strong" option. The simulation of the "weak-strong" option predicts a weak dependence of the IP beam size σ_0 on the opposite beam strength. has to be similar to the IP. One can remark, that $\sigma_X(3)$ (dark blue curve) does not change in accordance with the simulation. The vertical size (light blue) grows as a result of the counter beam focusing, which increases the radiation emittance and β_z in the point 3. Such beam behavior was observed up to electron beam current I^-=50 mA, that corresponds to the space charge parameter $\xi = \frac{N r_e \beta^*}{4\pi\gamma\sigma_0^2} \quad 0.1$

After "weak-strong" option study we have increased both beam current and relatively easy have got a luminosity value $L = 1\times10^{31} cm^{-2}s^{-1}$, that exceeds in few times the luminosity record of VEPP-2M on the same energy. More demonstrative advantages of the round beam option are presented in the Fig.3, where the specific luminosities are shown versus the electron beam current for flat beams (black points - VEPP-2M data [7]) and for round beams (red curve).

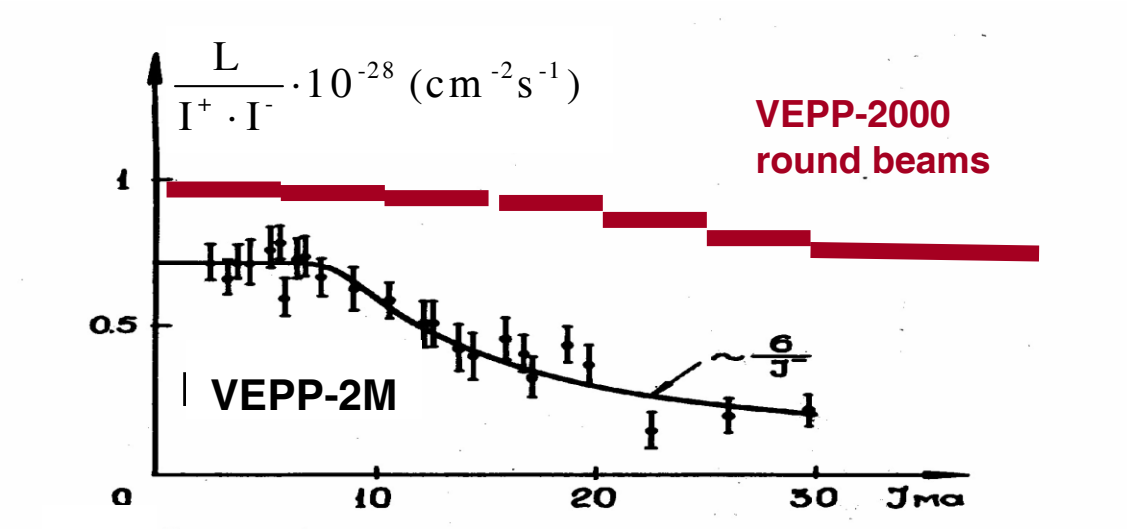

Figure 3: Specific luminosities versus electron current

CONCLUSION

The VEPP-2000 commissioning have been successfully carried out during 2007 year. Beam diagnostics calibration and vacuum conditioning have been done in the special optics without solenoids. The same regime was used for the solenoids alignment using CO offsets in recoils on each solenoid excitation.

The experimental results of the beam-beam study in the round beams mode have confirmed our expectations for the beam size behaviour in the "weak-strong" and "strong-strong" situations. In the "weak-strong" case the electron current achieves the value I^-=50 mA. It corresponds to the space charge parameter value $\xi = 0.1$ The record luminosity $L = 1\times10^{31} cm^{-2}s^{-1}$ has been achieved by the value $\xi \approx 0.08$ with beam currents $I^+ \times I^- = 35\times45\ (mA)^2$ and the life time $\tau \approx 1000\,s$. These numbers are dependent on a residual coupling and the tunes working point. We are planning to proceed with the beam-beam studies in the next run.

REFERENCES

[1] V.V.Danilov et al., in Proc of the EPAC 1996, Sitges, vol. 2, p.1149
[2] Yu.M.Shatunov at. al., in Proc. of the EPAC 2000, Vienna, p.439
[3] A.A.Valishev et al., in Proc. of the PAC 2003, Oregon, p.3398
[4] D.E.Berkaev et. al., in Proc. of the EPAC 2006, Edinburg p. 622
[5] D.E.Berkaev, et. al., in Proc. of the EPAC 2006, Edinburg, p. 628
[6] V.S.Arbuzov et al., in Proc. of Russian PAC, Dubna, (2004), p.324

COMMISSIONING OF CRAB CAVITY SYSTEM

K.Nakanishi*,K.Hara, A.Honma, K.Hosoyama, A.Kabe, Y.Kojima, H.Nakai
K.Akai, K.Ebihara, T.Furuya, S.Mitsunobu, Y.Morita, M.Ono, Y.Yamamoto
KEK, Tsukuba, Japan

Abstract

The electron positron collider KEKB is operating at KEK. At KEKB, the electron and positron bunches cross at an angle of 11 x 2 mrad. It is called finite angle collision. In this scheme, non-overlapping of the beam bunches at collision point causes beam instability. To cure this problem, the crab cavity was proposed. In the crab cavity, time varying magnetic field is applied to bunches. The field kicks the head and tail of bunches to opposite direction. And the axis of bunches are tilted. We called the motion crab motion. Effective head-on collisions can be realized using the crab motion while retaining the crossing angle. We called that crab crossing. The crab crossing is effective to boost the luminosity. According to the computer simulation, it is expected that the luminosity will be doubled with crab crossing.

The history of crab cavity was started about 20 years ago. The crab crossing scheme was proposed by R.B.Palmer for linear colliders in 1988[1]. K.Oide and K.Yokoya showed the scheme for storage rings in 1989[2]. The baseline design of crab cavity was shown by K.Akai et al in 1993 in collaboration with a Cornell university group/citeakai. In that design, the shape of cavity that was called squashed cell cavity was not axial symmetric. And it has the coaxial coupler and notch filter. R&D of the crab cavity for KEKB was started in 1994. Two crab cavities were finally installed to KEKB in 2006. The first crab crossing was realized on February@20, 2007. KEKB has been operated about one year with crab cavity. Some problems appeared and were overcome.

HARDWARE

Assembling the coaxial coupler

The cryostat for HER crab cavity was assembled first. The coaxial coupler assembling was started at the end of February 2006. A hard barrier was found soon. The coaxial coupler has two mechanical joint. To assemble them easily, the connections were designed like a single lens reflex. An installation tool that was prepared first was not sufficiently strong. It was expected that parts align by themselves, because it can move. But that is very difficult. The axis should be kept accurately. The improved installation tool is shown in figure 1. New tool was strong enough, and it can be measured the position and be adjusted well. To use the new tool, the coaxial coupler for HER crab cavity was assembled at the end of April. The HER crab cavity was opened long time. During assembling, dry and clean nitrogen gas was fed from another side of cavity. Even that, we expect that the property of the cavity was much degraded. But after RF processing, 1.8MV peak kick voltage was achieved. It is not needed to wash the cavity again. Later, The LER crab cavity was assembled smoothly.

Figure 1: The improved installation tool.

Tuner

To keep the resonance frequency constant, tuner was attached to the cavity. The coaxial coupler was moved longitudinally by tuner. The tuner is driven by a motor and a piezo stack. The tuner driven by motor that called motor tuner can move widely. But it is not suited for fine motion. The piezo stack is suited for fine motion. But the stroke of the element is only 0.2mm.

The properties of motor tuners are shown in figure 2. They are almost same, but the hysteresis of LER tuner is larger than HER's. The properties of tuner driven by piezo stacks that is called piezo tuner are shown in figure 3. The hysteresis width of LER is comparable with the piezo tuner stroke. In this situation, the piezo tuner for LER can not work to make fine tuning. And the piezo tuner for LER has one more problem. Each strokes of LER piezo tuner are not monotone function. To start decrease the frequency, the frequency should be increased once. This property make big frequency fluctuation. In practice, wide distribution of tuner phase is observed (figure 4). This fluctuation is suppressed by low level RF control system (LLRF). The phase distribution improved by LLRF is shown in figure 5. The LER phase distribution is improved from 9.5˚to 0.046˚

These tuners have another purpose. If the tip of coaxial coupler is moved horizontally, operation frequency RF can propagate coaxial coupler to HOM dumper as TEM mode.

* kota.nakanishi@kek.jp

To avoid the situation, the position of coaxial coupler can be adjusted by another motor that is called sub tuner. That function works well.

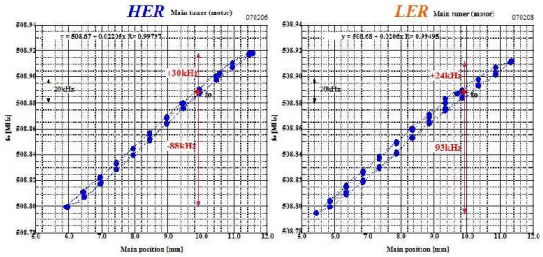

Figure 2: Properties of motor tuner.

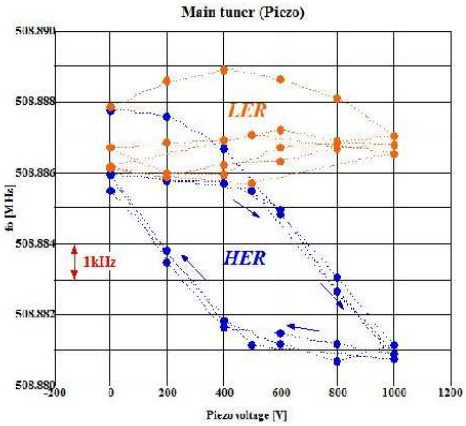

Figure 3: Properties of piezo tuner.

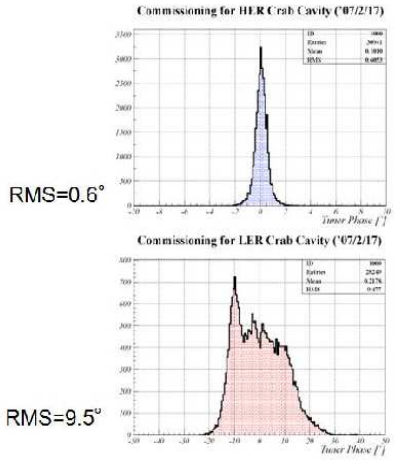

Figure 4: Response of resonance frequency of cavity for piezo voltage.

Ice balls

Boiled He gas returns to refrigerator through isolation pipe. To cool down the coaxial coupler, Liquid He was

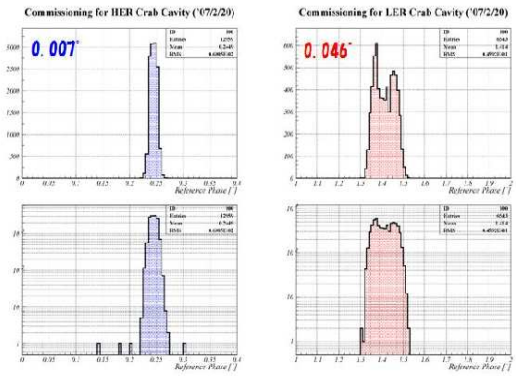

Figure 5: Response of resonance frequency of cavity for piezo voltage.

taken from He vessel. That gas return to suction of compressor through the normal (not isolated) pipe. Because the amount of He flow was expected very small (less than $10m^3/h$). Because only tip is exposed to high magnetic field, liquid He is supplied to tip of coaxial coupler. But the temperature of the tip of coaxial coupler is not measured. The temperature of the He outlet of coaxial coupler is measured. If outlet temperature is kept 4.2K, the tip of coaxial coupler can be kept 4.2K. It may be excessive. Now ice balls stick the He return pipe. They should be improved.

OPERATION

Instability in high current operation

In the high-current crab-crossing operation, we encountered a large-amplitude oscillation of beams and the crabbing field caused by the beam loading on crab cavities together with the beam-beam force at the IP[4]. We found that the oscillation can be avoided by shifting the crabbing phase, shifting the tuning offset angle, and adjusting the loop gain appropriately. Shifting the crabbing phase make actual beam kick. It is compensated by DC magnets.

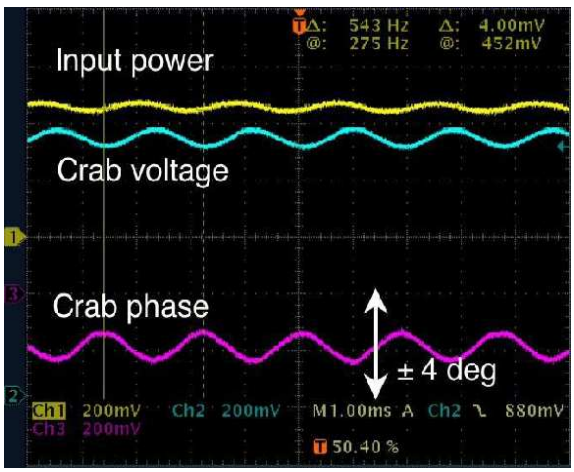

Figure 6: Instability in high current operation.

RF trip

The history of RF trip rate is shown in figure 7. KEKB operation with crab cavities was started in February 2007. Figure 7 is included data from February 2007 to March 2008. RF trip rate is looks influenced by operation condition namely kick voltage and beam current. The history of kick voltage and beam current is shown in figure 8. In November 2007, the LER kick voltage was set to 0.95MV. This kick voltage is much higher than before. The trip rate of LER is increased quickly, and KEKB parameter was changed to decrease the required LER kick voltage.

In almost case, degraded cavity's property can be recovered by a few hours aging effort. But big quench was occurred on March 17, 2007. The reachable kick voltage of LER crab cavity decrease from 1.36MV to 0.98MV. To cure this trouble, aging was done. But it was not recovered. Crab cavities were warmed up to 80K. After that, the reachable kick voltage was increased to 1.1MV The reachable kick voltage was gradually increased to 1.14MV by steady aging effort.

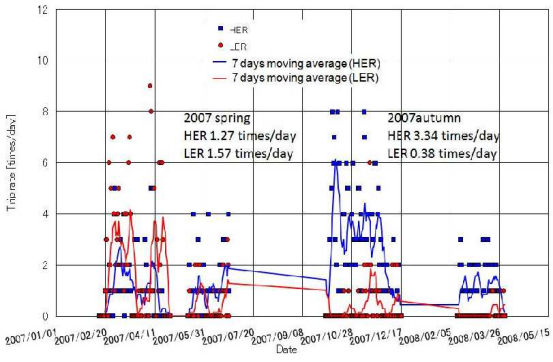

Figure 7: History of RF trip rate.

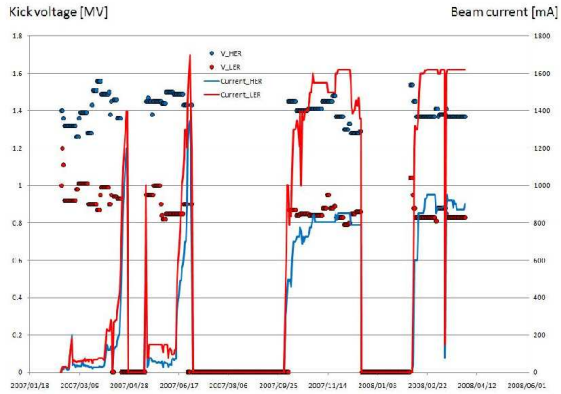

Figure 8: History of kick voltage of crab cavities and maximum beam current.

The luminosity

Specific luminosity of KEKB is shown in figure 9. The light blue line was shown the specific luminosity without crab cavities. At least, in low current operation, the specific luminosity was doubled by crab crossing. The detail of commissioning efforts may be introduced in other presentation.

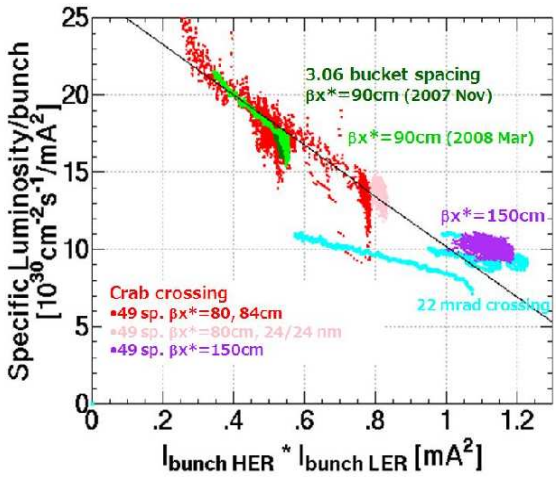

Figure 9: Specific luminosity versus product of bunch current.

SUMMARY

Two crab cavities were installed to KEKB. Crab cavities made kick voltage more than 1.8 MV at KEKB, at least they were new. The luminosity was increased at low bunch current operation with crab cavity. The peak luminosity reached to 15.1/nb/sec with crab cavities. The record of luminosity is 17.1/nb/sec without crab cavity. The tuner for LER crab cavity has big fluctuation. It is compensated by low level RF control system. At high current operation, RF instability was observed. It is suppressed by adjusting crabbing phase, tuning offset and feedback loop gain.

REFERENCES

[1] R.B.Palmer, SLAC-PUB-4707 (1988).

[2] K.Oide and K.Yokoya, Phy rev. A40, 315 (1989).

[3] K.Akai et al, Proc.IEEE Part. Accel. Conf., 757 (1993).

[4] K.Akai, Proc. of the 13th Workshop on RF Superconductivity (2007).

BEAM-BEAM EFFECTS AT CRAB CROSSING IN KEKB - I

K. Ohmi for KEKB commissioning group, KEK, Tsukuba, Japan

Abstract

In KEKB, collision with crab crossing has been examined since February 2007. The luminosity is still lower than the target. The status and studies why the luminosity is low are reported.

INTRODUCTION

In KEKB, crab crossing had constructed to boost-up the luminosity performance. The crab cavity is considered to work to increase the luminosity twice. Betatron resonances excited by odd order terms of the dynamic variable is eliminated by the symmetry in the head-on collision, and horizontal motion is integrable for the operating point close to the half integer.

Figure 1 shows the comparison of the specific luminosity measured and simulated in KEKB. Large blue and black dots show the specific luminosity given by the strong-strong simulation for the head-on collision and the crossing collision with 11 mrad, respectively. Light blue dots are measured luminosity for the crossing collision. Red and other (yellow, violet, light green) dots are measured luminosity for crab crossing collision in several operating conditions. The specific luminosity is as high as that given by simulation for the head-on collision for low current I^2=0.3 mA^2, but degrades at high current I^2=0.9 mA^2. The current product can be achieved I^2=1.25 mA^2 in the crossing collision, while 0.9 mA^2 for the crab crossing due to a short lifetime. The figure show that the measured luminosity distribute a line L_{sp}=27-17I^2. When horizontal emittance is changed, another line is drawn. The offset and gradient are high and steep for small horizontal. The light blue line is similar as a line with an emittance $\beta_x\varepsilon_x = \sigma_x{}^2+(\theta\sigma_z)^2$. Now it seems to face a beam-beam limit independent of the collision scheme.

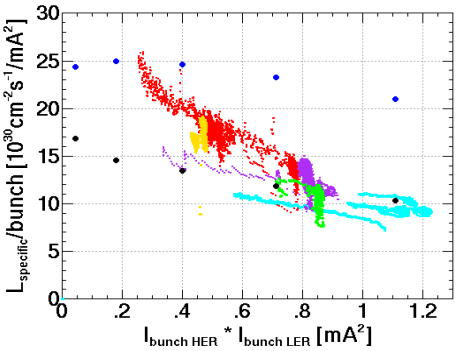

Figure 1: Specific luminosity as a function of the current product.

There are many mechanisms to cause degradation of the luminosity performance. The mechanisms, which we recognize, are summarized as follows,

1. Linear coupling at IP
2. Beam-beam halo
3. Touschek life couple to beam-beam
4. Nonlinearity of lattice
5. Fast noise
6. Wake force acting crabbing beam

We discuss 1-4 in this paper. 5-th mechanism has been discussed in [1,2]. 6-the, which will be discussed elsewhere, was not more serious than the strong head-tail instability for non-crabbing beam.

SIMULATION OF KNOB SCAN

Luminosity degradation due to linear coupling at IP has been discussed, since early stage of KEKB [3]. The effect of linear coupling had studied one by one in simulations. There are 12 coupling parameters, 4 for each of xy xz and yz. Actually, the coupling parameters are mixed complex in accelerators. In KEKB, the linear coupling parameters at the collision point are used as knobs for luminosity tuning. The knobs are scanned and optimized day by day. We simulate the knob scan process using a strong-strong beam-beam code, named BBSS [4]. The knobs in each ring are consists of four parameters related to the x-y coupling and two of vertical dispersion and its prime. Horizontal dispersion and vertical tilt in yz plane are recently taken into account in the machine operation, but are not discussed here. The waist position of the vertical beta function is also used as a knob, but is less frequently changed. Here we discuss the tuning using the 12 knobs with following beam parameters,

- Beam current 0.8/1.4 mA/bunch (HER/LER)
- ε_x = 24/18 nm (HER/LER) 1% coupling
- $\beta_{x/y}$ = 80/0.7 cm (both)
- $\nu_{x/y/z}$ = 0.511/0.580/0.025

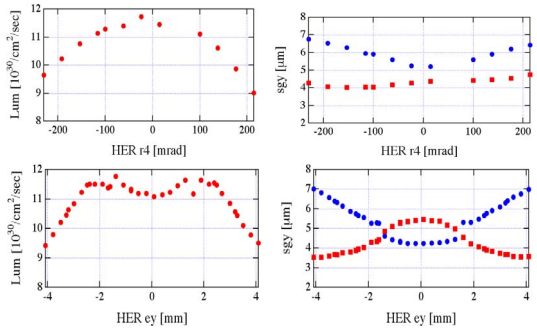

Figure 2 Examples of knob scan. Top plots are luminosity and beam sizes for HER R4. Bottom plots are those for HER ηy.

R1 and R4 are rotation of real and momentum space, respectively. The condition, R1(L)=R4(L)=R1(H)=R4(H) and others=0, in which both beam rotate an equal angle, therefore luminosity should not degrade under the condition. The simulation realizes that the one of R's is

chosen arbitrary, and found a solution except for the ambiguity of R1-R4.

The knob scan was iterated several times. In first iteration, several parameters are misled due to complex of errors in many parameters. After the second and third iterations, most of parameters go to zero, except for R1 and R2, with the result that a high luminosity > $2x10^{34}$ $cm^{-2}s^{-1}$ was achieved in the simulation.

Down hill simplex method for the 12 parameters is also used to optimize the luminosity. A simplex optimization with 4 parameters was tried after the first knobs scan. Details are published in EPAC08 [5].

BEAM LIFE TIME SIMULATION

Beam lifetime limits to operate high bunch current in present KEKB. It is shortened for increasing bunch current. The behavior is quite strange. The lifetime is asymmetry for the horizontal offset of colliding beam: that is, when positron beam is outside of ring for electron beam, both beams have shorter lifetime than opposite case. The vertical emittance of one beam is controlled by dispersion of arc section in the ring to reduce the beam-beam effect of another beam. When one beam is enlarged by the dispersion, the other beam is expected to be shrunk and to have longer lifetime. However though the other beam is shrunk somewhat, lifetime is not helped by the vertical size of colliding beam.

We first try the lifetime evaluation with a simple model, in which arc transformation is represented by a matrix transformation. Figure 3 shows beam particle distributions for 4 cases: no beam-beam, head-on, head-on with an offset and crossing collision, where H-axis 0-12.8σ_x (0.1σ_x/unit) V-axis 0-64σ_y (0.5σ_y/unit). They are depicted by contour plot with log scale. In every cases, the hor. and ver. halo do not matter for the operation, because of our aperture limit of 20-30σ_x and 80σ_y. A vertical halo is formed by a horizontal offset of collision as seen in the bottom left plot. Halo is bigger in finite crossing angle collision compare than crab crossing as seen in the bottom right plot.

Figure 4 shows the beam distributions for various vertical emittances of the target beam, ε_y=0.6x10^{-10}, 1.8x10^{-10} and 5.4x10^{-10} m. Vertical beam size and halo is smaller for higher vertical emittance of the target beam, while those of horizontal are independent of the vertical emittance of the target beam. The simulation behaviour is quite reasonable, but inconsistent with experiments in KEKB. The experiments showed that the vertical emittance control does not work the beam lifetime.

Similar simulations were carried out with including lattice nonlinearity with a code used in the latter section (SAD including 3D weak-strong beam-beam module). The results did not show remarkable difference from this simple arc model.

This type of halo did not seem to affect the beam lifetime of present KEKB.

The halo simulation did not give any asymmetry of beam lifetime. Smaller beam size gives short lifetime, namely, like the intra-beam effect [6].

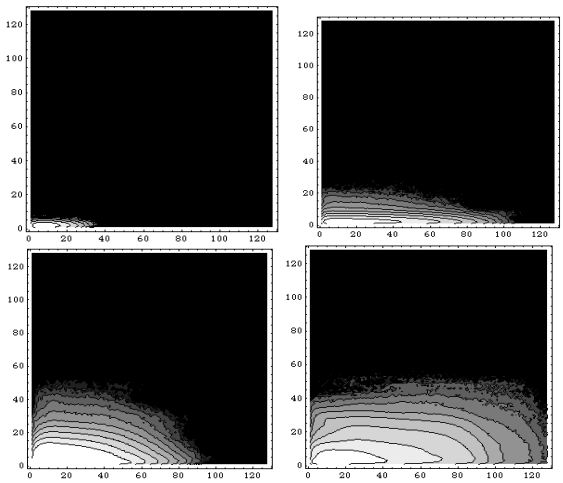

Figure 3 Beam particle distributions in the amplitude space ($J_x^{1/2}$,$J_y^{1/2}$,). Full ranges of the horizontal and vertical axes are 0-12.8σ_x and 0-64σ_y, respectively. Top left picture is given for no beam-beam interaction, Top right is for head-on collision, bottom left is for head-on but 50 μm offset (~0.5 σ_x), and bottom right is for a finite crossing collision with 11 mrad.

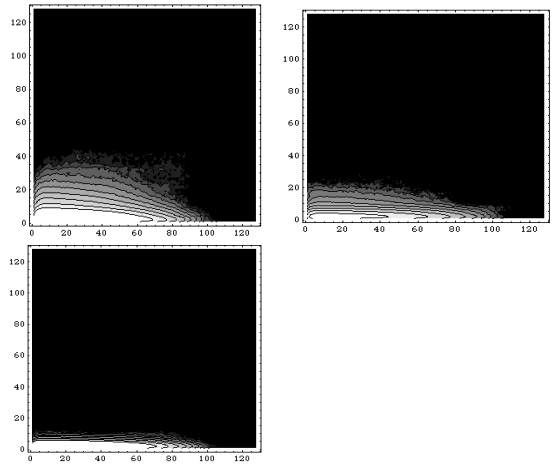

Figure 4 beam particles distributions for colliding beam with vertical emittances, ε_y=0.6x10^{-10}(top left), 1.8x10^{-10} (top right) and 5.4x10^{-10} m (bottom left).

TOUSCHEK LIFE TIME UNDER THE BEAM-BEAM INTERACTION

Touschek lifetime coupled to beam-beam effect is discussed. The cross section of the intra-beam scattering is expressed as follows,

$$\frac{d\sigma}{d\Omega} = \frac{4r_e^2}{\gamma^2 p_\perp^4}\left|\frac{4}{(1-\sin^2\theta\cos^2\varphi)^2} - \frac{3}{1-\sin^2\theta\cos^2\varphi}\right| \quad (1)$$

Touschek lifetime is given as

$$\frac{1}{\tau} = 2N \int d\Omega \int d\mathbf{x}_1 \int d\mathbf{x}_2 A(\mathbf{x}_1, \mathbf{x}_2, \theta, \varphi) \frac{d\sigma}{d\Omega} v_\perp \psi(\mathbf{x}_1)\psi(\mathbf{x}_2) \quad (2)$$

where the distribution function is normalized by

$$\int d\mathbf{x}\, \psi(\mathbf{x}) = 1 .$$

$A(\mathbf{x}_1, \mathbf{x}_2, \theta, \phi)$ characterizes whether two particles ($\mathbf{x}_1$, $\mathbf{x}_2$) kicked by a large angle θ, ϕ due to intra-beam scattering survive or not.

The integration in Eq. (2) is performed by Monte Carlo method. An equilibrium distribution is obtained under the beam-beam interaction at first.

$$\rho_p(\mathbf{p}) = \sum_{i=1}^{n} \delta(\mathbf{p} - \mathbf{p}_i) \quad (3)$$

$\Delta\delta$ is applied so that Eq. (1) is satisfied. Here Monte Carlo integration (summation) is taken with the weight in Eq.(1) for an uniform distribution of $\Delta\delta < \delta_{bucket}$.

$$\frac{1}{\tau} = \frac{32N\pi c r_e^2}{\gamma^3 V} \frac{\Delta\delta_{bucket}}{n} \sum_{i=1}^{n} A(p_{\perp,i}, \Delta\delta_i) \frac{1}{p_{\perp,i}^4} \left[\frac{2\gamma^3 p_{\perp,i}^3}{\Delta\delta_i^3} - \frac{\gamma p_{\perp,i}}{\Delta\delta_i} \right] \quad (4)$$

The particle distribution and A was evaluated by SAD code including a weak-strong beam-beam module. Tracking with several 1000 revolutions forms an equilibrium macro-particle distribution. Intra-beam kicks (p, $\Delta\delta$) are applied randomly for every macro-particles and A(p, $\Delta\delta$) of them, which characterize inside or outside of aperture, are evaluated. Taking the summation, the lifetime integral is evaluated.

The simulation gives a short lifetime in LER, ~53 min, while a longer lifetime for HER, ~297 min. HER seems to have a sufficient lifetime.

The lifetime issue is still mysterious in KEKB.

LUMINOSITY SIMULATION INCLUDING LATTICE NONLINEARITY

Lattice nonlinearity may affect luminosity performance. Several signs in which nonlinearity affects luminosity have been observed in KEKB.

1. Existence of Golden orbit
2. Luminosity performance depended on something run by run, even though IP parameters were tuned hardly.
3. Integer part of tune affected the luminosity performance.
4. Beta distortion in wiggler section made worse the luminosity.

Errors in transverse positions of sextupoles are generated and induced linear coupling and dispersion at IP are corrected. The vertical emittance is chosen to be 1% coupling. Using the lattice, beam-beam tracking is performed. A 3D weak-strong beam-beam module is implemented in SAD.

Figure 5 shows the specific luminosity given by the simulation. Lattice nonlinearity does not affect strongly. Three blue lines, are seen in the figure, correspond to the specific luminosities for head-on and crossing collision given by the strong-strong simulation code (BBSS), and measured specific luminosity fitted in Figure 1. Errors degrade the luminosity performance, but the coupling correction at IP renovates it.

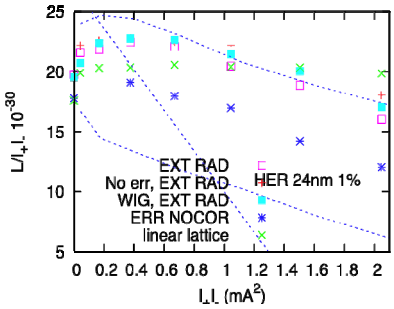

Figure 5: Specific luminosity given by a weak-strong simulation including lattice nonlinearity.

ACHIEVED BEAM-BEAM PARAMETER OF E+E- COLLIDERS

Achieved beam-beam parameters of e+e- machines in the world are listed in Table 1. Parameters for DAFNE and BEPC-II are tentative, because the calibration of the luminosity monitors is in progress [7,8]. Here the beam-beam parameter is defined as a normalized luminosity as follows,

$$\xi_N = \frac{2 r_e \beta L}{\gamma N f} . \quad (5)$$

KEKB achieved 0.057 for crab crossing, while 0.043 for crossing collision. The beam-beam parameter for crab crossing is higher than that of crossing collision. However the luminosity is lower than that of crossing collision, because the current product is limited by a short lifetime.

SUMMARY

Simulations have not given to explain the bad luminosity performance at KEKB yet.

It is not clear whether the luminosity and lifetime issues are caused by an origin or independent two origins. At least, lifetime limits the bunch current product. However even a lower current product, higher luminosity is predicted.

New knobs for correction of lattice nonlinearity may be necessary, though present simulation results showed “no” now.

REFERENCES

[1] J. Augustin, Orsay Report No. 36-69 (1969).
[2] K. Hirata, Phys. Rev. Lett. 74, 2228 (1995).
[3] K. Ohmi, M. Tawada, Procedings of PAC2003.
K. Ohmi, Proceedings of e+e- Factories 1999.

[4] K. Ohmi, Phys. Rev. E62, 7287 (2000).
[5] Tawada et al., to be published in proceedings of EPAC08.
[6] K. Oide, Y. Ohnishi, private communications.
[7] P. Raimondi et al., private communications.
[8] Q. Qin et al., private communications.

Table 1: Beam-beam parameters for e+e- colliders (April 2008). KEKB-1 and 2 are for crossing collision and crab collision, respectively. DAFNE-1 and 2 are before 2007 and after 2008.

	KEKB-1	KEKB-2	DAFNE-1	DAFNE-2	BEPC-II	CESR	VEPP2K	PEP-II
C (m)	3016	3016	97	97	240	768	24.4	2200
N_{bunch}	1388	1584	110	80	90	45	1	1722
E (GeV)	3.5/8	3.5/8	0.51	0.51	1.89	5.3	0.51	3.1/9
I (A)	1.66/1.2	1.6/0.9	1.1/1.5	0.9/1.2	0.5	0.35	0.04	2.9/1.9
ε_x (nm)	18/24	18/24	340	250	144	205	47	27/50
ε_y (nm)	0.18/0.24	0.18/0.24	1.7	1.25	1.44	0.205	47	0.38/1.3
β_x(cm)	55	90	170	23.4	100	94	5	40
β_y(cm)	0.6	0.6	1.7	0.9	1.5	1.8	5	0.97
τ/T_0	4000	4000	1.1e5	1.1e5	3.2e4	9000		1e4/0.5e4
L (mes.)	1.71e34	1.5e34	1.5e32	2e32	1e32	1.25e33	1e31	1.2e34
ξ_N	0.043	0.057	0.015	0.014	0.0073	0.056	0.057	0.036

COLLECTIVE BEAM-BEAM INSTABILITIES OF BUNCHES WITH TUNESPREADS

D.V. Pestrikov, Budker Institute of Nuclear Physics, 630090 Novosibirsk, Russian Federation

Abstract

We discuss effects of Landau damping on the stability of coherent oscillations of short identical colliding bunches. Near the sum-type resonances $n/(2m)$, where n and m are integers, these oscillations are unstable. Comparing the stopbands calculated for monochromatic and non-monochromatic bunches, we have found that the beam-beam tunespreads increase the widths of the stopbands of coherent modes thus, resulting in Landau anti-damping of coherent beam-beam oscillations. The tunesperads due to octupole fields do not eliminate Landau anti-damping.

INTRODUCTION

Periodic perturbations of the particle oscillations at the interaction point (IP) of a collider by space charge forces of the counter-moving colliding bunches result in numerous resonant instabilities which can limit the operational performance of the collider. In particular, such beam-beam perturbations can result in the resonant instabilities of coherent oscillations of the colliding bunches. In the simplest case, if $\nu_{1,2}$ are the tunes of the betatron oscillations of particles in the colliding bunches 1 and 2, coherent oscillations of these bunches become unstable provided that the oscillation tunes approach the sum-type resonance region [1] $m_1\nu_1 + m_2\nu_2 = n$. Here, $m_{1,2}$ and n are positive integers. Nonlinear dependencies of the beam-beam forces on particle coordinates in the bunches produce the tuneshifts and the tunespreads of the particle oscillations. Therefore, some Landau damping of unstable modes could be expected. However, a qualitative study made in Ref.[2] has shown that the beam-beam tunespread is not sufficient to suppress the beam-beam coherent instability and that near the resonant tunes still can exist unstable coherent beam-beam modes. Using a different approach, this result was confirmed numerically for the beam-beam π–modes in Ref.[3].

Descriptions of such instabilities are usually complicated by a generic self-consistency of the beam-beam interactions. We simplify calculations of Landau damping effects of self-consistent coherent oscillations of short identical colliding bunches using the model described in Refs.[1, 2, 3], or in Ref.[4]. Using the technique developed in Refs.[5] and [6], we calculate the stopbands for coherent oscillations of colliding bunches taking into account and/or ignoring the beam-beam and others tunespreads. For the last case, we call colliding bunches as the monochromatic ones. Comparing results of such calculations, we find out that Landau damping due to the nonlinearity of the beam-beam forces, generally, increases the widths of the stopbands of coherent beam-beam modes. It also can change positions of the stopbands of unstable modes relative to the values of the resonant tunes. These features mean that together with the damping of unstable modes of the monochromatic colliding bunches the tunespreads result in the instabilities for the regions of tunes where the modes of the monochromatic bunches were stable – i.e. in the Landau anti-damping. Such an anti-damping is a specific feature for resonant instabilities of coherent oscillations near the sum-type coupling resonances [7].

THE MODEL

We consider collisions of two identical short counter-moving relativistic electron and positron bunches, which move in separate storage rings and interact head-on at a single interaction point (IP). In our calculations we assume a zero dispersion function at the IP. Incoherent e.g. the horizontal oscillations of particles in the bunches are described using $x = \sqrt{J\beta}\cos\psi$ and $p_x = px'/R_0 = -p\sqrt{J/\beta}\sin\psi$. Here, $I = pJ/2$ and ψ ($\psi(\theta + 2\pi) = \psi(\theta) + 2\pi\nu_x$) are the action-phase variables of the unperturbed incoherent oscillations, $\Pi = 2\pi R_0$ is the perimeter of the closed orbit, $s = R_0\theta$ is the path along the closed orbit, primes mean $d/d\theta$, $p = \gamma Mc$ is the value of the momentum of the reference particle, β denotes the value of the β-functions of the horizontal oscillations at the center of IP.

Coherent oscillations of bunches are described using harmonics of their distribution functions f in phases ψ. We use a special model, where the bunches have very flat unperturbed distribution functions so that $f^{(1,2)}(I_y, x, \psi, \theta) = \delta(I_y)f^{(1,2)}(x, \psi, \theta)$,

$$f^{(1,2)}(x, \psi, \theta) = \frac{e^{-x}}{p\epsilon} + \sum_{m=-\infty}^{\infty} f_m^{(1,2)}(x, \theta)e^{im\psi}, \quad (1)$$

(y marks the values relating to the vertical oscillations, $I = xp\epsilon$, ϵ is the horizontal bunch emittance) and where the bunches execute coherent oscillations only in the horizontal plane. Assuming also that the bunches move in the rings with identical lattices, $p\epsilon|f_m^{(1,2)}| \ll 1$, and neglecting in the linearized Vlasov equations for $f_m^{(1,2)}$ the fast-oscillating terms, we find that the combinations

$$\begin{aligned} f_m^{(\pm)} &= f_m^{(1)} \pm f_m^{(2)} \\ &= e^{-x}p_m^{(\pm)}(x)\frac{x^{m/2}}{i^m}\sum_{n=-\infty}^{\infty}\frac{e^{-i(\nu+n)\theta}}{\nu + n - m\nu_x(x)} \end{aligned}$$

describe normal modes of identical colliding bunches [8]. Since the functions $f_m^{(1,2)}$ are linear combinations of the

modes $f_m^{(\pm)}$, coherent oscillations of identical colliding bunches are stable only in the regions, where both modes $f_m^{(+)}$ and $f_m^{(-)}$ are stable. For small values of the beam-beam parameter $\xi = Ne^2/(2\pi pc\epsilon)$ (e.g. $B = 2\pi\xi < 1$) and near the resonances $\nu_x = n/(2m)$, we can neglect in equations for $f_m^{(\pm)}$ the contributions of non-diagonal in $|m|$ modes. Resulting equations for $p_m^{(\pm)}(z_1, x)$ read (more details in Ref.[6], $m > 0$)

$$\frac{d}{dx}\left(x^{m+1}\frac{dp_m^{(\pm)}(x)}{dx}\right) = \pm e^{-x}x^m V(x)\, p_m^{(\pm)}(x). \quad (2)$$

These equations should be solved with the boundary conditions $p_m^{(\pm)}(z_1, 0) = 1$, and $dp_m^{(\pm)}(z_1, 0)/dx = \pm V(0)/(m+1)$. The dispersion equations of the problem read

$$p_m^{(\pm)}(z_1, \infty) = 0. \quad (3)$$

Here, $V(x) = 2\delta(x)/(z_1^2 - \delta^2(x))$ ($\mathrm{Im} z_1 > 0$), and

$$z_1 = \frac{1}{m\xi}\left(\nu - \frac{n}{2}\right),\ \delta(x) = \frac{1}{\xi}\left(\nu_x(x) - \frac{n}{2m}\right), \quad (4)$$

n is the azimuthal number of the resonance harmonic.

RESULTS

Near the resonances $\nu_x \simeq n/(2m)$ Eqs.(2) and (3) always have solutions with the eigenvalues $\mathrm{Re}(z_1) = 0$ and $\mathrm{Im}(z_1) \neq 0$ [2]. Since $p_m^{(\pm)}(z_1, \infty)$ are functions of z_1^2, these solutions describe unstable modes. The values of the increments of unstable modes as well as the widths of relevant stopbands and their positions in ν_x are found solving Eqs.(2) and (3) numerically. In these calculations we also took into account self-consistent variations of the oscillation tunes and of β-functions by the beam-beam interactions: $\cos\mu_0 = \cos\mu_x + B\sin\mu_x$, $\beta\sin\mu_x = \beta_0\sin\mu_0$, where $\mu = 2\pi\nu$, the subscript 0 marks bare values. Below, we neglect possible flip-flop spitting of the betatron functions. Using simulations, we have found that in our model the tunes depend on x according to

$$\nu_x(x) = \nu_x - \Delta\nu_x(0)\left(1 - \frac{1 - e^{-x}}{x}\right), \quad (5)$$

where $\Delta\nu_x(0) = \nu_x - \nu_0$ is the linear beam-beam tuneshift (e.g. in Fig. 1) Calculating increments for the modes $(\pm)$ with $1 \le m \le 5$ and $1 \le n \le 4$, we find the stopband depicted in Fig. 2. Although only the segment $0 \le \nu_x \le 1/2$ is shown in Fig. 2, the stopbands for higher, or lower values of ν_x appear periodically with a period in ν_x of $1/2$. For dipole oscillations $m = 1$ we have found no roots of the dispersion equation (3) for $0 \le \nu_x \le 1/2$. This result means that only $(-)$ dipole mode has the stopband below the resonance $\nu_x = 1/2$. The stopband for the mode $(-, 2)$ starts slightly below the resonance $\nu_x = 1/4$. The lower ends of all other found stopbands are found to be close to the corresponding resonant tunes $\nu_x = n/(2m)$. Numerical values of the maximum increments and of the widths

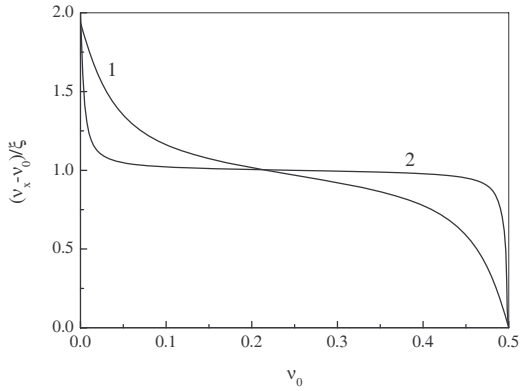

Figure 1: Dependence of the linear beam-beam tune shift on the bare tune (ν_0); line 1 – $\xi = 0.05$, line 2 – $\xi = 0.005$.

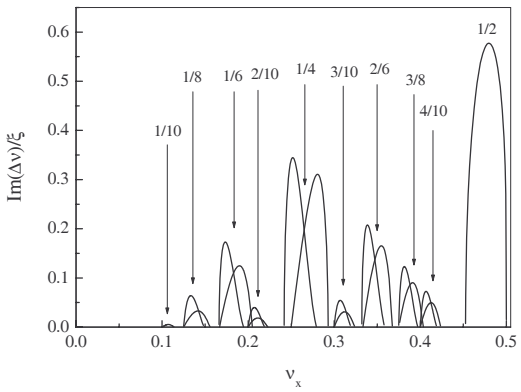

Figure 2: Dependencies of the increments of the coherent beam-beam modes on the tune of the horizontal incoherent betatron oscillations (ν_x). Modes $1 \le m \le 5$, arrows show positions of stopbands near particular resonances, wider curves to the right from the resonances $\nu_x = n/(2m)$ depict the increments of the modes $(+)$, $\xi = 0.05$.

of the stopbands for modes $(-)$ and $1 \le m \le 3$ in Fig. 2 are in general agreement with similar results reported in Ref.[3] and obtained using a different approach. We note that the values of the maximum increments for the modes $m \ge 3$ are a bit smaller in the region $\nu_x < 1/4$ than that above $\nu_x = 1/4$. The maximum increments of the modes near the resonances $\nu_x = 1/(2m)$ tend to zero, when ν_x approaches the border value

$$(\nu_x)_{\min} = \frac{1}{2\pi}\arccos\frac{1 - B^2}{1 + B^2}. \quad (6)$$

This fact is in a general agreement with experimental observations of the beam-beam instabilities in the electron-positron colliders. Although it is not shown here, a decrease in ξ results in decreases in the values of the mode increments ($\mathrm{Im}\nu$) and in the narrowing of the widths of the stopbands in ν_x. However, the ratios $\mathrm{Im}\nu/\xi$ and of these widths to ξ remain the same.

Outside the spectrum of incoherent oscillations (e.g. $z_1^2 > \delta^2(0)$) Eqs.(2) and (3) may have solutions with

$\mathrm{Re}(z_1) \neq 0$ and $\mathrm{Im}(z_1) = 0$. To avoid the mode interference, coherent tuneshifts of such stable solutions should not enter the stopbands of unstable modes.

To figure out effects of Landau damping on the stability of coherent beam-beam oscillations we compared the stopbands calculated for monochromatic and non-monochromatic bunches. For monochromatic bunches the roots of the dispersion equations corresponding to the largest increments are calculated using ([6]) $z_1^2 = \delta^2 \pm 2\Lambda_m\delta$, where the sign $+$ is taken for the modes $(-)$ and

$$\Lambda_m = \frac{4}{m\,(m+2)}\,\frac{1}{\left(1+\frac{1}{m+1}\right)^{m+1}}. \qquad (7)$$

For the dipole mode $(-)$ Landau damping results only in minor changes of the stopband of the monochromatic bunches (Fig. 3). The maximum values of the increments almost coincide, Landau damping suppress the instability within a narrow band A′A and decreases the oscillation increments within the segment AB. Within the segment BC the beam-beam tunespread slightly increases the increments of unstable modes hence, resulting in some Landau anti-damping. Stronger Landau anti-damping indicate the stopbands of the modes with higher betatron multipole numbers ($m \geq 2$, e.g. in Fig. 4 and 5). For such modes, the beam-beam tunespread although decreases the values of the maximum increments, moves the lower border of the stopbands of the modes $(-)$ towards the resonant tune $n/(2m)$ and substantially increases the widths of the stopbands. Except for the case $m = 2$, the stopbands of the multipole modes $(\pm)$ are placed above the resonant tunes almost entirely. Hence, the beam-beam tunespread suppressing the modes of the monochromatic colliding bunches opens new wide regions of the tunes ν_x where the oscillations become unstable. The described Landau anti-damping of the coherent oscillations of the colliding bunches is a generic phenomenon for the coherent beam-beam interactions. These instabilities occur due to the coupling of the modes m and $-m$ near the sum-type resonance $m(\nu_x^{(1)}+\nu_x^{(2)}) = 2m\nu_x = n$. According to general properties of such instabilities [7] any damping can stabilize coupled coherent modes only in the case, when both coupled modes are damped sufficiently strongly. Otherwise, the oscillations become unstable.

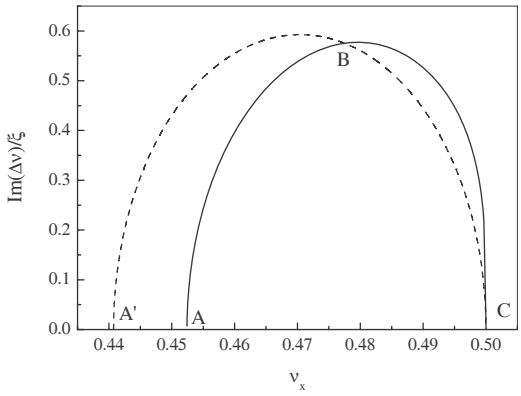

Figure 3: Dependence of the increment of the dipole mode $(-)$ on the tune of the horizontal incoherent oscillations ν_x. Solid line – Landau damped coherent oscillations, dashed line – monochromatic bunches, $\xi = 0.05$.

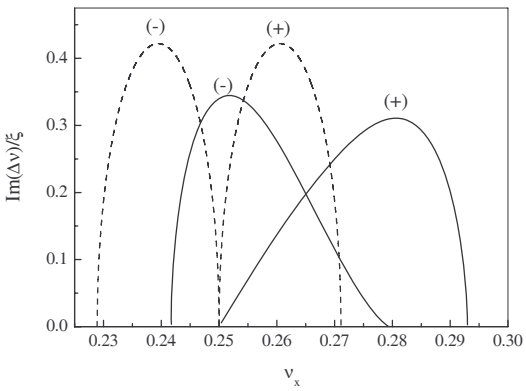

Figure 4: The stopbands of coherent oscillations near the resonance $1/4$. Solid line – Landau damped coherent oscillations, dashed line – monochromatic bunches, the symbols $(\pm)$ mark the curves for modes $(\pm)$, $\xi = 0.05$.

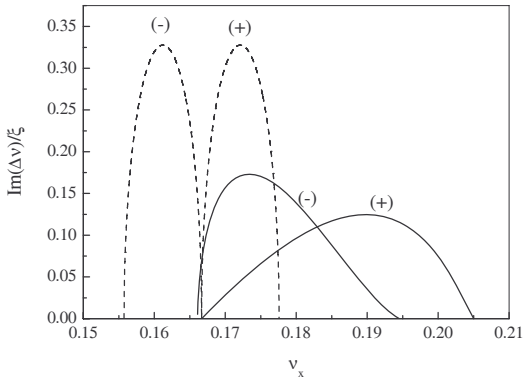

Figure 5: Same as in Fig. 4, but near the resonance $1/6$.

Replacing ν_x by $\nu_x + ax$, we can also inspect some effects of the octupole lattice non-linearity on the stability of coherent beam-beam oscillations. According to data depicted in Figs. 6 and 7, the octupole fields do not cancel the described Landau anti-damping. However, it can decrease the strength of the instability provided that the sign of the non-linearity is correct.

Additional suppression of the strength of the coherent beam-beam instability can occur in collisions of long bunches due to hour-glass effect [9]. In the simplest case and provided that the disruption parameter of the bunches $4\pi\xi\sigma_s/\beta$ is small, the stopbands of the betatron modes of the bunches with the lengths σ_s comparable to β can be calculated using Eqs.(2) and (3) after a reduction in Eq.(2) of the function $V(x)$ by the suppressing factor times. According to data depicted in Fig. 8, the hour-glass suppres-

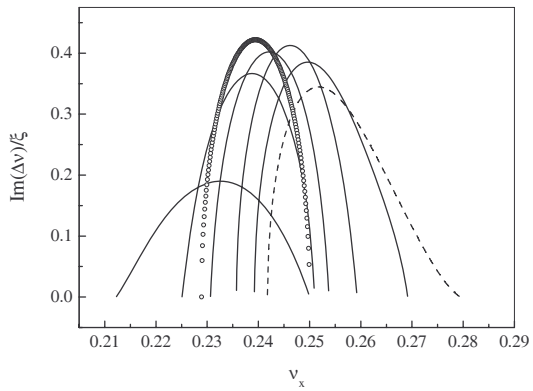

Figure 6: Modifications of the stopband of the $(-)$ mode near $\nu_x = 1/4$ due to octupoles. Solid lines right to left $a/\xi = 0.1, 0.2, 0.3, 0.4, 0.8$; dashed line $a = 0$, open circles – the stopband for monochromatic bunches, $\xi = 0.05$.

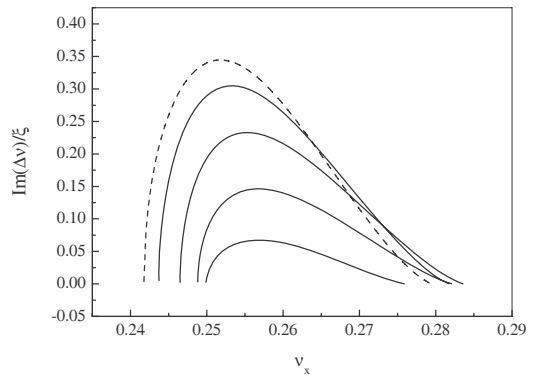

Figure 7: Same as in Fig. 6, but top to bottom $a/\xi = -0.1, -0.3, -0.6, -1$; dashed line: $a = 0$.

sion decreases the increments of unstable modes and the width of the stopband, but does not eliminate Landau anti-damping of the modes.

CONCLUSIONS

Using the simplifying model, we have studied the influence of tunespreads on the stability of coherent oscillations of short, identical colliding e^+e^- bunches. Comparing the spectra of coherent oscillations which are calculated taking into account and/or ignoring the tunespreads we have found out the Landau anti-damping of coherent oscillations of colliding bunches. Namely, together with the damping of unstable modes of the monochromatic colliding bunches the tunespreads result in the instability of coherent oscillations in the regions of betatron tunes ν_x where coherent oscillations of monochromatic bunches were stable. Effects of this anti-damping increase with an increase in the value of the betatron multipole number m. It is almost negligible for the dipole modes, but for the modes with $m \geq 2$ the calculations ignoring the beam-beam tunespread result in strong underestimation of the widths of the stopbands

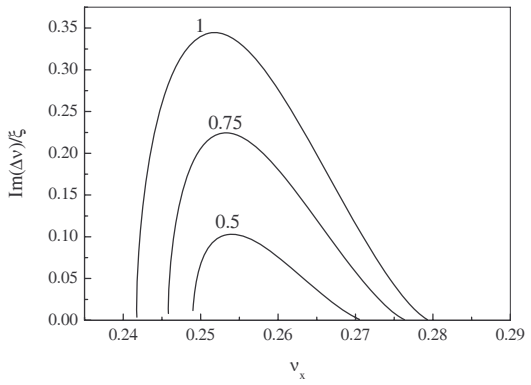

Figure 8: Modifications of the stopband of the $(-)$ mode near $\nu_x = 1/4$ due to hour-glass like suppression. The figures above the curves give the values of the suppression factors, $\xi = 0.05$.

of coherent oscillations of the colliding bunches as well as in wrong positions of these stopbands relative the resonant values of the tunes ν_x. Generally, effects of the tunespreads decrease the maximum values of the oscillation increments as compared to those calculated for monochromatic bunches. Octupole fields do not cancel Landau anti-damping, but can decrease increments of unstable modes. Initial estimations also show, that the hour-glass reductions do not eliminate Landau anti-damping of the coherent beam-beam modes.

We simplified our half-analytic calculations ignoring possible effects of incoherent beam-beam resonances on the stability of collective beam-beam modes assuming that only small amount of the bunch particles are captured in the resonance buckets. If the incoherent resonances are strong and/or are wide enough in ν_x, the described calculations may predict the results which are not reliable (see, e.g. in Ref.[10]). In such cases, the stability of collective beam-beam modes should be studied using numerical simulations.

REFERENCES

[1] N. Dikansky and D. Pestrikov, Part. Acc. **12** (1982) 27.

[2] D. Pestrikov, SLAC-PUB-5510, SLAC, 1991.

[3] P. Zenkevich and K. Yokoya, Part. Acc. **40** (1993) 229.

[4] Dikansky N.S., Pestrikov D.V., Physics of Intense Beams and Storage Rings. AIP PRESS, New York, 1994.

[5] D. V. Pestrikov, Nuclear Instruments and Methods in Physics Research A 578/1 (2007) 65.

[6] D.V. Pestrikov, Nuclear Instruments and Methods in Physics Research, A 588/3 (2008) 336.

[7] Ya.S. Derbenev, N.S. Dikansky, In Proc. of All Union Part. Acc. Conf.; Moscow 1970, v.2, 391.

[8] A.W. Chao, R.D. Ruth, Part. Acc. **16** (1985) 201.

[9] D. Pestrikov, SLAC-PUB-5575, SLAC, 1991.

[10] L. Jin, J. Shi, G.H. Hoffstaetter, Phys. Rev. E **71**, 036501, (2005).

EXPERIMENTAL BACKGROUND STUDY IN THE BEPC Ⅱ/BESⅢ*

D.P. Jin#, N. Huang†, S.M. Yang, J. Xing, J.S. Cao, X.Y. Zhao, Q.J. Zhang, Q.B. Wu, Q. Qin, G. Xu, Y.Z. Wu, W.G. Li, Y.F. Wang, C. Zhang, J.Q. Wang, L. Ma, Y.N. Guo, IHEP, Beijing 100049, China

Abstract

Experimental beam-related background study is introduced with the BEijing Spectrometor (BESⅢ) [1] off the interaction region (IR) of the BEPCII [2]. Only safety issues are studied carefully so far for the not good enough detector`s accuracy. Various experiments are carried out and effective ways to reduce the doses to the IR are found. The results show that the BESⅢ is safe enough when it is pulled to the IR.

Key words: background, BEPC Ⅱ, BESⅢ, collimator, injection

GENERAL DESCRIPTION

With the progress of the BEPC Ⅱ commissioning, experimental beam-related background study becomes very urgent. There are two related issues, one is the safety of the detectors, especially for the CsI crystals (<500rads/year) since they will always be exposed to the radiation doses, the other is the data acquisition environment for physics studies. Pin Diodes [3] and RADFETs [4] are used to measure the doses. Beam Loss Monitors (BLM) [5] are used to measure the rate of charged particles. With the large integrated doses during the commissioning of the BEPC Ⅱ, the accuracy of the two types of detectors gets worse and worse, which cannot fulfil the requirements of steady run backgrounds. So, only safety issues are studied in detail. Simulation study for steady run backgrounds is provided in Ref. [6].

The commissioning of the BEPC Ⅱ in the past has two phases. One is from the late of 2006 to the summer of 2007 with the backup lattice (two normal quadrupoles and one normal dipole instead of the two superconducting Quadrupoles – SCQ) used in the IR, the other is from the autumn of 2007 to the beginning of 2008 with the two SCQs there.

In the phase Ⅰ running, no collimators are installed and only measurements are done. In the phase Ⅱ running, some movable and fixed collimators are installed, experiments are designed and done.

RESULTS FROM PHASE Ⅰ RUNNING

Measurements from the phase Ⅰ running show that backgrounds due to injections are much more serious than those due to steady runs and the total integrated doses are much higher than the safety margin of the CsI crystals. Integrated doses to the crystals within one day can be 15 rads, which is about 10 times the safety margin per day.

Fig. 1 and Fig. 2 show the dose rate of a pin diode and integrated doses of 4 RADFETs respectively. The pin diode in Fig. 1 locates at the crotch pipe upstream of the interaction point (IP) for the electron beam. The RADFETs in Fig. 2 locate at 1.75m upstream of the IP for the electron beam and 30 to 60cm from the centerline of the BESⅢ in downward direction. The distance between the inner most crystals and the centerline of the BESⅢ is about 50cm.

The positron beams have little affection to the detectors in the electron beam side as seen from the two figures.

How to reduce backgrounds due to injections to guarantee the safety of the crystals when they are there becomes one of the central tasks in the phase Ⅱ running.

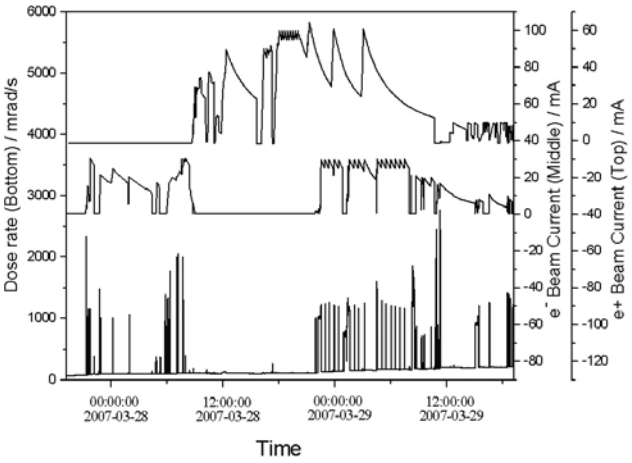

Figure 1: Pin diode dose rate to beam current.

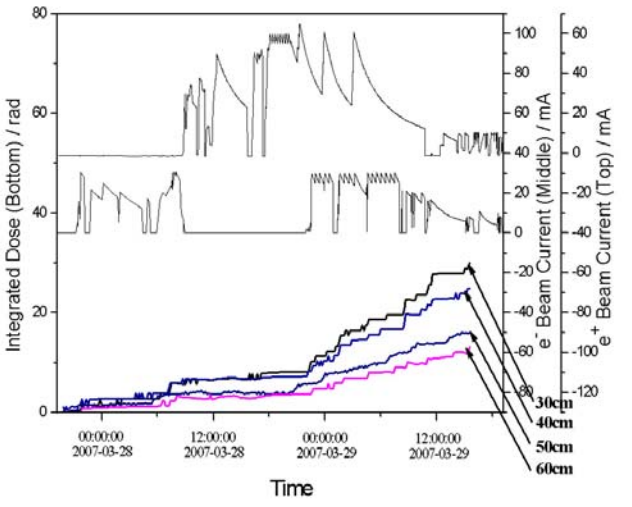

Figure 2: Integrated doses near the crystals.

*Work supported by National Natural Science Foundation of China(No. 10491300), National Science Fund for Distinguished Young Scholars(No. 10225524) and Major Programs of the Chinese Academy of Sciences(No. KJ95T-03).

#jindp@ihep.ac.cn; †huangn@ihep.ac.cn

RESULTS FROM PHASE Ⅱ RUNNING

To get as clear as possible understanding of the backgrounds, the following experiments are done with the results illustrated.

1. Aperture adjustment of the collimator about 8m upstream of the IP for the electron beam. For the half aperture down to 11σ, no obvious effects are seen to reduce injection backgrounds.

2. Aperture adjustment of the collimators downstream of the IP for the electron beam. No obvious effect to reduce injection backgrounds is found. Injection rate is stable with half apertures down to 12σ in both horizontal and vertical directions. Injection rate gets 30% lower with a 10σ half aperture in vertical direction.

3. Aperture adjustment of collimators on the transport line. With an aperture of ±0.3% for energy dispersion collimator and that of ±3mm (±1.7σ) for emittance one, the integrated dose of one electron injection to the pin diode reduces from several rads to point several rads at the upstream crotch pipe and the rates from Beam Loss Monitors at the same position decrease with a factor of about 10 as shown from Fig. 3 to Fig. 5. Assuming 20 injections per day, the integrated dose is less than 10rads at the crotch pipe, and that to the crystals should be less than 0.3 rad, which is well below the safety margin.

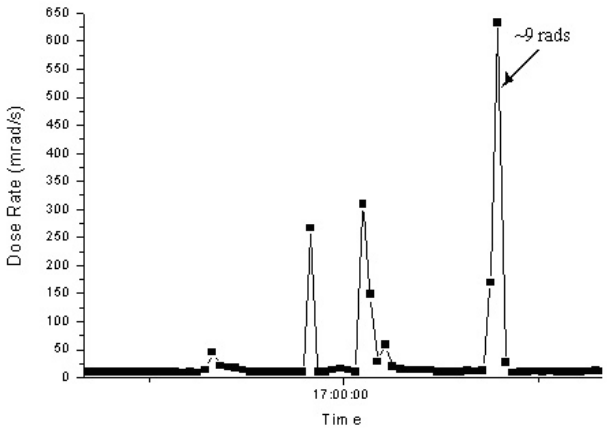

Figure 3: Dose rate at the upstream crotch pipe with the collimators on the transport line opened.

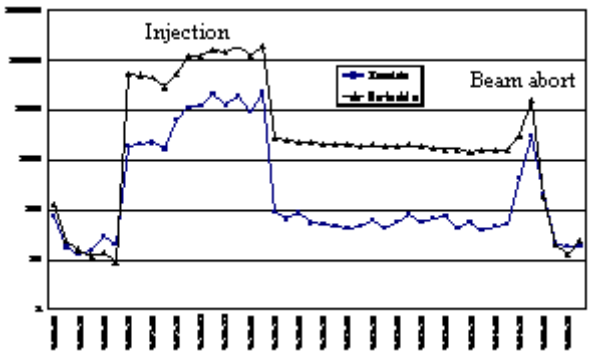

Figure 4: Rates of BLM at the crotch pipe with the collimators on the transport line opened.

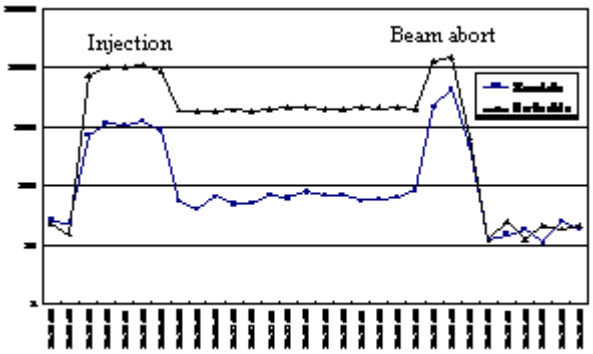

Figure 5: Rates of BLM at the crotch pipe with the collimators on the transport line closed.

4. Beam abort experiment. At first, only one of two injection kickers is used to abort the beam and large dose rates to the IR are seen. After that, two kickers are used to abort the beam. There is no obvious dose rate to the IR from then on.

5. Lead bricks experiment. In real case, there are iron plates neighboured to the crystals in the longitudinal direction and lead pieces just under them in the radial direction. Five lead bricks are used to simulate the real situation as shown in Fig. 6. With the lead bricks, doses to the crystals decrease about 50%.

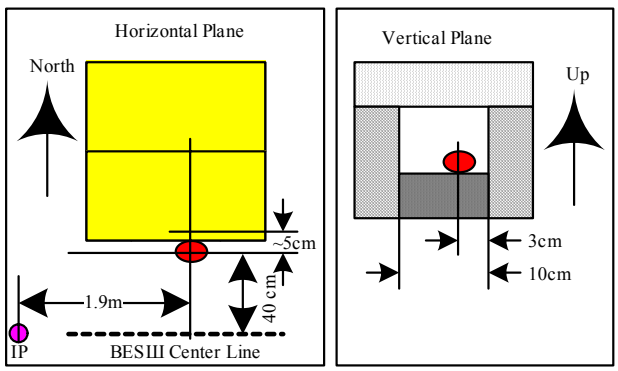

Figure 6: Arrangement of the lead bricks.

6. Doses due to synchrotron radiation runs. BEPC II provides dedicated synchrotron radiation runs besides colliding experiments. So, doses to the crystals due to these runs should be studied. Normally, there are 3 injections per day. From the results of pin diodes and RADFETs, doses due to injections are negligible as shown in Fig. 7.

FURTHER STUDIES

The BESIII detector will be rolled in the IR in mid-April. In order to reduce background for detector safety and clean data acquisition, as much as possible shielding and pin diodes & RadFETs for radiation and background diagnostics will be mounted in the IR. In the storage rings, more collimators will be installed. Beam injection will be further optimized especially for electrons. Fast beam abort system will be applied when beams are dumped. A

luminosity-based collision feedback (x, y, y') will be developed for improving integrated luminosity, providing operational stability, reducing injection and beam-beam backgrounds. Finally, different background sources such as beam-gas scattering, Touscheck effect, luminosity background as well as beam-beam interactions will be investigated experimentally together with vacuum pressure and optimisation of orbits and lattice parameters in order to reduce the background in the BES III .

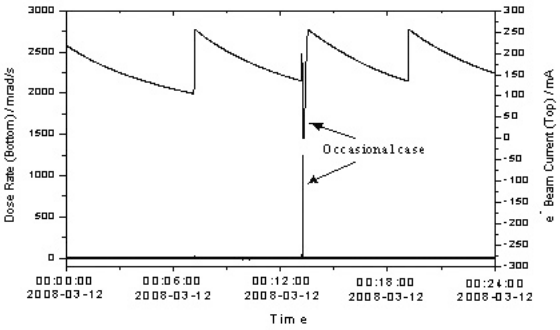

Figure 7: Dose rates of pin diodes in the IR during synchrotron radiation runs.

SUMMARY

Various experiments are done to study the behaviour of the backgrounds and means to reduce them are found. The results from both colliding and synchrotron radiation operation show that it is safe for the BESIII to be pulled to the IR. The backgrounds due to steady runs and ways to reduce them should be studied thoroughly in the BEPC II /BESIII joint experiments.

REFERENCES

[1] BESIII design report, http://epc2.ihep.ac.cn/epc/design/design1.htm

[2] BEPC II design report, http://acc-center.ihep.ac.cn/bepcii/cdr_download.htm

[3] Detection Technology, Inc. High-Performance Diodes XRB-series. August 2000, http://www.deetee.com/ion_radiation.htm

[4] H. Gong and other, "Study of the Features of 400nm IMPL RADFET Dosimeter", Chinese Physics C, (2007) Vol. 31, No. 3, P283-287 (in Chinese), http://hepnp.ihep.ac.cn/qikan/manage/wenzhang/2006-0149.pdf

[5] Bergoz Instrumentation, Beam Loss Monitor, http://www.bergoz.com/products/BLM/BLM.html

[6] http://epc2.ihep.ac.cn/epc/design/English_reports/4.doc

INTERACTION REGION DESIGN AND REALIZATION FOR BEPCII

C. H. Yu, Y. Z. Wu, Z. S. Yin, J. F. Zhang, M. T. Wang, Q. L. Peng, J. B. Pang, Y. Yang, X. W. Dai
IHEP, Beijing, P.R. China

Abstract

The BEPC (Beijing Electron Positron Collider) is being upgraded as a double-ring factory-like collider (BEPCII). A New and compact interaction region (IR) has been designed to afford a peak luminosity of $10^{33}cm^{-2}s^{-1}$ with an equal beam energy of 1.89 GeV, a cross angle of ±11 mrad, 93 bunches and maximum beam current of 0.91 A. All the components of the IR have been fabricated successfully. During the commissioning of BEPCII the operation experience shows that the IR components have excellent performance and meet the design requirements. The design and realization of the interaction region for the BEPCII will be introduced in detail.

LAYOUT OF THE IR

The central part of the BESIII detector is a cylindrical drift chamber surrounded by electromagnetic calorimeters. The geometry of the drift chamber has a direct bearing on the IR design. It requires that the accelerator components inside the detector must fit within a conical space with an opening angle of 21.5˚. The first accelerator element can only approach to 0.55m on each side of the IP.

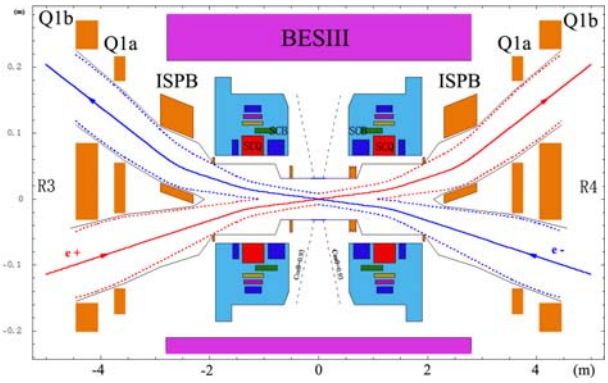

Figure 1: The layout and beam separation scheme in the IR for the colliding mode.

To ensure adequate quantum lifetime, the beam stay clear is defined to accommodate at least 14σ+2 mm in the IR [1]. The beam line layout in the central part of the IR is shown in Fig. 1. On each side of the IP, a doublet of quadrupole is used to provide the focusing optics at the IP. The first vertical focusing quadrupole, SCQ, connects the outer and inner rings, which are shared by both beams. Two beams collide with a horizontal crossing angle of 22 mrad at the IP. A horizontal bending magnet ISPB, which is located just beyond the vertical focusing quadrupole, will enhance the separation between electron and positron beams. ISPB is a septum magnet which acts on the outgoing beam-line only. The second element of the doublet is horizontal focusing quadrupoles Q1a and Q1b. In order to achieve the aims of keeping the symmetrical structure of two rings and saving space, the quadrupoles Q1a and Q1b are designed as a two-in-one type. Two separate beam channels for the incoming and outgoing beams have same field strength.

BEPCII will be operated not only for high energy physics (colliding mode) but for synchrotron radiation application (SR mode). The switch of two modes is to control the power supplies of SCQ and SCB. The bending dipoles SCB which are only used for the synchrotron radiation mode connect the outer-ring. During the SR mode operation two SCQs are turned off.

SUPERCONDUCTING MAGNETS

The superconducting magnet [2] has a multi-function coil pack. As shown in Fig. 1, it consists of independent quadrupole (SCQ), horizontal dipole (SCB), vertical dipole (VDC), skew quadrupole (SKQ) and three anti-solenoid (AS1, AS2, AS3) windings. The cryostat has a warm bore with an inner diameter of ϕ132mm and outer diameter of ϕ326mm. The endcan of cryostat has an outer diameter of ϕ640mm.

The main mechanical work of superconducting magnets was completed in China and the main coils were wound at BNL laboratory in U. S.

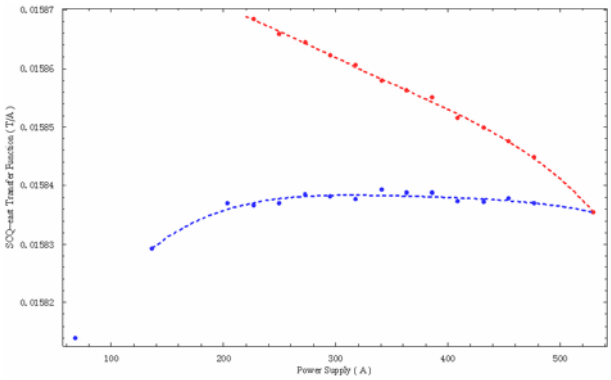

Figure 2: The measurement transfer function of SCQ.

The field measurements of the superconducting quadrupoles and dipoles have been performed at IHEP. The transfer function of SCQ is shown in Fig. 2. The harmonic components were measured by the rotating coil system. The integral gradient, offset and tilt angle were measured by SW system. Furthermore, the characteristics of each magnet have been studied in detail according to various performance possibilities.

The harmonic requirements for SCB and SCQ at the reference radius are SCB (R=38mm) $B_n/B_1<5\times10^{-4}$ and SCQ (R=50mm) $B_n/B_2<3\times10^{-4}$. Field measurement results show that there is a larger sextupole component of 7.0×10^{-4} in the superconducting quadrupole which is located in the east region. Other components of this quadrupole satisfy the requirements. The field quality of

the other superconducting quadrupole and both superconducting bending magnets can satisfy the requirements.

COMPENSATION OF SOLENOID FIELD

For the colliding mode, the detector solenoid has an effective length of ±1.8m around the IP. The maximum field strength of solenoid is 1.0T so that the particle motion between the horizontal and vertical planes will be coupled strongly. It's impossible to meet higher luminosity without the dedicated coupling compensation of solenoid field. According to the requirements of high energy physics, the collider will be operated at the energy range from 1.0GeV to 2.1GeV, so the compensation system should be powerful enough to work perfectly for particles within the relevant momentum range. For this purpose a special anti-solenoid system has been designed to realize the local compensation of solenoid.

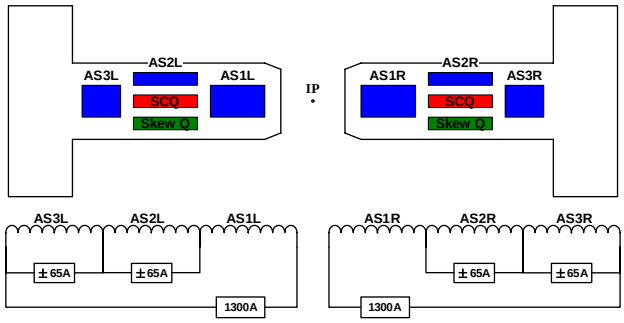

Figure 3: The wiring schematic diagram of anti-solenoids.

This system consists of three anti-solenoids AS1, AS2 and AS3 and a skew quadrupole SCSKQ which are all inside the superconducting cryostat. AS1 locates between the IP and the superconducting quadrupole (SCQ). AS2 and the skew quadrupole SCSKQ overlap the SCQ, while AS3 locates after the SCQ.

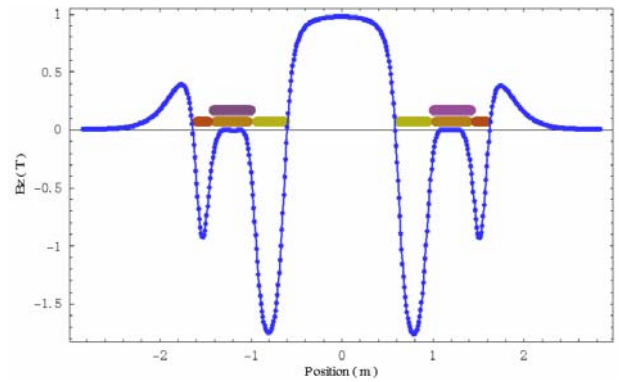

Figure 4: The combination magnetic field Bz along the axis of BESIII detector after compensation.

The local compensation layout of BEPCII and wiring schematic diagram are shown in Fig. 3. AS2 and AS3, which have their own independent trim circuits to allow fine tuning of the anti-solenoid compensation scheme, are in series with AS1. Since the compensation of longitudinal field within the SCQ region is a key to control the vertical beam size at the IP, the skew quadrupole SCSKQ is used to make fine tuning of longitudinal field over the SCQ region instead of the mechanical rotation method.

With this local coupling compensation scheme, the integral field $\int B_z ds$ between the IP and the SCQ is zero. The longitudinal field over the SCQ is nearly zero and the integral field $\int B_z ds$ between the SCQ and the first horizontal focusing quadrupole is zero too. The field measurements of the detector solenoid, anti-solenoid and the combination field have been finished. The distribution of the combination magnetic field B_z along the axis of the BESIII detector after compensation is shown in Fig. 4.

SEPTUM BENDING MAGNET ISPB

Figure 5: The shape of ISPB.

Two ISPB [3] magnets shown in Fig. 5 have been successfully fabricated. The field measurements show that its performance meets the requirements of beam dynamics with $B_n/B_1 < 5 \times 10^{-4}$.

SPECIAL QUADRUPOLES Q1a AND Q1b

The separation between two beams is about 185 mm at the inboard face of Q1a [3] and 231 mm for Q1b while the beam stay clear (BSC) is 95mm and 102mm respectively. The space for the design of septum is very limited. The following accelerator elements are quadrupoles Q2, Q3 and Q4 where the separation of two beams is large enough to allow them to be installed side by side into the two rings.

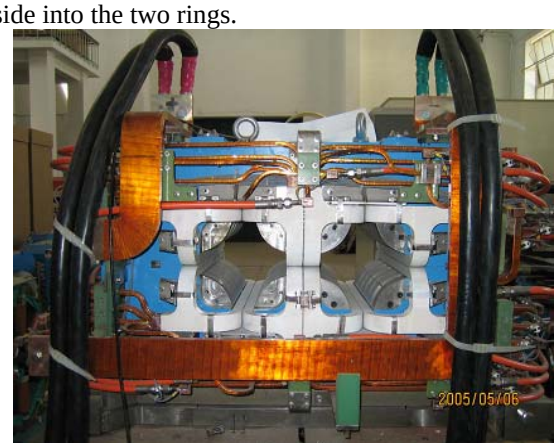

Figure 6: The shape of Q1a/Q1b.

The fabrication of Q1a and Q1b were completed at the IHEP workshop with the shape shown in Fig. 6. The measurements of the magnetic field were finished. After being shimmed by the method of edge harmonic compensation developed by IHEP, all the components of higher order magnetic fields of Q1a and Q1b are less than the design requirements 4×10^{-4} (R=53.5mm)and 3×10^{-4} (R=61.5mm) respectively.

SYNCHROTRON RADIATION

The colliding and SR modes have different synchrotron radiation sources and different synchrotron radiation fan distributions.

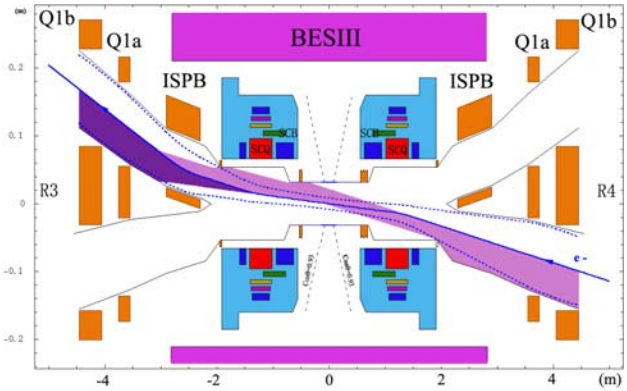

Figure 7: The SR fan of e- beam of colliding mode.

The colliding mode will be operated at the energy range of 1.0GeV to 2.1GeV. However, the case with maximum SR power distribution is 1.89GeV, as well as beam current of 0.91A. For the e- beam, synchrotron radiation fans of the IR shown in Fig. 7 are mainly generated from the final bending magnet R4OWB and from the IR quadrupoles due to the crossing angle trajectory. As the e-beam travels through the final bending magnet R4OWB (13.4m from the IP) and enters the IR, it generates SR fan with the total power 396W (Ec=0.7keV). The SR fan of center beam passes through the IP and spreads horizontally up to 0.5m from the IP. It contributes about 3.0W of SR power on the 0.5m~0.7m beam pipe. There are 6 quadrupoles between R4OWB and the IP. Among them R4SCQ magnet is the largest radiation source due to its off-axis installation. The total SR power generated by the R4SCQ magnet is 95.2W (Ec<1.2keV). About 19.2W of SR power from R4SCQ can strike on the 0.5m~0.7m beam pipe. The rest of SR fans travels out of the near IR and is absorbed on the surface at 3m~4m. Most of the synchrotron radiation power (521.3W) generated by R3SCQ and ISPB magnets hits the beam pipe at 3.0m~4.4m from the IP.

The SR mode will be operated at energy of 2.5GeV. The maximum beam current is 250mA. The SR powers are mainly generated by the final bending magnet R4OWB, the superconducting bending magnets R4SCB and R3SCB nearby the IP. For the SR mode, only e- beam is employed. As the e- beam travels through the final bending magnet R4OWB and enters the IR, it generates SR fan with the total power 333W (E_c = 1.7 keV). The SR fan of center beam passes through the IP and spreads horizontally up to 0.5m from the IP. It contributes about 2.5W of SR power on the 0.5m~0.7m beam pipe. The total power of the SR fan generated by R4SCB is 223W (E_c = 2.3 keV). About 25.3W of SR power from R4SCB can strike on the region of 0.5m ~ 0.7m of the beam pipe. The rest of the SR fan from R4SCB travels out of the near IR and is absorbed on two surfaces, one is a mask placed in front of the ISPB septum, and the other is the beam pipe at 3m ~ 4m. About half of the SR power 223W generated from R3SCB hits the mask placed in front of the ISPB septum. The remainder mainly strikes the beam pipe between the R3Q1a and R3Q1b

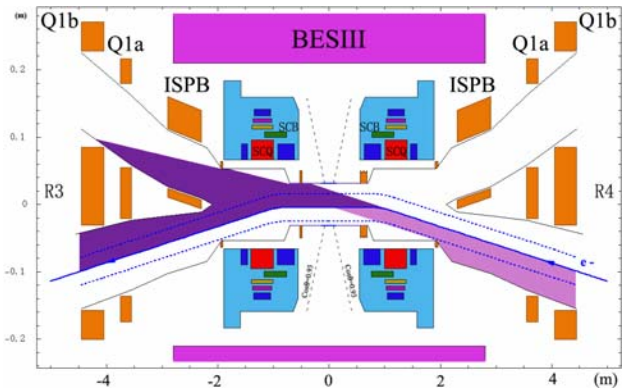

Figure 8: The SR fan of SR mode.

For the present IR design, it's very difficult to stop both direct and once-scattered photons emitted within $10\sigma_x$ of beam size at all magnets hitting on the detector beryllium pipe. The critical energy of photons is less than 0.7keV during the operation of colliding mode. The simulation results show that the SR background level is acceptable.

IR VACUUM CHAMBER

The central part of the beam pipe is a double-wall beryllium structure with a 1mm gap of cooling channel. It is ± 0.15 m long around the IP with the ID of 63 mm. The inside wall of Be pipe will be coated by gold. The Be pipe is welded to a copper cylinder which is connected to the SCQ chamber through a special CF63 bellows [4].

The SCQ chamber is about 1.24 m long with an inner diameter of 111 mm. It is connected to the Y-Type chambers through special CF100 flange. The Y-type chamber is about 0.3 m long in which a bellows, one NEG pump, and two BPMs are installed. At the end of the Y-type section the vacuum chambers are completely separated for each beam. Both Q1a and Q1b chamber have an inner diameter of 104 mm. After Q1b the vacuum chamber has a transition to the standard chamber.

The water cooling structure have been designed in the beam pipe 0.5~0.7m away from the IP, the crotch beam pipe, the SCQ beam pipe and the beam pipe 3.0~4.0m away from the IP, to avoid the heat problem in these region. Except for the Be pipe, copper was chosen for the vacuum chamber within ±3.5m as its low coefficient of photon-induced gas desorption, large photon absorption coefficient and high thermal conductivity [5].

There are 132 thermocouples in the IR to monitor the temperature raise and SR fans behavior. During the operation of both colliding and synchrotron radiation modes, the temperatures of vacuum chambers were controlled effectively.

COLLISION TUNNING MONITORS

The beam-beam deflection technique [5] is adopted in the BEPCII to find and maintain the collision conditions.

For the consideration of phase advance and beta function, the BPMs between Q1a and Q1b are set to measure horizontal beam-beam kicker angle. The BPMs on the crotch beam pipe are set to measure vertical beam-beam kicker angle. The measured signals of beam-beam kicker during collision tuning are shown in Fig. 9.

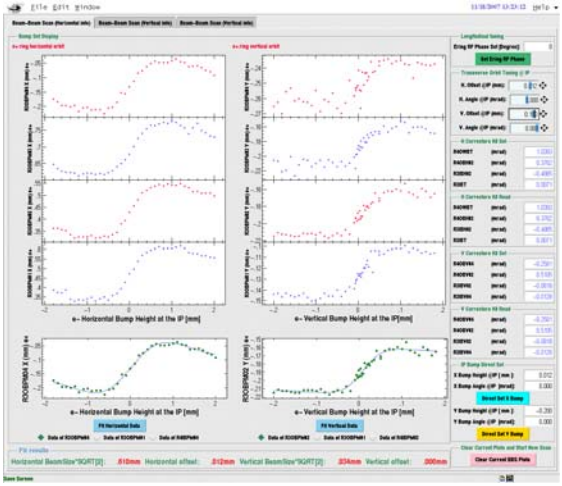

Figure 9: The measured signals of beam-beam kicker

A pair of Cherenkov luminosity detectors which measure the radiative Bhabha photons are installed to monitor positron and electron beam, respectively. They worked well during the last collision tuning operation.

SUPPORTING SYSTEM

The cryostat of superconducting magnet, transfer line, service cryostat and ISPB, Q1a, Q1b etc. are supported by a movable stage. This movable stage could move along the beam line by approximately 3m. With this motion the superconducting magnets could be pulled out and pushed into the detector [7]. The drawing of the supporting system of IR is displayed in Fig. 10.

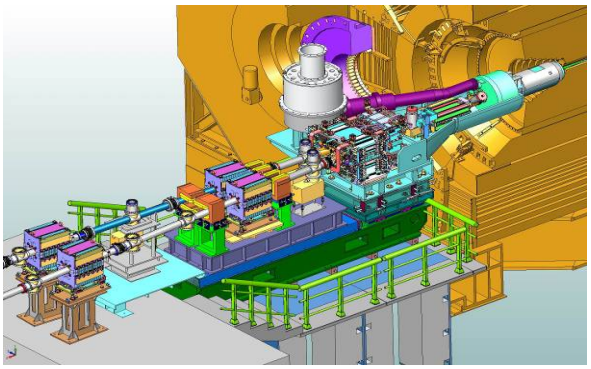

Figure 10: The supporting system of IR.

The measurements of ground vibration in the IR have been finished. The results of data analysis indicate that the average rms displacement is about 10nm. The IR is a good place with a low cultural noise. The inherence frequency of supporting system has been optimized to avoid the resonance from noise frequency [8]. The power spectral density of ground motion is shown in Fig. 11.

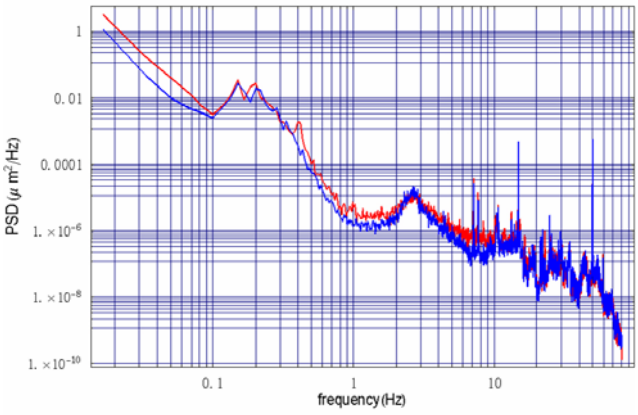

Figure 11: Power spectral density of ground motion.

DISCUSSIONS

The design and realization of interaction region for the BEPCII have been introduced in detail. The detector will be rolled into the interaction point this summer. Coupling compensation, background issues, radiation dose, etc. will bring new challenges for the commissioning of the BEPCII.

REFERENCES

[1] C. H. Yu, "Beam physics issues of the BEPCII interaction region", Proceedings of Mini-Workshop on the BEPCII Interaction Region., January 2004.

[2] Brett Parker, "Review of operating currents, forces and torques for the BEPCII IR magnets", The 2'nd BEPCII Videoconference, May 2003.

[3] J. B. Pang, Z. S. Yin, "The design of special magnets in the IR", Proceedings of Mini-Workshop on the BEPCII Interaction Region., January 2004.

[4] Y. Yang, "The design for the IR vacuum chamber", Proceedings of Mini-Workshop on the BEPCII Interaction Region., January 2004.

[5] X. W. Dai, "The heating analysis for the vacuum chambers in the IR", Proceedings of Mini-Workshop on the BEPCII Interaction Region., January 2004.

[6] D.A. Edwards and L.C. Teng, IEEE Trans. Nucl. Sci. 20, 3 (1973).

[7] M. T. Wang, "Support and vibration in the IR", Proceedings of Mini-Workshop on the BEPCII Interaction Region., January 2004.

[8] C. H. Yu, "The measurement of ground motion in the IR", internal report, 2005.

OPTICS CORRECTION IN BEPCII USING RESPONSE MATRIX *

Y.Y. Wei #, Q. Qin, G. Xu, W.B. Liu, D.M. Zhou, Y. Chen, IHEP, CAS

P.O. Box 918, Beijing 100049, P.R. China

Abstract

The second phase commissioning of the BEPCII (Beijing Electron Positron Collider II) had been made a great progress. The optics correction using LOCO based on orbit response matrix contributed a lot to the successful commissioning. This paper discusses mainly on the procedure and results of optics correction at BEPCII. Using LOCO, we have determined the errors of quadrupole strengths, BPM gains and corrector kicks, and found the quadrupole strengths that restore the design optics well. Optics measurement after correction also shows the real optics agrees well with the design one.

INTRODUCTION

The BEPCII is constructed for both high energy physics and synchrotron radiation (SR) users. The storage ring for collision consists of a positron (BPR) and an electron ring (BER), and the outer parts of the two rings contribute to the SR ring.

To satisfy both the collision and the SR modes, the geometric and optics design of BEPCII are relatively complex. No 4-fold symmetric structure exists. The arc region consists of 6 quasi-FODO cells, and the quadrupoles and sextupoles of arc region are installed very closely. Furthermore, a number of different kinds of quadrupoles with independent power supplies are used at BEPCII, such as the superconducting quadrupole SCQs to squeeze the vertical beta function at the IP and bend the beam, the warm bore quadrupoles to connect the arc and IP, the dual aperture quadrupoles, quadrupoles inherited from BEPC, and so on. Thus, a good agreement between the real optics and the model is essential for BEPCII to achieve the optimum performance.

From the beginning of the BEPCII commissioning, we have used the orbit response matrix method base on LOCO [1] (the Linear Optics from Closed Orbits) codes to correct the optics successfully. In this paper, we present the results of BEPCII commissioning from Oct. 2007, including a brief introduction of the LOCO algorithm, the analysis and optics measurement on the three storage rings, and some problems identified by response matrix method.

THEORY

The orbit response matrix M defines the relationship between the shift at each BPM and a change in strength of each corrector:

$$\begin{pmatrix} \Delta x \\ \Delta y \end{pmatrix} = M \begin{pmatrix} \Delta\theta_x \\ \Delta\theta_y \end{pmatrix}, \qquad (1)$$

where $\Delta x, y$ are the orbit changes due to the changes of corrector strengths $\Delta\theta_{x,y}$. By varying the parameters in model matrix M_{model}, which is calculated by accelerator modelling code such as AT [2], the difference between model response matrix and measured matrix M_{meas} are minimized with [3]:

$$\chi^2 = \sum_{i,j} \frac{(M_{\mathrm{mod},ij} - M_{meas,ij})^2}{\sigma_i^2} \equiv \sum_{i,j} V_{ij}^2 \ . \qquad (2)$$

where σ_i is the measured noise levels for the BPMs, V_{ij} is the function of the parameters varied in model lattice. With the residual error of M_{meas} and M_{model} converges to the noise level of BPM, the quadrupole gradient differences between the model and real storage ring as well as BPM gains and corrector kicks are determined. The model optics derived from LOCO after fitting can predict the real machine optics. When the gradient errors are corrected, the design optics can be restored.

ANALYSIS FOR COLLISION MODE

After the SCQs were moved to IR, we started the second phase commissioning of the BER and BPR, respectively. To make the injection relatively easier, a lattice with beta function at the IP, i.e., β_x^*/β_y^* = 2m/5cm, and the tunes of ν_x/ν_y=6.54/5.59 was chosen for both rings. Applying all the quadrupole fudge factors of last run, the beam accumulated in BER and BPR smoothly. Then we optimized the optics to the lattice of β_x^*/β_y^* = 1m/1.5cm by the lattice of β_x^*/β_y^* = 2m/3cm. When the status of beam was good enough to measure the response matrix, we attempted to do the optics correction.

Before the orbit response data was collected, beam based alignment was done to determine all BPM offsets, and orbit was corrected to the centre of quadrupoles.

There're 34 horizontal correctors, 33 vertical correctors and 67 double-view BPMs are available in both BPR and BER, respectively. This results in that (34+33)×67×2 =8978 elements can be used for fitting in model optics.

BER Optics Analysis

Response matrix was measured with sextupoles on, then we fitted the model to the measured response matrix using LOCO codes. BPM gains, corrector kicks and quadrupole strengths were varied in the model with some constraints listed as following:

- Because the change of SCQs' strength will affect the orbit, SCQs' strengths are not fitted in LOCO.

#weiyy@mail.ihep.ac.cn

- R3IQ1A and R3IQ1B, R4OQ1A and R4OQ1B, R3IQ02 and R3IQ03, R4OQ02 and R4OQ02 are couples of adjacent magnets which have the same polarity. If the two quadrupoles in the magnet couple are fitted independently, the strength errors derived from LOCO may fight each other. To avoid this problem only Q1Bs and Q02s in the magnet couples serviced as parameters when fitting.
- R4OQ1B and R3IQ1B are fed by the same main power supply, and different auxiliary supplies. They can only be adjusted independently within a very limit region, so their strengths vary simultaneously when fitting.

After fitting the model response matrix to the measured matrix, the rms error between them is about 0.007mm (some abnormal data removed), and the measured BPM resolution is smaller than 0.01mm. The distribution of residuals for the response matrix is normalized by the noise level of the BPMs, and the distribution has a width roughly equal to 1, which indicates the fitting in LOCO converged to the noise level of BPM.

Fig.1 shows the errors of quadrupole fudge factors. The quadrupole amplitude fudge factor AF describes the correction to restore the design optics:

$$K^i = AF^i \cdot K_0^i . \qquad (3)$$

Here, for the i^{th} quadrupole, K is the correction strength, and K_0 is the design value. Fudge factors can be derived from the strengths found by LOCO:

$$AF^i = K_n^i / K_L^i . \qquad (4)$$

In eq. (4), K_L is the strength determined by LOCO, and K_n the nominal strength when response matrix is measured.

From the initial result of BER fudge factors, which is shown in Fig.1 marked by "before R1OQ16 problem resolved", we notice that the fudge factor error of R1OQ16 exceeds 15%. That means the real strength of R1OQ16 is much lower. On Dec.25, 2007, the shortcut between R1OQ16 magnet poles was confirmed. After that, we measured the response again and fitted a new set of quadrupole strengths, which is marked by "after R1OQ16 problem resolved" in Fig.1.

Furthermore, we applied the fudge factors of qudrupoles to BER. Optics measurement was performed to examine the difference between the real and the design optics.

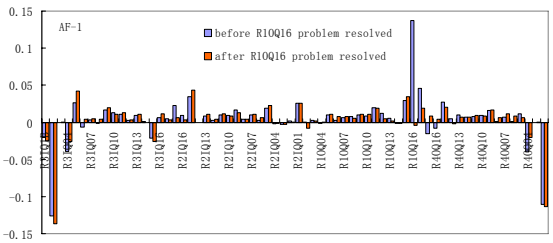

Figure 1: Errors of BER quadrupole fudge factors.

The nominal tunes of the design optics are 6.5434/5.6396, and measured tunes after correction are 6.5474/6.6377.

Beta function was measured using quadrupole modulation method. Fig.2 and Fig.3 show the comparison of the measured and design beta function. Before optics correction, beta function errors in some region even exceed 100%. After correction, the measured beta function agrees well with the design one.

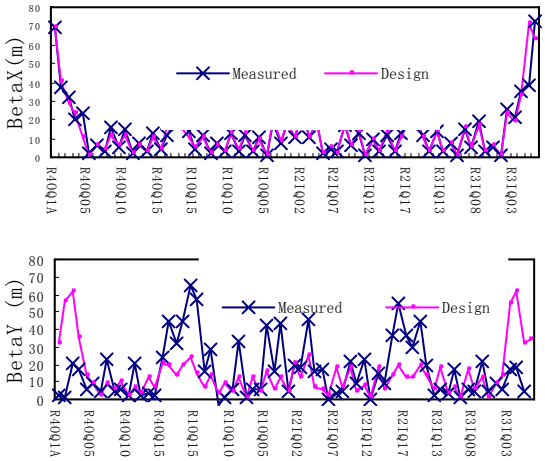

Figure 2: The comparison of the measured and design horizontal (upper) and vertical (bottom) beta function before BER optics correction.

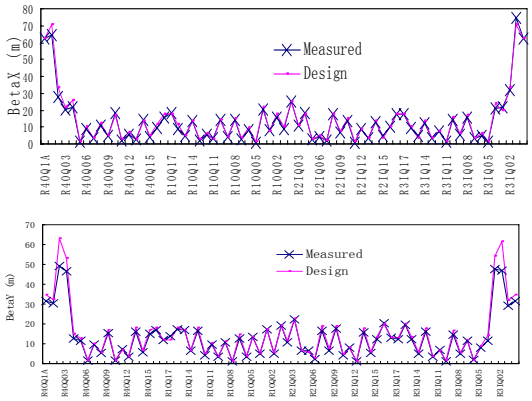

Figure 3: The comparison of the measured and design horizontal (upper) and vertical (bottom) beta function after BER optics correction.

BPR Optics Analysis

For BPR optics correction, the method and constraints fitting in LOCO are similar to BER. Only the results are presented here.

Fig.4 shows the errors of quadrupole fudge factors of BPR, marked by "SCQ:AF=1". From Fig.1 and Fig.4 we find out the fudge factor errors of Q2s in IR are all relatively large, amounting to 10%. Because Q2s have the same polarity as SCQs, we wonder if the changes of Q2s' strength are to compensate the SCQs' gradient errors. Then we decreased the strength of SCQs by 0.2%,

measured the response matrix and fitted. The fudge factor errors of Q2s reduced from 10% to 7%.

Additionally, in the SR mode, the SCQs are not used, and the fudge factor errors of Q2s are less than 1%. It seems to support our hypothesizer again.

Some simulations were also made. We increased the SCQs' strength by 1% in model lattice and fitted by the same way in LOCO. That is to assume the SCQs' strengths of real machine are higher than the design value by 1%. The results of BPR are displayed in Fig.4, marked by "SCQ:AF=1.01". All the Q2s' fudge factor errors of both rings appear to be less than 1%. The result of BER is similar to BPR.

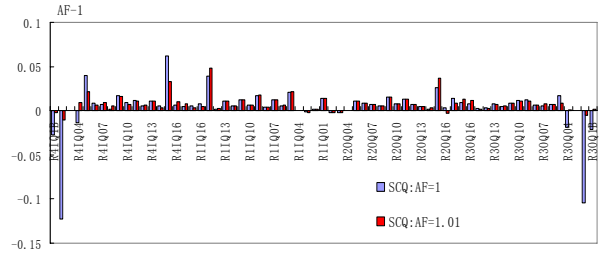

Figure 4: Quadrupole fudge factor errors of BPR with increasing SCQs' strengths by 1% in model.

All the above is not yet enough to confirm the problem on SCQs' gradients. Experiments at real machine are necessary in the future to draw the conclusion.

The optics correction of BPR succeeded to restore the design. After the fudge factors were applied, the discrepancy between the measured and theoretical beta function is within ±10% at most quadruples. For the tunes, the nominal values are 6.54/5.59, and the measured are 6.540/5.596 after correction. We also measured dispersion, as shown in Fig.5, and the deviation from design is less than 10% except for some invalid data due to bad BPMs.

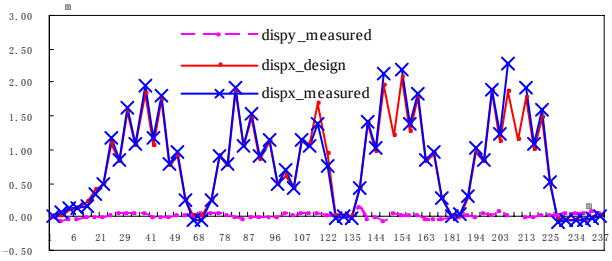

Figure 5: The comparison of the measured and design dispersion (several data is removed due to BPM problem).

Tune split method is applied to measure the transverse coupling for both BPR and BER at BEPCII. As a result, the transverse coupling of BPR is about 1.02% shown in Fig.6, and the coupling of BER is about 1.24%.

Collision tuning started based on the good agreement between the real optics and the design one. Besides the Beam-Beam Scan in longitudinal, horizontal and vertical direction, some optics including the transverse coupling is also adjusted to find out the best status of collision.

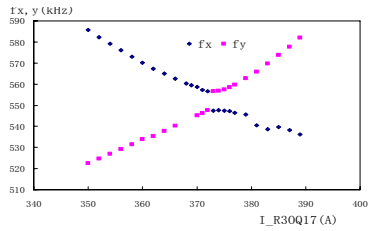

Figure 6: The measurement of BPR transverse coupling.

At BEPCII, because of the limit space, only 4 skew quads are installed in each ring, and adjusted for the IP coupling tuning locally. For the global transverse coupling, since the optics is well corrected, we can form vertical bumps across sextupoles very locally. By changing the bump height thus the vertical orbit in the sextupoles, the transverse coupling can be adjusted. In the second phase commissioning in Jan. 08, the bump height at R1IS5 and R2IS5, which have the relatively strong strengths were changed to tune the coupling of BPR and BER effectively. Parts of the results are listed in Table 1.

Table 1: The BER coupling tuning by changing the bump height at R2IS5

Bump height (mm)	Coupling (%)
0	0.477
-4	5.44
-2	2.15
-1.5	1.53
-1	1.08
-0.5	0.723

ANALYSIS FOR SR MODE

The BEPCII is a double ring collider with separated electron and positron storage rings. In the SR mode, two outer half-rings of the BSR and BER form another electron ring called BSR, which is used as a light source. The two superconducting dipole coils on the both sides of IP connect the two half-rings. The goal of SR mode is designed at 2.5GeV, and the maximum beam current is 250mA. In Mar. 08, during the second phase commissioning of BEPCII, we chose the tunes of ν_x/ν_y=7.28/5.18. The emittance at 2.5GeV is 138nm·rad.

In the SR mode, 5 wigglers are installed to produce stronger SR. Because of the vertical focusing effect caused by wigglers, the vertical tune increased by 0.08. The distortion of the vertical beta function was as much as 30%. Additionally, the effect of wigglers can change the vertical beam size and sometimes excite the structural resonances thus shorten the beam lifetime. To improve the performance of SR mode, the focusing of the wigglers must be compensated.

After orbit correction of BSR, we measured response matrix with wigglers on, and varied all the independent quadrupole strengths in LOCO to determine the changes of strength that best compensate the wiggler focusing. Actually, in the SR mode there exist 63 quadrupoles whose fields can be independently adjusted. R3OQ1A and R4OQ1A are fed by one power supply, thus their

strengths must change together. The SCQs, Q1Bs and Q03s in IR are off. Additionally, a quadrupole named QSR at the north crossing point is used.

The fitting result of user mode shows the quadrupole strengths where wigglers located change intensively. We also examined the optics after correction. The tunes appeared to consist with the design value, and the beta-beating is reduced largely except for the region where wigglers located.

Understanding the Fudge Factor

Examining the errors of quadrupole fudge factor of the three rings derived from LOCO, 40% fudge factor errors exceeding 1%. Some systematic component must exist. The short distance between qudrupoles and sextupoles, and the fringe field effect may be partly responsible for the large errors.

An experiment was done at BSR based on the mode without wigglers and fudge factors applied. The nominal tunes are 7.28/5.38, the measured are 7.1685/5.2834. On one side, we increased the strengths of qudrupoles in arc by 0.6% to compensate the effect of sextupoles, the tunes measured moved to 7.1917/5.3174. On the other side, we setup the model lattice including the fringe field effect of dipoles and qudrupoles. When the modified lattice was applied to BSR, the measured tunes changed to 7.2005/5.3413. Then the two situations were all considered, the measured tunes were 7.225/5.379, which are very close to the nominal tunes on vertical direction, but still have 0.055 discrepancy left on transverse direction.

The experiment partly explained for the large fudge factors. The modified model may be adopted in fitting with LOCO in the future, and studies on other sources are still under way.

Application of Response Matrix

In the SR mode the stability of orbit is very important for the users. But in fact, the orbit drifts with time due to the effects caused by stability of power supplies, the beam, environmental temperature, and so on. To constrain the orbit drifts accurately we setup the slow orbit feedback (SOFB) system.

The SOFB system is only applied on vertical plane currently. The vertical beam size is about 100μm at the extraction point of beam line. After SOFB system applied, the orbit drift reduced from nearly 100μm to ±5~±10μm.

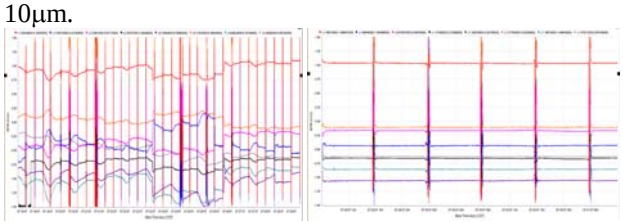

Figure 6: The orbit drifts before (left) and after (right) SOFB system is applied at the extraction points of beam lines (Jun.07, the current is 100~180mA).

During the SR runnin in June 2007, we observed several abrupt changes of orbit shown in the upper one of Fig.7. Based on the measured orbit response matrix, we found out the origin of the orbit abrupt drifts can be regard as the strength change of R2OBV07. At last, the shortcut between R2OS7 magnet poles which is located near the R2OBV07 was confirmed.

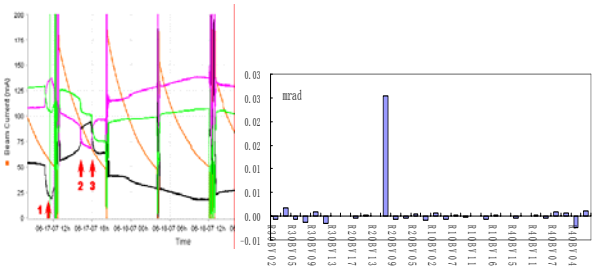

Figure 7: The abrupt changes of orbit (left) and the strength change of all vertical correctors analyzed most likely to cause the abrupt orbit changes (right).

CONCLUSION

Analysis of the orbit response matrix not only determined the quadrupole strength errors, BPM gains, corrector kicks at BEPCII, but also revealed some problems on magnets. 40% fudge factor errors of quadrupoles are more than 1%. An experiment indicates one contributed to this systemic component is the interaction of quadrupoles and their adjacent sexupoles due to their short distance. Another may be the fringe filed effect. Further studies are necessary to confirm the sources. The analysis also gave the best settings for quadrupoles to restore the design optics with sextupoles on even with all the wigglers used in SR mode. After correction, the measured beta function of BPR and BER at most quadrupoles can be restored within ±10% of design model. In SR mode, the application of response matrix method on BSR SOFB system, global orbit analysis and correction are also successful. In the future, studies on coupling correction based on response matrix, determinination the strength errors of SCQs and parasitical mode will be developed.

ACKNOWLEDGEMENTS

The programme used to collect the data and measure the optics is coded with SAD script from KEK, and LOCO is provided by SLAC. Thank all the member of the BEPCII team.

REFERENCES

[1] http://www.slac.stanford.edu/~safranek/loco/
[2] http://www-ssrl.slac.stanfor.edu/at/
[3] J. Safranek, “Experimental determination of storage ring optics using orbit response measurements”, Mucl. Inst. And Meth. A388, 27(1997).

TRENDS IN FAST FEEDBACK R&D

Alessandro Drago
Istituto Nazionale di Fisica nucleare, Laboratori Nazionali di Frascati, Frascati, Italy

Abstract

In this paper, starting from the basic description of the equation that governs the bunch motion and looking at the advances of the technology, three examples of feedback designs versus technology trend are presented and discussed. In particular the author compares three digital systems implemented or proposed for DAΦNE and other e+/e- accelerators. Descriptions of some relevant features are also done. Conclusions on the digital feedback design trend are reported.

INTRODUCTION

In the last two decades, the impressive progress of the digital electronics has stunned and delighted designers and users. In the same years, feedback systems with increasing complexity have been designed to control the beam motion in lepton accelerators and colliders with more and more high currents.

In the following, some general consideration on fast bunch-by-bunch feedback systems are presented as well as the present digital electronics trends with special regards to commercially available DSP (Digital Signal Processor) and FPGA (Field Programmable Gate Array) technology. The synergy between development systems and beam-feedback simulators is also highlighted. Old and new DAΦNE bunch-by-bunch feedback systems are described with special attention to the last upgrade of the recent iGp system.

BUNCH MOTION EQUATION

The n-th bunch can be described as an individual harmonic oscillator moving rigidly in the longitudinal plane (energy oscillations), or in the X, Y transverse panes (betatron oscillations) according to the classic harmonic equations. In the longitudinal plane, the dynamic of the system is described by the following equation [1]:

$$\ddot{\tau}_n + 2d_r\dot{\tau}_n + \omega_s^2\tau_n = -\frac{\alpha_c e}{E_0 T_0} V_n^{wk}(t) \quad (1)$$

where τ_n is the arrival time (time delay) of the n-th bunch relative to the synchronous particle, d_r is the natural radiation damping, ω_s is the natural (synchrotron) oscillation frequency, α_c is the momentum compaction, E_0 is the nominal energy, $eV_n^{wk}(t)/T_0$ is the rate of energy loss due to the superposition of the wake forces of the other bunches.

The action of the feedback consists in individual kicks to each bunch increasing the damping term d_r by a voltage opposing to the wake field one. In presence of an active feedback system the equation (1) becomes:

$$\ddot{\tau}_n + 2d_r\dot{\tau}_n + \omega_s^2\tau_n = \frac{\alpha_c e}{E_0 T_0}[V_n^{fb}(t) - V_n^{wk}(t)]$$

where $V_n^{fb}(t)$ represents the feedback kick applied to the bunch n-th at the time t.

FEEDBACK MAIN BLOCKS

To introduce the discussion, in the following section we analyze, as example, the DAΦNE longitudinal feedback system (LFB) consisting of three main blocks (see fig.1); similar considerations can be done for transverse systems. The blocks are the following:

(i) A longitudinal pickup detecting a signal from the bunch passage and sending it to an analog front end followed by a programmable delay, to detect the error signal of each bunch. The function of the programmable delay is to synchronize the output signal of this block with the digital part.

(ii) A digital part, to manage separately the signal of every bunch with individual band-pass filters having a convenient gain and phase response. The global phase response of the feedback must give a 90 degrees phase shift at the dipole frequency to have a damping effect.

(iii) An analog back end (BE) followed by a second programmable delay, power amplifiers, and kicker. The BE programmable delay has the task of synchronizing the peak of the n-th kick with the passage of the n-th bunch through the kicker.

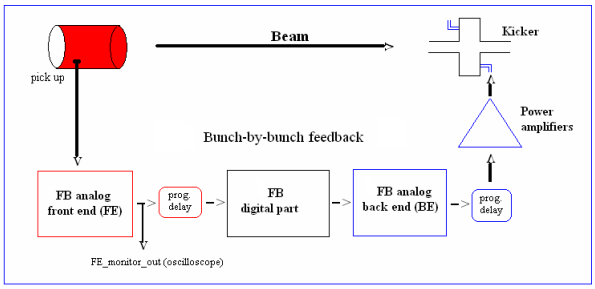

Fig.1 – DAΦNE longitudinal feedback main blocks

In the digital part, the FE output signal is sampled by an analog-to-digital converter working at RF frequency. After this task a demultiplexer separates the signal of each bunch in different slower computing paths.

A digital signal processor (DSP) farm is used to implement band-pass filters [finite impulse response (FIR) or infinite impulse response (IIR)]. Number of taps, gain with sign, center frequency, filter shape, and phase response are programmable by the user looking at the behaviour of the beam. The loaded filters are identical for

all bunches, even if it is possible to run an ‘‘exception’’ filter for just one bunch.

In general, the IIR filter can be described by the following “conceptual” formula in which the output is function of the previous input and output bunch values:

$$y_n = \sum_{k=1}^{N} a_k y(n-k) + \sum_{j=0}^{M} b_j x(n-j)$$

Differently, implementing a FIR filter, the output is function only of the previous input bunch values:

$$y_n = \sum_{j=0}^{M} c_j x(n-j)$$

In general, there are infinite damping solutions for the coefficient a_k, b_j and c_j to be used to solve the motion equation see in the previous paragraph. The damping coefficients can be found experimentally or computed using a model. Amplitude and phase response versus frequency of a FIR filter implemented in the DSP farm for high current beam are shown in the fig. 2. The synchrotron frequency is drawn by a dotted line.

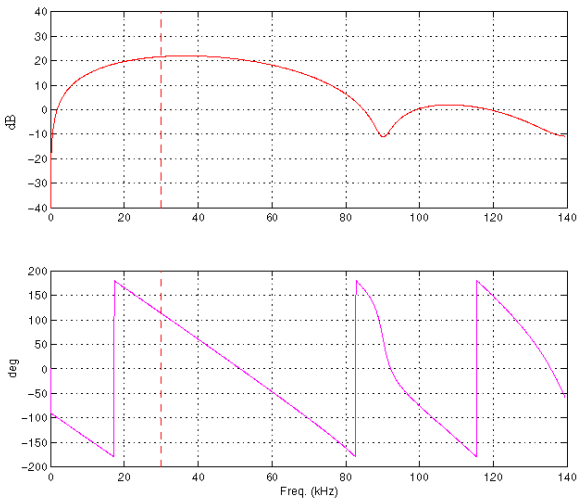

Fig.2 – FIR filter amplitude and phase response versus frequency

PROGRESS IN DIGITAL PROCESSING

As well known, in the last two-three decades, impressive progresses have been done in the digital electronics. DSP (digital signal processor) units are single-chip microprocessors invented in the mid-80’s to process mainly voice and audio signals (.1-10kHz bandwidth). DSP units have dedicated instruction set to perform real time (but at low frequency) signal processing.

As shown in the next paragraph, during the 90’s a SLAC-LBNL-LNF collaboration has built a bunch by bunch longitudinal system (still used) designed around a 16 bits fixed point DSP by ATT.

In the second half of 90’s, the designers watched a new powerful technological improvement: the FPGA (field programmable gate array) units were put on the market. As it is well known, the FPGA’s are digital components with extremely high number of circuits in a single chip and the possibility to be reprogrammed “on the field” any time is necessary. The FPGA’s became so powerful to begin to include PowerPc and many DSP units inside a single component.

The main FPGA producer, Xilinx Inc., foresees the impressing processor performance trend shown in the fig.3 [2]. The Xilinx Virtex-5 SX95T has 640 built-in 18x25 bits DSP allocated in only one chip running at 550Mhz. Powerful software environment makes possible to integrate beam-feedback simulators written in MATLAB language together with the FIR/IIR filter codes downloaded in the real hardware.

To compare the computing power now available, we should consider that the most recent version of digital feedback used at DAFNE is based on the Virtex-II that is shown on the low left side of the fig. 3.

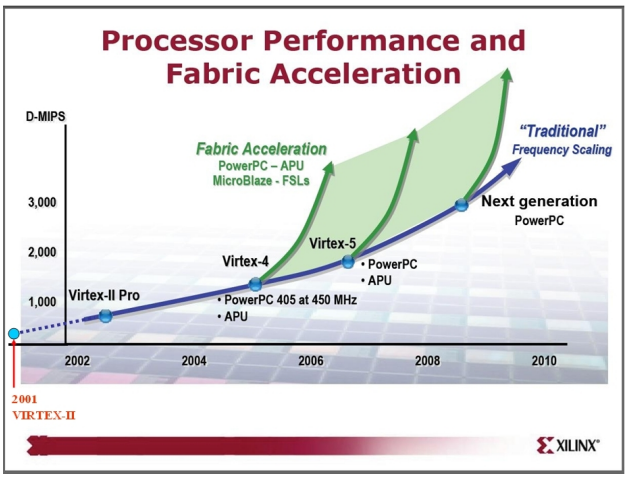

Fig.3 – Xilinx FPGA processor performance

BUNCH-BY-BUNCH DIGITAL FEEDBACK VERSIONS

Looking back at the past feedback versions related to DAΦNE, we will find a first collaboration developing the longitudinal bunch-by-bunch digital feedback in the years 1992-1996 by a SLAC–LBNL-LNF team [3]. This system has still worked in the current year 2008 at PEP-II, DAFNE and ALS. It is based on a VXI crate and with up to 4 VME panels managing 5 DSP boards each. In every VME board 4 DSP units are allocated. In total the system can manage up to 80 DSP and each of them can elaborate up to 32 bunches. This feedback system was designed only to damp longitudinal oscillations and not transverse, because the betatron motion is generally present at too high frequencies.

In the September 2003 a new feedback design has been proposed for both longitudinal and transverse system by J.D.Fox and D.Teytelman at the ICFA’03 Workshop hold at Alghero [4]. This project, called GBoard, is based on at least four FPGA components, probably seven units in total, and is designed to be able to sample at 1.5 GS/sec using an 8 bits analog-to-digital converter. The processing

speed is foreseen to manage the whole flux of data without need of downconversion for the input signals.

The “iGp” (integrated Gigasample processor) system has been developed by a collaboration of KEK-SLAC-LNF starting around 2002-2003 as a ”small” prototype system for the “big” GBoard feedback system.

The iGp feedback system is a baseband bunch-by-bunch signal processing channel designed around a single Virtex-II FPGA by Xilinx.

It can be used for longitudinal and transverse feedback applications in storage rings as well as for bunch-by-bunch diagnostics. The “iGp” system has processed more than 5000 bunch signals sampled at ~500 MHz by an 8bits A/D converter. It uses EPICS as operator interface and distributed control system, working in Linux environment both in the IOC and in the client sides. MATLAB post-processing programs are used to analyze feedback performances and beam instabilities [5].

DAΦNE has 4 “iGp” feedback units currently running on the e+/e- transverse planes. At SLAC D.Teytelman and J.D.Fox have built ~15 units of the “iGp” system, some of them have been planned for working as bunch-by-bunch diagnostics systems. At KEK, M.Tobiyama and T.Obina have built a version the “iGp” system made in Japan, to be used in the longitudinal plane of the B-Factory and in the Photon Factory. Last but not least, at ALS (LBNL) one iGp unit is in phase of installation on the longitudinal plane replacing the old DSP-based system.

The iGp system is evolving fast and the last gateware (FPGA code) and software version has been tested at DAΦNE on the first week of April 2008 by D.Teytelman and myself. All the four iGp systems have been updated to the same software version based on a powerful Fedora rev. 8 Linux client personal computer.

A new important feature is a complete efficient control of the timing setup. This improvement has permitted to remove the Colby delay lines in the front end and the old analog delay lines in the back end stage.

The front-end amplifiers have been also removed in all the transverse planes to have a smaller crosstalk between bunches by using all the frequency band of the sharp input beam pulse. Now the pickup signal, after passing through the H9 hybrids making the difference operation, enters directly in the iGp unit.

The iGp feedback has also, as further features, many diagnostic tools included in the system. As example from the Epics panels it possible to make:

- input signal record with sw trigger from operator i/f;
- grow/damp record with sw trigger from operator i/f;
- data record during the injection using a hw trigger coming from the DAΦNE timing system;

From the off-line MATLAB environment it is possible:

- to store recorded data in a time-stamped database creating two files in .mat format;
- to make post-processing analysis on the database;
- to do beam modal analysis (mode # and grow rate);
- to make injection transient data analysis to study the injection kicker effects versus kicker setup and timing;
- to do bunch-by-bunch tune spread analysis.

As example, in the horizontal e+ plane, grow/damp data have been recorded at 355 mA; the off-line data analysis has shown the presence of a strong -1 mode and an extremely fast damping of the feedback of the order of 2.5 microseconds rate.

The bunch-by-bunch tune analysis, made off-line on data recorded, has shown that a large tune spread along the train can be observed in the horizontal plane while a much smaller tune spread is present in the vertical plane.

Another interesting real time feature is shown in the fig.4. The frequency power spectrum of the beam signal (the low square on the right) is able to show the rejecting frequency corresponding to the betatron tune.

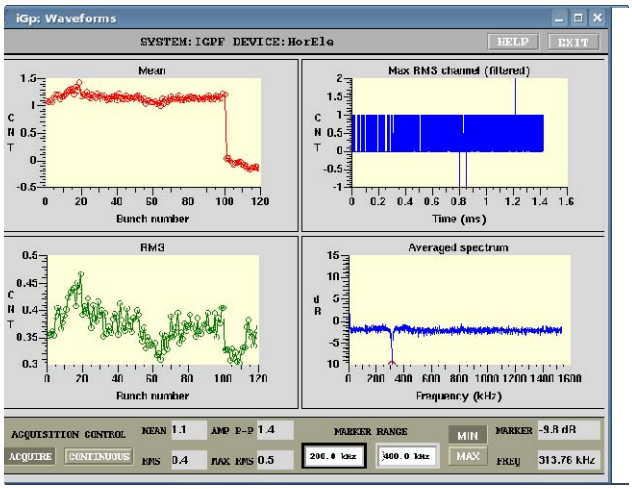

Fig.4 – iGp Waveform panel

CONCLUSION

The FPGA (Field Programmable Gate Array) technology upgrades very fast its performances: this trend should be considered in designing future feedback projects to foresee new features and more powerful capabilities. The iGp (integrated Gigasample processor) feedback is a single FPGA system with many new interesting features. Powerful diagnostics inside the system can help to understand beam current limits and evaluate feedback performances. In DAFNE e+ horizontal plane an extremely fast mode -1 and a large tune spread limit the beam stability and the storable beam current.

REFERENCES

[1] A.Drago, *et al.* "Longitudinal Quadrupole Instability and Control in the Frascati DAFNE e- Ring",PRST-AB,Vol.6,pagg.052801-1/11, 2003.

[2] Xilinx Inc., X-FEST 2007.

[3] J.D.Fox, *et al.* "Operation and Performance of a Longitudinal Damping System using Parallel Digital Signal Processing", EPAC 1994.

[4] J.D.Fox, D.Teytelman, “Multi-Bunch Feedback and High-Current Factories”, presented at “Workshop on e+e- in the 1-2 GeV range”, Alghero, Sept.2003.

[5] D.Teytelman, *et al.*, THPCH103, EPAC2006.

PERFORMANCE OF THE TRANSVERSE COUPLED-BUNCH FEEDBACK SYSTEM IN THE BEPCII STORAGE RING

Junhui Yue*, Li Ma, Jianshe Cao, Lin Wang, IHEP, Beijing, China

Abstract

In order to cure the transverse coupled bunch instabilities due to higher order modes of RF cavities and resistive wall impedance in the BEPCII storage ring, an analog bunch-by-bunch feedback system was designed and used. The main components are two sets of beam oscillation detectors, betatron phase adjuster, notch filter and stripline kicker. This paper will describe system parameters, specifications of key components and experiment results.

INTRODUCTION

BEPCII is an upgrade project of the Beijing Positron Electron Collider (BEPC), in which a new inner ring has been installed inside the old one. BEPCII will provide colliding beams with 910mA at the centre-of-mass energy 1.89GeV in colliding mode. There are 93 bunches in every rings, the bunch spacing is 2ns. In the last commissioning stage, over 500mA beam has been successfully stored in both rings, the colliding luminosity has been reached to 1×10^{32} $cm^{-2}s^{-1}$. When the current reaches to 200mA, strong transverse instabilities occurred in both BEPCII electron and positron rings which limited the maximum storable currents. In order to cure these instabilities, two sets of transverse bunch-by-bunch feedback systems for both rings have been developed and put into operation. The transverse feedback systems suppress the instabilities and make the beams stable to collide.

Table 1: Feedback related parameters of BEPCII rings

Parameters	**value**	**unit**
Energy	1.89	GeV
Circumference	240	m
Bunch current	9.8	mA
Number of bunches	93	
Revolution frequency	1.2621	MHz
RF frequency	499.8	MHz
Radiation damping times	25	ms
Tunes	6.46/7.42	
Most fast rising time of instabilities (ECI)	0.5	ms
Kicker shunt impedance (at 125MHz)	4000	Ω

The system is an analog bunch-by-bunch system in time domain with frequency domain bandwidth of 125MHz. The first operation of the BEPCII rings has suggested that this feedback system can provide 40dB damping of beam oscillation in full bandwidth. Table 1 gives us some feedback related parameters. In this paper, we will describe the design and operation results of this system.

TRANSVERSE FEEDBACK SYSTEM

The idea of transverse feedback system is based on the feedback systems developed in NSLS [1], ALS [2], PLS [3] and KEKB [4]. The BEPCII transverse feedback system consists of pickup electrodes, signal processing electronics, power amplifiers, and a stripline kicker. Figure 1 shows an overview of the transverse feedback system. Two x (or y) signals from pickups located about 90 degrees apart in betatron phase are added together with appropriate coefficients to produce a 90-degree betatron phase shift between the pickup signal and the kicker for arbitrary kicker location and betatron tune. The beam oscillation signal is detected at the third harmonic of the RF (1.5GHz) in order to take advantage of the good sensitivity of the button pickups at this frequency; the signals then are demodulated to the baseband with heterodyne receivers. The DC offset at the pickups is removed by two ways, one is that a fraction of sum signal is added to or subtracted from the beam moment signal, and another is to use a two-tap notch filter. The one-turn delay is provided by coaxial cable. In each ring there is one stripline kicker and four 75-watt power amplifiers for both directions to apply the correction kick signal to the beam.

Front-end electronics

The signals from pickup is firstly divided into three branches by a power combiner and summed up again by another power combiner. Three cables have different length and the difference is the wavelength of the 1.5GHz detection frequency. Two combiner and three cables make up of a very effective FIR filter, the magnitude-frequency characteristic is shown as figure 2. The centre frequency is 1.5GHz and bandwidth is 480MHz. Then the filtered signal passed a hybrid network, the true x and y signal and the sum signal will be produced. The local DC rejection circuit in fixed-voltage mode [4] is used. Some fraction of sum signal is added to or subtracted from the beam moment signal. The magnitude of sum signal is changed by a manual attenuator (here is double balanced mixer) to make the magnitude of the original beam moment signal changing to zero. This circuit can provide 20dB rejection of orbit offset [5]. Subsequently, the signals are down-converted to baseband using heterodyne mode detection.

*yuejh@mail.ihep.ac.cn

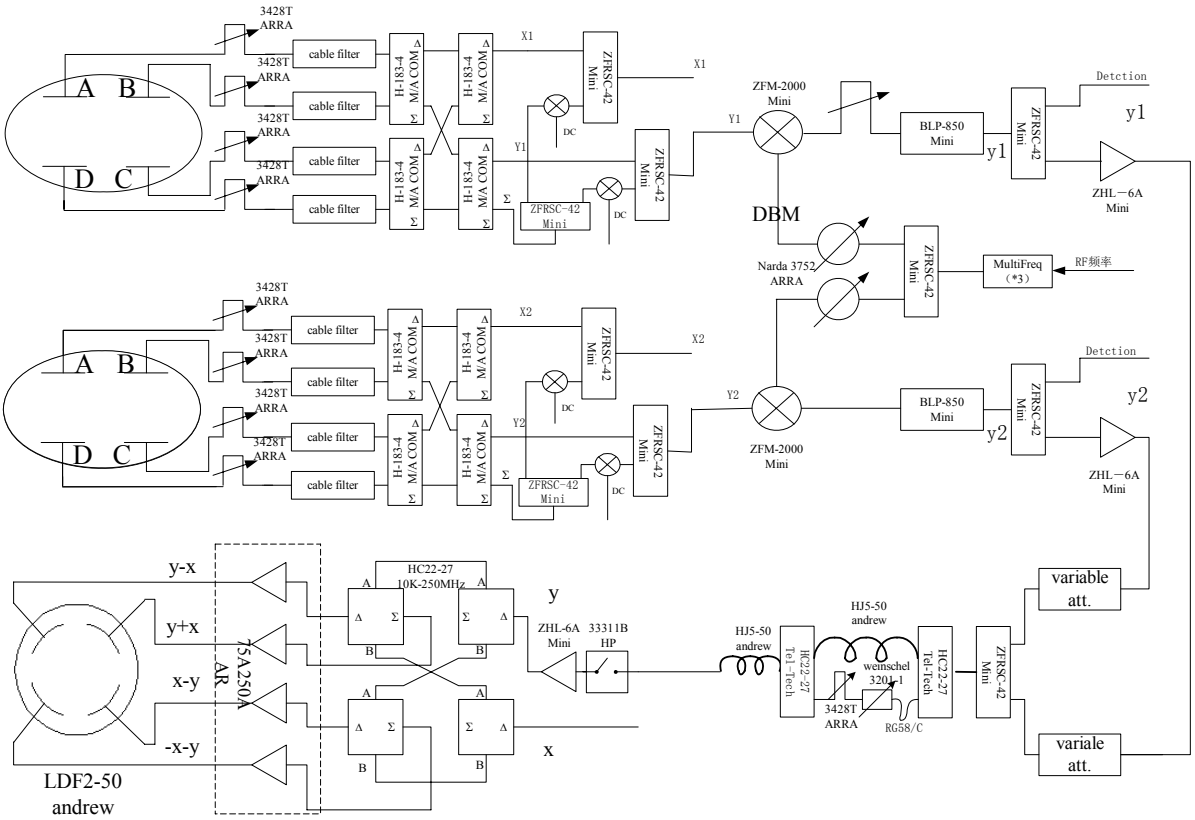

Figure 1: An overview of transverse feedback system of BEPCII.

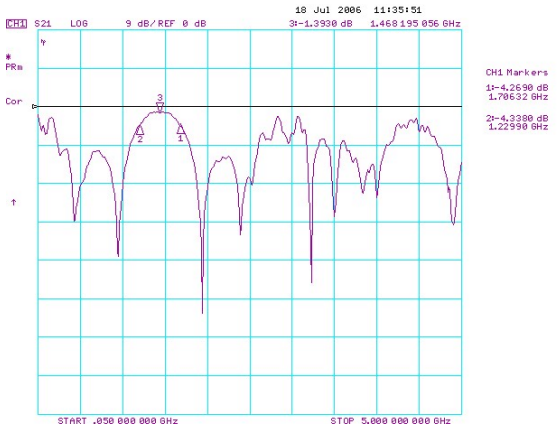

Figure 2: Magnitude-frequency characteristic of three cable filter.

Signal processing system

The two beam pickup signals are attenuated by mechanic attenuators and vector summed. By setting different attenuations of the two beam signals, the phase between the pickup and kicker can be changed in the range of 360 degrees. In order to reject the DC offset signal, a two-tap coax-cable notch filter is used to reject the revolution frequency component. As shown in figure 3, the notch depth reaches up to -41dB. After a long cable for one-turn delay, the output signal from the notch filter is sent to a hybrid network to make a correct signal for the stripline kicker.

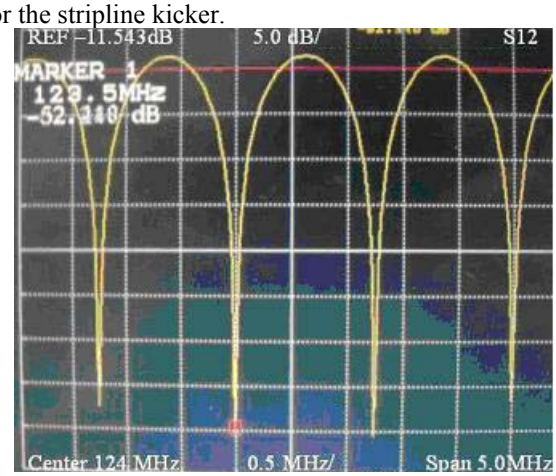

Figure 3: The performance of the notch filter.

Power amplifier and kicker

Four 75-watt AR amplifiers are used for each ring. Each ring has only one kicker with four-stripline for both transverse directions because of the tight space in the rings. The stripline is 600mm (λ/4 of 125MHz) long. All striplines are careful assembled to match 50Ω impedance. 4kΩ shunt impedance is obtained at the frequency of 125MHz. The kicker electromagnetic design has been carried out mainly by means of the Hewlett&Packard

high frequency structure, the test and operation results are good.

Performance of the transverse feedback system

In the last commissioning stage of BEPCII, 500mA beam current has been reached in positron and electron rings, respectively. In any ring, when the beam current is over 200mA, the transverse instabilities occurred and the beam blows up. It can be seen that the sidebands disappears when the feedback is on; the beam profile is stable and then the beam current can be increased again. At last, we can realize 500mA×500mA colliding beams, the luminosity reached the aim we expected.

Fig.4 shows the beam sidebands with the transverse feedback turning off and on. It was measured by a spectrum analyzer when the positron ring operated on the colliding mode at 243mA with 93 bunches. The background frequency lines are revolution frequency harmonics and the dark-coloured lines are instability sidebands. We can see that the magnitude of instability sidebands is attenuated more than 30dB when the feedback is on. Fig.5 shows the beam profiles with the transverse feedback turning off and on.

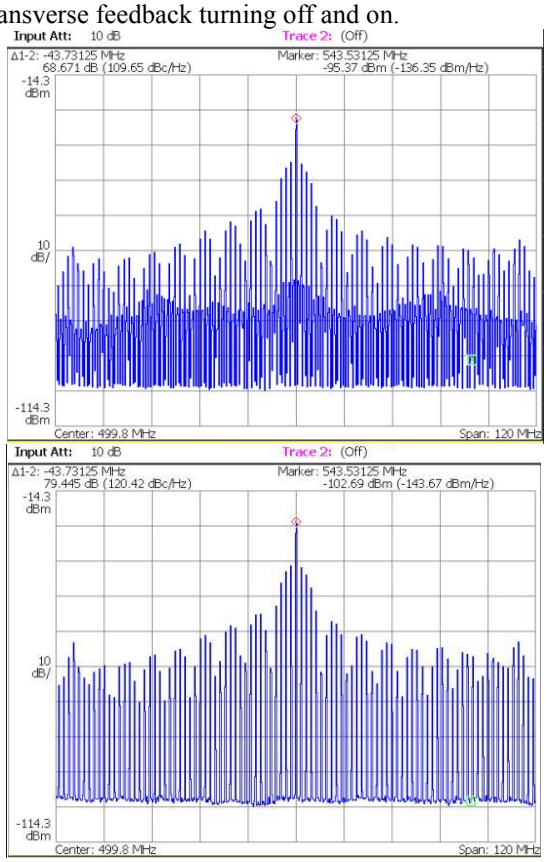

Figure 4: The sidebands of beam with the transverse feedback turning off (upper) and turning on (lower).

SUMMARY

The transverse feedback systems of BEPCII have been installed and played an important role during the commissioning of BEPCII double rings. It can suppress the strong multibunch instabilities at the higher beam current of over 500mA. In the next stage, we need careful tuning the system and make sure of suppressing the transverse instabilities at more higher current. In addition, remote control and damping time measurement will be completed.

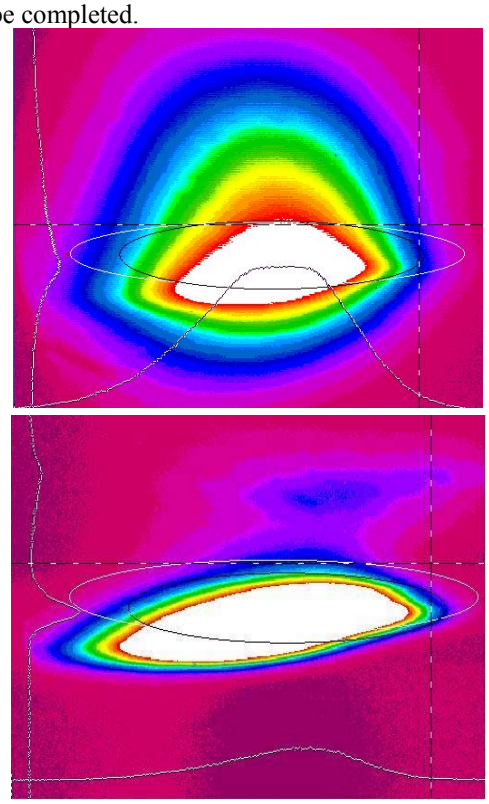

Figure 5: The beam profiles with the transverse feedback turning off (upper) and turning on (lower).

ACKNOWLEDGEMENT

The authors would like to express their sincere appreciations to M.Tobiyama and E.Kikutani for helpful suggestions and thoughtful discussion.

REFERENCES

[1] J.Galayda, “Performance of a Correlator Filter in Betatron Tune Measurement and Damping on the NSLS Booster”, IEEE Transaction on Nuclear Science, Vol. NS-32, No.5, October 1985, p2132-2134.

[2] W.Barry, J.Byrd, J.Corlett et al., “Design of the ALS transverse coupled-bunch feedback system”, PAC1993, Washington D.C., p2109-2111.

[3] J.Y.Huang, M.K.Park, D.T.Kim et al., “Transverse beam feedback system for PLS storage ring”, Nuclear Instruments and Methods in Physics Research, A467-468 (2001), p103-105.

[4] Makoto.Tobiyama, Eiji.Kikutani, “Bunch-by-bunch feedback systems for KEKB Rings”, PAC2001, Chicago, U.S.A., p1246-1248.

[5] W.Barry, J.Corlett, M.Fahmie, “Status of the PEP II transverse feedback systems”, PAC1998, p2344-2346.

THE *SUPERB* ACCELERATOR: OVERVIEW AND LATTICE STUDIES

M.E. Biagini, INFN-Laboratori Nazionali di Frascati, Frascati, Italy
on behalf of the *SuperB* Accelerator Team*

Abstract

SuperB [1] aims at the construction of a very high luminosity (10^{36} cm^{-2} s^{-1}) asymmetric e^+e^- Flavour Factory, with possible location at the campus of the University of Rome Tor Vergata, near the INFN Frascati National Laboratory. In this paper the basic principles of the design and details on the lattice are given.

INTRODUCTION

Attempts to design a Super B-Factory date to 2001. The initial approach at SLAC and KEK had much in common: they were extrapolations of the very successful B-Factory designs, with increased bunch charge, more bunches, and crab cavities to correct for the crossing angle at the Interaction Point (IP). These proposed designs reached luminosities of 5 to 7 x 10^{35} cm^{-2} s^{-1} but had wall plug power of the order of 100 MW. This daunting power consumption was a motivation to adapt linear collider concepts from SLC and ILC to the regime of high luminosity storage ring colliders. Among the possible schemes were a two arcs SLC-like layout and a 2 Linacs (ILC-like) layout.

The implementation of a new colliding scheme [2] with the combination of "large Piwinski angle", low β_y*, ultra low emittances and "*crab waist*" transformation opened new possibilities with the return to the usual two rings layout. This allowed for the design of a *SuperB* Factory with a target luminosity two orders of magnitude higher than presently achieved, by overcoming some of the issues that have plagued earlier super e^+e^- collider designs, such as very high beam currents and very short bunches.

In the most recent *SuperB* design an electron beam (7 GeV, HER) and a positron beam (4 GeV, LER) are stored in two low-emittance damping rings similar to those designed for an International Linear Collider (ILC) or the next generation light source. An ILC style Interaction Region (IR) is included in the rings to produce sub-millimeter vertical beta functions at the collision point. A large crossing angle (+/- 24 mrad) is used at the IP to allow better beam separation. A "*crab waist*" scheme is used to reduce the hourglass effect and restore peak luminosity. Beam currents of the order of 1.9 A can produce a luminosity of 10^{36}/cm^2/s with upgrade possibilities. Such a collider would produce an integrated luminosity of about 10,000 fb^{-1} (10 ab^{-1}) in a running year (10^7 sec) at the Y(4S) resonance. A longitudinally polarized electron beam in the HER, with injection of a transversely polarized electron beam and a spin rotator section, will allow for producing polarized τ leptons, opening an entirely new realm of exploration in lepton flavour physics.

A Conceptual Design Report (CDR) [3] was issued in May 2007, with about 200 pages dedicated to the accelerator design. This report discusses site requirements, "*crab waist*" compensation, parameters optimization in order to save power, IP quadrupole design, Touschek backgrounds, spin rotator scheme, and project costs. As many as 320 scientists from 85 Institutions, spread in 15 countries, have signed the CDR. The contribution to the accelerator design, about 200 pages, came from machine experts from LNF (Italy), SLAC (US), KEKB (Japan), BINP (Russia), BLNL (US) and Cockcroft (UK).

In order to evaluate the proposal, an International Review Committee (IRC) has been established in 2007, chaired by J. Dainton (Daresbury, UK). In November 2007 and April 2008 two IRC meetings were organized for the presentation of the various aspects of the proposal. The final report is due on May 2008. A presentation to the CERN Strategy Group before any formal approval and funding model definition is foreseen for fall 2008, a Technical Design Report (TDR) will be then issued on the time scale of 1.5 years.

A possible location of *SuperB* at Tor Vergata University near Rome, - in synergy with the FEL SPARX project to be built on the same grounds, – is shown in Figure 1.

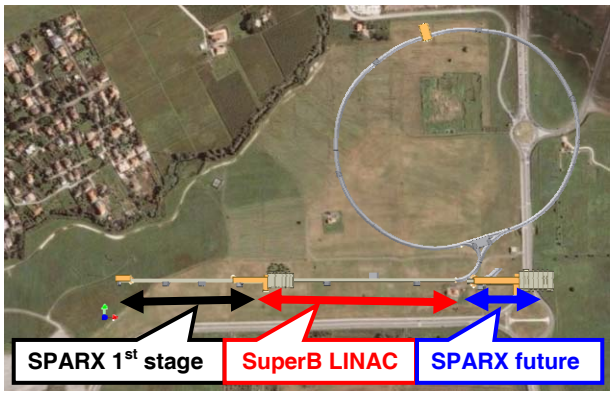

Figure 1: Possible *SuperB* location at Tor Vergata University with a ring circumference of 1800 m and an injector located adjacent to the future SPARX FEL.

*M.E. Biagini, M. Boscolo, R. Boni, A. Drago, S. Guiducci, M. Preger, P. Raimondi, S. Tomassini, C. Vaccarezza, M. Zobov (INFN/LNF, Italy), Y. Cai, A. Fisher, S. Heifets, A. Novokhatski, M.T. Pivi, J. Seeman, M. Sullivan, U. Wienands (SLAC, US), K. Ohmi, Y. Ohnishi (KEK, Japan), I. Koop, S. Nikitin, E. Levichev, P. Piminov, D. Shatilov (BINP, Russia), A. Wolski (Liverpool University, UK), M. Venturini (LBNL, US), S. Bettoni (CERN, Switzerland), E. Paoloni, G. Marchiori (Pisa University, Italy), A. Variola (LAL/Orsay, France)

BASIC CONCEPTS

B-Factories (PEP-II and KEKB) reached very high luminosity (>10^{34} s^{-1} cm^{-2}), but to increase luminosity of about two orders of magnitude borderline parameters are needed, such as:

- very high beam currents;
- smaller damping times;
- very short bunches;
- crab cavities for head-on collision;
- higher power.

However this may result in a difficult and costly operation. On the contrary *SuperB* exploits an alternative approach, with a new IP scheme:

- small beams (ILC-DR like);
- large Piwinsky angle and "*crab waist*" transformation;
- currents comparable to present Factories.

New collision scheme

The novel collision scheme uses frozen variables in parameter space to ascend to a new luminosity scale, by effectively exchanging the roles of the longitudinal and transverse dimensions. The design is based on collision with a "large Piwinski angle" and small beam sizes, plus the so-called "*crab waist*" transformation. In the new scheme, the Piwinski angle ϕ:

$$\phi = \frac{\sigma_z}{\sigma_x}\tan\frac{\theta}{2} \approx \frac{\sigma_z}{\sigma_x}\frac{\theta}{2}$$

(σ_x being the horizontal rms bunch size, σ_z the rms bunch length and θ the horizontal crossing angle) is increased by decreasing the horizontal beam size and increasing the crossing angle. In this way, the luminosity is increased, and the horizontal tune shift due to the crossing angle decreases. The most important effect is that the overlap area of colliding bunches is reduced, as it is proportional to σ_x/θ. Thus, if β_y^* can be made comparable to the overlap area size, several advantages are gained, as small spot size at the IP, i.e. higher luminosity, a reduction of the vertical tune shift, and suppression of vertical synchro-betatron resonances. Moreover the problem of parasitic collisions (PC) is automatically solved by the higher crossing angle and smaller horizontal beam size, which makes the beam separation at the PC larger in terms of σ_x.

However, a large Piwinski angle itself introduces new beam-beam resonances and may strongly limit the maximum achievable tune shifts. This is where the "*crab waist*" innovation is required, boosting the luminosity mainly by suppression of betatron and synchro-betatron resonances, through vertical motion modulation by horizontal beam oscillations. "*Crab waist*" sextupoles near the IR introduce a left-right longitudinal waist position variation in each beam allowing a vertical beta function which is much smaller than the bunch lengths. The "*crab waist*" transformation can easily be realized with two sextupole magnets on both sides of the IP, in phase with the IP in the x plane and at $\pi/2$ in the y plane.

This scheme is being firstly tested at the upgraded DAΦNE Φ-Factory in Frascati, with very encouraging results so far [4]. The details on the scheme features and principles can be found in [5]. Figure 2 shows the left-right *crab waist* compensation at the IP. Figure 3 shows the beam cross sections at the IP with unequal emittances but equal beam-beam tune shifts without and with the crab sextupole transformation.

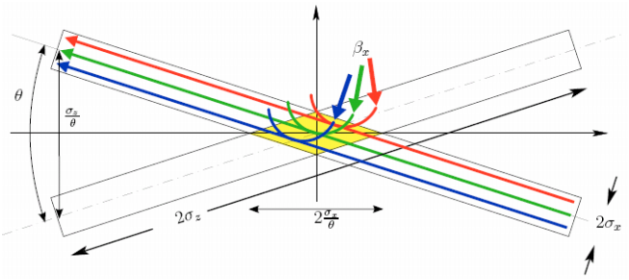

Figure 2: Interaction region showing two beams crossing at a large angle with the *crab waist* to improve the beam-beam interaction.

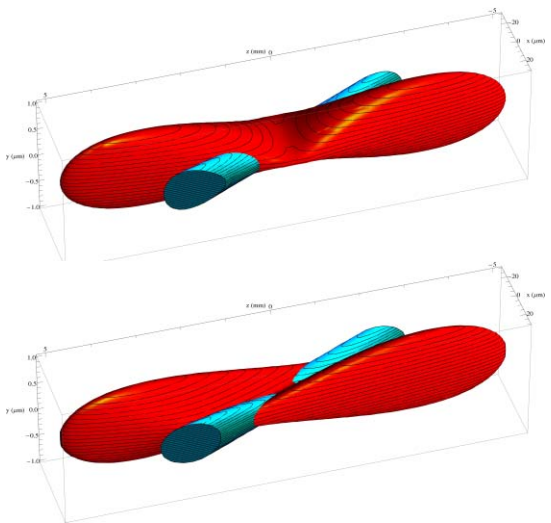

Figure 3: Beam distributions at IP. Top: *crab waist* sextupoles OFF, bottom: crab sextupoles ON.

TRANSPARENCY CONDITIONS

In order to have equal tune shifts for the two beams, asymmetric B-Factories operate at unbalanced beam currents, with a current ratio inverse to the energy ratio. For *SuperB*, with an energy ratio of 4/7 and a large crossing angle, new conditions for having equal tune shifts are possible. LER (+) and HER (-) beams can have different emittances and β^* but equal currents:

$$\xi^+ = \xi^- \Leftrightarrow \frac{\beta_y^+}{\beta_y^-} = \frac{E^+}{E^-} \qquad (1)$$

Then, in order to have equal vertical beam sizes at IP, the LER and HER vertical and horizontal emittances must be:

$$\varepsilon_y^+ = \frac{E^-}{E^+}\varepsilon_y^-, \quad \varepsilon_x^+ = \frac{E^-}{E^+}\varepsilon_x^- \qquad (2)$$

with the horizontal beam sizes in the inverse ratio with the beam energies. Thus, the LER beam sees a shorter interaction region, in a ratio 4/7, with respect to the HER beam. This allows for further β_y* reduction, a larger emittance, increased the Touschek lifetime, and reduced injection rates. Table 1 summarizes *SuperB* beam parameters for the three operational scenarios, nominal, upgrade and ultimate with increasing peak luminosity.

Table 1: *SuperB* main parameters

Parameter (LER/HER)	Nominal	Upgrade	Ultimate
Energy (GeV)	4/7	4/7	4/7
Luminosity ($cm^{-2}s^{-1}$)	$1x10^{36}$	$2x10^{36}$	$4x10^{36}$
C (m)	1800	1800	1800
N. of bunches	1251	1251	2502
F_{RF} (MHz)	476	476	476
N. part/bunch	$5.5x10^{10}$	$5.5x10^{10}$	$6.8x10^{10}$
I_{beam} (A)	1.85/1.85	1.85/1.85	3.7/3.7
β_x* (mm)	35/20	35/20	35/20
β_y* (mm)	0.22/0.39	0.16/0.27	0.16/0.27
ε_x* (nm rad)	2.8/1.6	1.4/0.8	1.4/0.8
ε_y* (pm rad)	7/4	3.5/2	3.5/2
σ_x* (μm)	10/5.7	7/4	7/4
σ_y* (μm)	0.039	0.023	0.023
σ_z (mm)	5./4.3	5./4.3	5./4.3
θ_{cross}(mr)	48	48	48
α_c ($x10^{-4}$)	3.2/3.8	3.2/3.8	3.2/3.8
$\tau_{x,y}/\tau_s$ (ms)	40/20	28/14	28/14
x-tune shift	0.004/0.003	0.006/0.003	0.006/0.003
y-tune shift	0.15	0.20	0.20
RF power (MW)	17	24	50

SUPER-B FACTORY LAYOUT

The two rings each have four arcs and two long straight sections. One straight is for the IR, the other is for diagnostics, RF and injection. The two rings will be crossing in only one IR at a horizontal angle of about 50 mrad and will have ultra low-emittances, similar to those of the ILC Damping Rings [6]. Beam currents will be lower than 2 A per beam, a number close to the achieved currents in the present e^+e^- Factories. The Final Focus (FF) section design is similar to that designed for FFTB/ILC.

RINGS LATTICE

The lattice design is based on the reuse of all PEP-II magnetic elements, vacuum system and RF system (for a total RF power of 17 MW, lower than the PEP-II one). The overall length, including the spin rotator sections, will be about 1.8 Km.

After the CDR completion, the work on the lattice design has continued in order to decrease power consumption and costs, optimize the *"crab waist"* compensation by sextupoles and the FF design. The updated lattice presents a larger horizontal phase advance μ_x in the arc cell, with consequent smaller intrinsic emittance, so that for the nominal phase operation it will not be necessary the insertion of wigglers to reach the emittances and damping times needed. Without wigglers damping times increase by 30% but the RF power decreases, with a net operational costs saving. Beam-beam simulations (see for example in [3], page 211) have studied the degree to which an increase in the damping time affects the luminosity and beam-beam induced tails: an increase by a factor of 2.5 does not lead to any substantial luminosity degradation. In the new lattice the longitudinal damping times are of the order of 20 msec in both rings, about 1.3 times larger than the CDR values but still below the threshold of beam tail growth. Space in the lattice has been provided in each ring for the installation of two wigglers, 40 m long, for the achievement of the emittance and damping times for the upgrade parameters.

LER and HER lattices are very similar: The arcs have an alternating sequence of two different cells: a $\mu_x = \pi$ cell, that provides the best dynamic aperture, and a μ_x = 0.72 cell that has a much smaller intrinsic emittance and provides a phase slippage for the sextupoles pairs, in such a way that one arc corrects all the phases of the chromaticity. As a consequence, the chromatic functions W_x and W_y are lower than 20 and the second order dispersion is almost zero everywhere except in the IR. With this arrangement, the number of arcs can be reduced to 4, with two 40 m long "empty" wiggler sections for the upgrade scenario. With 14 cells in each arc a horizontal emittance of 1.6 nm in HER and 2.8 nm in LER are obtained, the LER lattice having still room for further reduction. The 2 different phase arc cells for HER (top) and LER (bottom) are shown in Fig. 4.

The ring circumference was also shortened, better fitting the proposed construction site. Background studies have continued after the CDR, in synergy with the detector experts, in order to optimize the collimators set for backgrounds reduction and the design of the Final Focus.

Several spin rotation schemes for the e^- beam in HER have been studied to provide longitudinal polarization at the IP, and implementation into the lattice is in progress.

Dynamic aperture and working point optimization for both rings is in progress (see in [7]).

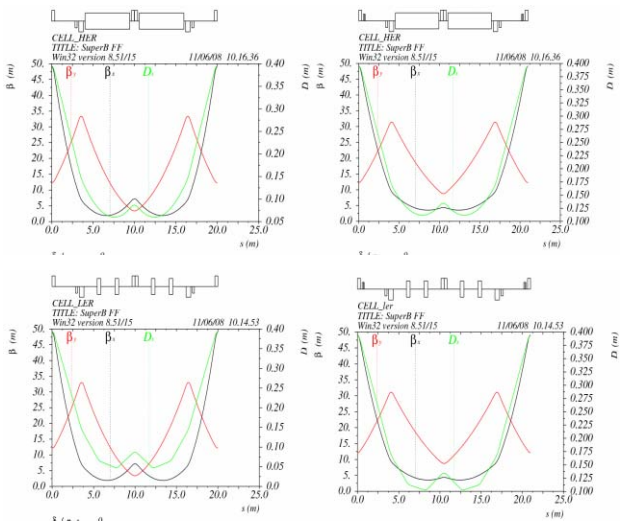

Figure 4: HER (top) and LER (bottom) arc cells: $\mu_x = 0.72$ (left), $\mu_x = 0.5$ (right).

Figure 5 shows the optical functions for the LER ring (HER's being very similar). The spin rotator sections are not included.

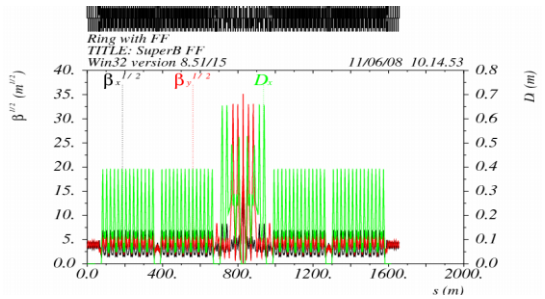

Figure 5: LER optical functions.

INTERACTION REGION

The IR layout (see Figure 6) was designed to leave about the same longitudinal free space for the detector as that presently used by BABAR or BELLE, but with superconducting quadrupole doublets QD0/QF1 as close to the IR as possible.

The Final Focus is based on an ILC/FFTB-like design and complies with all the requirements in terms of high order aberrations correction, needs to be slightly modified for LER to take care of energy asymmetry.

The final doublets must provide a pure quadrupole field on each of the two beams to avoid high background rates in the detector. Because of the small separation of LER and HER beams the influence of each winding on the other one is not negligible and, for the same space limitation, a multi-layer configuration is not suitable to compensate the high order multipoles. A novel helical-type superconducting design has been then studied [8] to compensate the fringe field of one beam line quadrupole onto the other one.

The choice for a finite crossing angle at the IP greatly simplifies the IR design, naturally separating the beams at the parasitic collisions. The beams enter the IP nearly straight to minimize synchrotron radiation and lost particle backgrounds, and are bent more while exiting the IR to avoid parasitic collisions and the resulting beam-beam effects. Half IR optical functions ($\sqrt{\beta}$) are shown in Fig. 7.

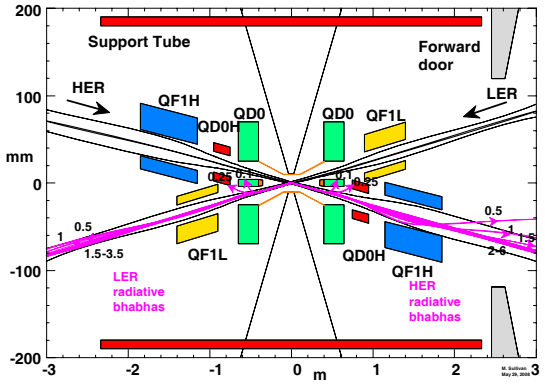

Figure 6: Near IP Interaction Region for two asymmetric beams.

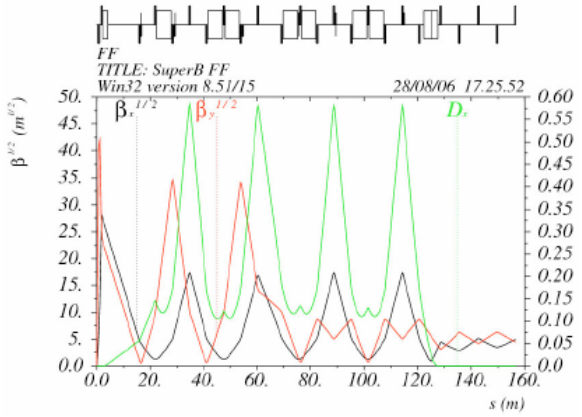

Figure 7: Optical functions in half IR ($\sqrt{\beta}$). IP is at s=0, crab sextupole at s = 140.

POLARIZATION

Polarization of one beam is included in *SuperB*:

- either energy beam could be the polarized one
- the LER would be less expensive, the HER easier

Longitudinal polarization times and short beam lifetimes indicate a need to inject vertically polarized electrons. There are several possible IP spin rotators: solenoids look better at present, since vertical bends will give unwanted vertical emittance growth.

The expected longitudinal polarization at the IP is about 87% (injected beam) x 97% (ring) = 85% (effective).

Several spin rotation schemes for the e^- beam in HER have been studied (see for example in [9]) to provide longitudinal polarization at the IP.

POWER REQUIREMENTS

The power required for this collider is the sum of power for the magnets, RF system, cooling water, controls, and the accelerator operation. The present estimates indicate about 17 MW is needed for the nominal case. These values do not include the campus power requirements or that of the particle physics detector. There are upgrade possibilities for this collider to 2 to 4 times the design luminosity that will require more power. Due to the advantages of the very low emittances and the *crab waist* collision scheme, the power requirements are significantly lower than those of the present B-Factory colliders.

CONCLUSIONS

SuperB is a new machine that can exploit novel very promising design approaches:

- large Piwinski angle scheme will allow for peak luminosity of the order of 10^{36} cm^{-2} s^{-1}, well beyond the current state-of-the-art, without a significant increase in beam currents or shorter bunch lengths;
- "*crab waist*" sextupoles will be used for suppression of dangerous resonances;
- the low beam currents design presents reduced detector and background problems, and affordable operating costs;
- a polarized electron beam can produce polarized τ leptons, opening an entirely new realm of exploration in lepton flavor physics.

SuperB studies are already proving useful to the accelerator and particle physics communities. The principle of operation is being tested at DAΦNE**.**

The baseline lattice, based on the reuse of all PEP-II hardware, fits in the Tor Vergata University campus site, near Frascati.

A CDR is being reviewed by an International Review Committee, chaired by J. Dainton (UK). A Technical Design Report will be prepared to be ready by beginning of 2010.

REFERENCES

[1] M.Giorgi, "The *SuperB* project", this workshop.
[2] P. Raimondi, 2nd LNF Workshop on SuperB, 16-18 March 2006, LNF, Frascati, Italy, also at http://www.lnf.infn.it/conference/superbf06/
[3] *SuperB* Conceptual Design Report, INFN/AE-07/2, SLAC-R-856, LAL 07-15, March 2007, also at http://arxiv.org/abs/0709.0451, 480 pp.
[4] C. Milardi et al, "Crab waist experiment results", this workshop.
[5] P. Raimondi, D. Shatilov, M. Zobov, "Beam-beam issues for colliding schemes with large Piwinski angle and *crab waist*", LNF-07/003 (IR), January 2007.
[6] S. Guiducci, "Damping rings issues", this workshop.
[7] P.Piminov, E.Levichev, "Dynamic Aperture Optimization", this workshop.
[8] E. Paoloni et al, "Design of the QD0 for *SuperB* IR", this workshop.
[9] I. Koop, "Longitudinally polarized electrons in *SuperB*", this workshop.

BEAM-BEAM RESONANCES FOR DIFFERENT COLLISION SCHEMES

D. Shatilov, BINP, Novosibirsk, Russia
for LNF-BINP "Beam-Beam Team" [*]

Abstract

One of the main advantages of proposed by P. Raimondi "Crab Waist" collision scheme [1] is a strong suppression of betatron resonances excited by beam-beam interaction. Some qualitative explanations with numerical examples, describing beam-beam resonances for different collision schemes, were given in [2]. This paper can be considered as an "appendix" (additional illustration) to that one. We performed a number of full 2D betatron tune scans (beam-beam simulations) for different collision schemes, so one can easily see how the beam-beam resonances appear and disappear, depending on the colliding conditions.

INTRODUCTION

Performing a wide range tune scans we cannot avoid a number of serious simplifications. First of all, as our main goal was to investigate beam-beam resonances only, lattice was represented as simple as possible: just a linear 2x2 block-diagonal matrix. We used the same diagonal noise matrix for all working points, providing that the generated emittances (without beam-beam) will be also the same. Of course, this approach is not "realistic", as near the main coupling resonance the vertical emittance must grow. But we simply had no other choice, since all these distortions very much depend on the actual lattice, which we don't know, especially taking into account a huge number of working points tested for each scan (about 40000). On the other hand, there is a clear advantage of such approach: we studied "pure" beam-beam effects without any other nonlinearities, that makes the results clearer and easier to understand.

One more important restriction is bound up with the fact that we performed "weak-strong" simulations. It implies that in the "bad" working points the numbers (luminosity, vertical blowup) are not correct. On the other hand, we don't need exact numbers in the "bad" areas, we need them only in the "good" ones, where blowup is small, and "weak-strong" approach works well there. Besides, we need to know where the "good" and "bad" areas are located in the space of betatron tunes, and "weak-strong" simulations are quite relevant for this purpose.

Also we should mention that Parasitic Crossings and beam tails (lifetime) were not taken into account. Our main concerns were the luminosity and beam core blowup, their dependence on the betatron tunes. The main goal was to illustrate how the resonances excited by beam-beam interaction depend on the colliding conditions (hour-glass, crossing angle, Piwinski angle, Crab Waist). So, the most informative are comparisons of different pictures (scans) and the numbers of maximum luminosities. These comparisons can be not exact in terms of numerical values, but we believe that qualitatively they are quite relevant.

SET OF PARAMETERS

For the basis we took the SuperB set of parameters of 15.11.2006, electrons being the "strong" beam (7 GeV) and positrons – the "weak" one (4 GeV):

Table 1: Nominal set of parameters

Horizontal beta	β^*_x (mm)	20
Vertical beta	β^*_y (mm)	0.30
Horizontal emittance	ε_x (nm)	1.6
Vertical emittance	ε_y (nm)	0.004
Bunch length	σ_z (mm)	6
Energy spread	σ_E	10^{-3}
Synchrotron tune (e+)	ν_s	0.02
Damping decrements	$\alpha_{x,y}$	$1.175\cdot10^{-4}$
Circumference	C (m)	2250
Number of bunches	N_b	1733
Particles per bunch (e–)	N_s	$3.52\cdot10^{10}$
Particles per bunch (e+)	N_w	$6.16\cdot10^{10}$
Crossing angle (full)	θ (mrad)	34
Piwinski angle	ϕ	18
"Nominal" tune shifts	ξ_x, ξ_y	1.26, 3.09
"Actual" tune shifts	ξ_x, ξ_y	0.004, 0.171
Luminosity	L	10^{36}

The definition of Piwinski angle and basic relations for beam-beam tune shifts are given below:

$$\phi = \frac{\sigma_z}{\sigma_x} tg\left(\frac{\theta}{2}\right) \quad \xi_y \propto \frac{N\cdot\beta_y}{\sigma_x\sigma_y\cdot\sqrt{1+\phi^2}} \quad \xi_x \propto \frac{N}{\varepsilon_x\cdot(1+\phi^2)} \qquad (1)$$

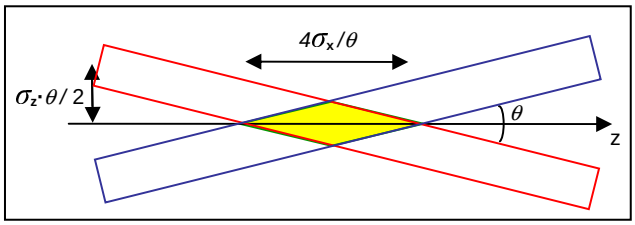

Figure 1: Collision with a crossing angle.

We performed 2D tune scans for the following cases:

- Head-on collisions, different hour-glass: suppressed ($\sigma_z << \beta_y$), normal ($\sigma_z = \beta_y$), and enhanced ($\sigma_z >> \beta_y$).
- Collisions with small Piwinski angle: from 0.2 to 1.2.
- Collisions with large Piwinski angle and different β_y: large (equal to σ_z) and small (equal to σ_z/ϕ), with and without Crab Waist.

We tried to keep the nominal set of parameters as close as possible. However, for head-on and small Piwinski angle

collisions we had to change some parameters in order to obtain acceptable tune shifts. The idea was to keep the ξ value close to the limit in "good" areas, in this case the pictures of resonances will be the most clear and informative. It should be noted that collisions with changed parameters were not optimized for themselves: we made only minimal changes to get the "correct" ξ value. As we did not take into account PCs, the number of bunches was used only for the total luminosity calculation. We assumed the same N_b in all our simulations, that obviously was very optimistic for head-on and small Piwinski angle collisions. The idea was to compare single bunch luminosities, but renormalized to the total luminosity as for SuperB.

HEAD-ON AND HOUR-GLASS

First of all, β^*_y must be increased by a factor of 20 to match the bunch length. Also, we decided to have the same β^*_x/β^*_y ratio, the same bunch length and bunch current. If the emittances would be also the same, the "nominal" $\xi_{x,y}$ would not change as well. But we need to reduce them to acceptable values, let's say ξ_y=0.07. To achieve this, we increased both emittances by a factor of 44. In this case ξ_x=0.0286, and the same crossing angle of 34 mrad would result in Piwinski angle ϕ = 0.6. Simulation results for the "nominal" hour-glass ($\sigma_z=\beta_y$) are shown on Fig. 2 (a,b,c). The "geographical map" colors are used there: red corresponds to the maximum luminosity, blue – to the minimum.

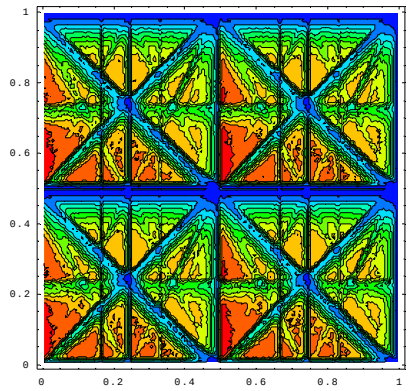

Figure 2a: $\sigma_z=\beta_y$, $L_{max} = 2.45\cdot10^{34}$

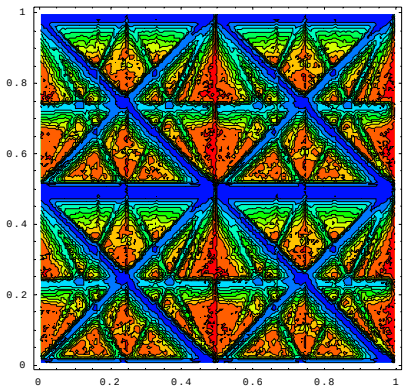

Figure 2b: $\sigma_z=\beta_y$, inverse vertical blowup

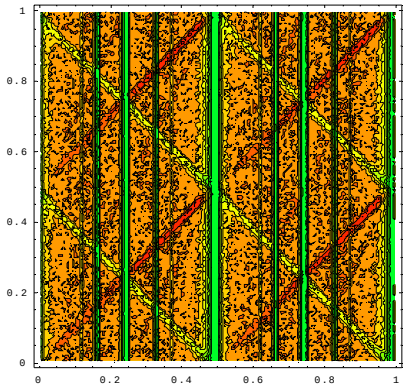

Figure 2c: $\sigma_z=\beta_y$, inverse horizontal blowup

The X-Y betatron resonances appear due to the vertical beam-beam kick's dependence on the horizontal particle's coordinate (amplitude modulation). The horizontal kick also depends on the vertical coordinate, but for the flat beams this dependence is much weaker. The luminosity plot combines both the vertical and horizontal blowups, but for high-order resonances it is better to look at the vertical blowup plot. Resonances $L\cdot\nu_x + M\cdot\nu_y = K$ (L, M – even numbers) are shown on Fig. 3, red lines – up to 4th order, green – 5th and 6th orders. All these resonances are clearly seen on Fig. 2.

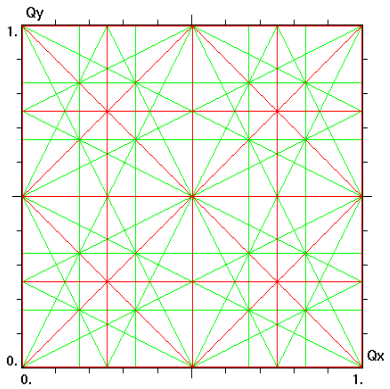

Figure 3: Resonance lines up to 6th order.

Hour-glass effect appears due to Collision Point (CP) longitudinal shift for particles with non-zero Z coordinate. Here CP is a point where a particle meets the center of the opposite bunch, see Fig. 4.

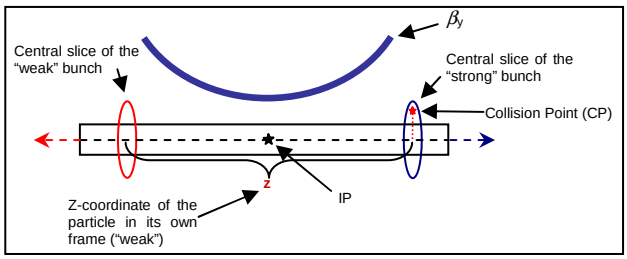

Figure 4: Hour-glass effect

Since β_y has a minimum at the IP, ξ_y increases when CP is shifted. Synchro-betatron resonances appear due to the vertical betatron phase modulation at CP and amplitude modulation (ξ_y dependence on CP). Strength of these

resonances strongly depends on synchrotron tune: the larger – the worse. On the other hand, the vertical betatron phase averaging over the Interaction Region (IR) results in high-order vertical resonances suppression. Simulation results for suppressed hour-glass are shown on Fig.5 (a,b).

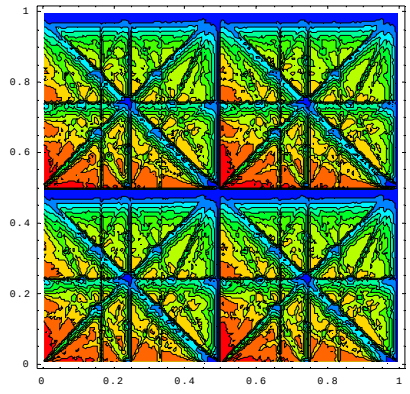

Figure 5a: $\sigma_z=\beta_y/100$, $L_{max} = 3.17\cdot10^{34}$

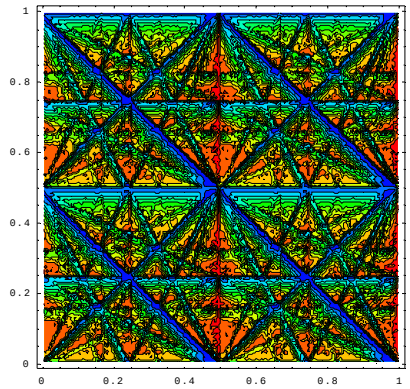

Figure 5b: $\sigma_z=\beta_y/100$, inverse vertical blowup

As we can see, luminosity increases due to geometrical factor and resonance lines become thin, since the synchro-betatron satellites disappeared. On the other hand, more high-order resonances become visible, since the vertical betatron phase averaging disappears, so a particle feels a "solid" kick in a constant phase. Simulations for enhanced hour-glass effect are shown on Fig. 6 (a,b).

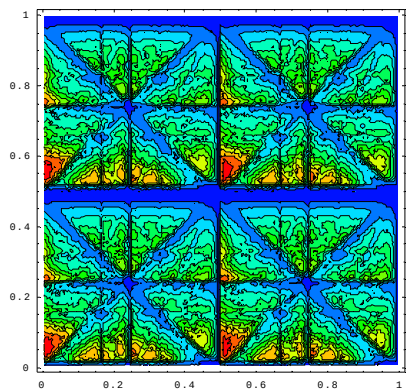

Figure 6a: $\sigma_z=\beta_y\cdot3$, $L_{max} = 1.62\cdot10^{34}$

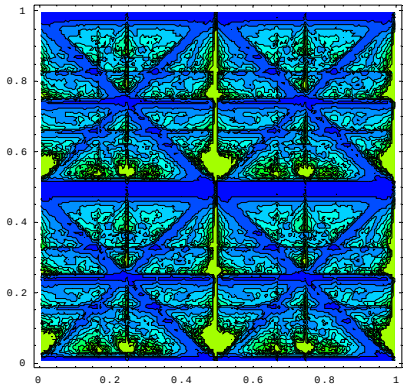

Figure 5b: $\sigma_z=\beta_y\cdot3$, inverse vertical blowup

Here luminosity decreases due to geometrical factor, and synchro-betatron resonances become much stronger: more satellites, wider resonance lines. So, we cannot find any working point without strong vertical blowup. Taking into account the beam tails, situation looks even worse. Actually it means that the beam-beam tune shift exceeds the limit and must be decreased.

SMALL PIWINSKI ANGLE

In collisions with a crossing angle the horizontal coordinate of CP (in the strong bunch's coordinate frame) depends on its longitudinal coordinate, see Fig. 6. As a result we obtain amplitude modulation of both horizontal and vertical beam-beam kicks by the particle's synchrotron oscillations, thus exciting strong synchro-betatron resonances. One more important consequence of the crossing angle: it breaks the X-symmetry, so the betatron resonances $L\cdot\nu_x + M\cdot\nu_y = K$ with odd L numbers appear. In particular, low-order resonances $\nu_x \pm 2\nu_y = k$ become very strong.

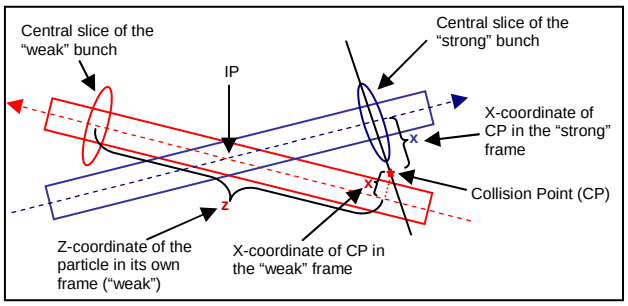

Figure 6: Collision with a crossing angle.

When increasing the crossing angle, luminosity and actual tune shifts decrease due to geometrical factor. Betatron resonances $\nu_x \pm 2\nu_y = k$ become stronger since they need X-asymmetry. On the other hand, "old" betatron resonances (as for head-on) become weaker since the horizontal coordinate of CP (in the strong bunch's coordinate frame) now depends more on the particle's longitudinal coordinate and less on its horizontal betatron coordinate. See the simulation results on Fig. 7 (a, b, c).

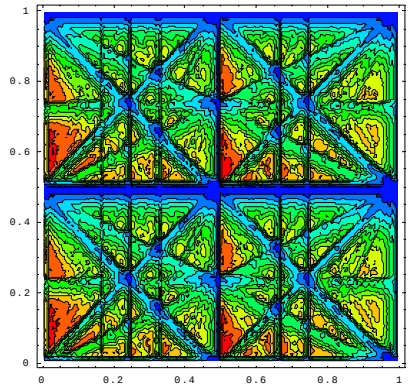

Figure 7a: $\phi = 0.2$, $L_{max} = 2.38 \cdot 10^{34}$

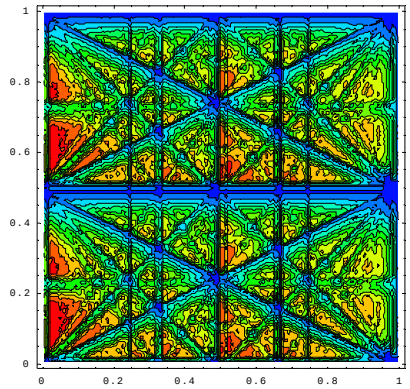

Figure 7b: $\phi = 0.6$, $L_{max} = 2.05 \cdot 10^{34}$

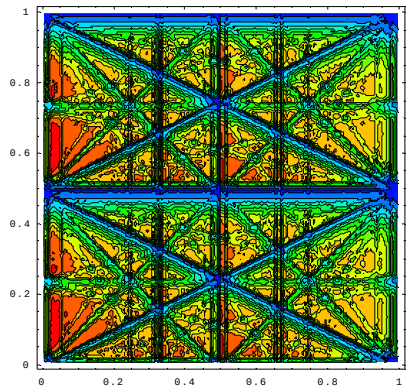

Figure 7c: $\phi = 1.2$, $L_{max} = 1.61 \cdot 10^{34}$

LARGE PIWINSKI ANGLE

In general, it looks like the larger Piwinski angle – the worse, but for $\phi >> 1$ we need to change the concept of CP, and this makes a difference. Indeed, for large horizontal separations (in units of σ_x) the vertical beam-beam kick drops as $1/R^2$, while the horizontal one drops as $1/R$. It means that for the vertical kick the center of the opposite bunch becomes not so important and can be not seen at all by the particles with large longitudinal displacements due to large horizontal separation. Thus CP has to be defined in a different way: it is *the point where a test particle crosses the longitudinal axis of the opposite beam*. In particular it means that the X-coordinate of CP in the "strong" frame is always zero, by the definition.

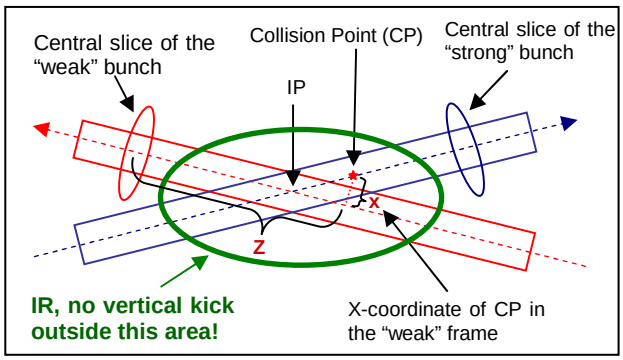

Figure 8: Collision with large Piwinski angle.

Now we simply return back to small emittances and β_x, as specified in Table 1, thus obtaining Piwinski angle ϕ=18. For the beginning we did not change β_y and keep it equal to the bunch length – just to see the effect of the new CP concept. However, we decreased the bunch current by a factor of ten in order to keep acceptable tune shifts. Since the distance between IP and CP is negligible as compared to β_y, the vertical beam-beam kick's dependence on the particle's X-coordinate becomes very small. This makes X-Y betatron resonances much weaker than even in the ordinary head-on collisions, see Fig. 9.

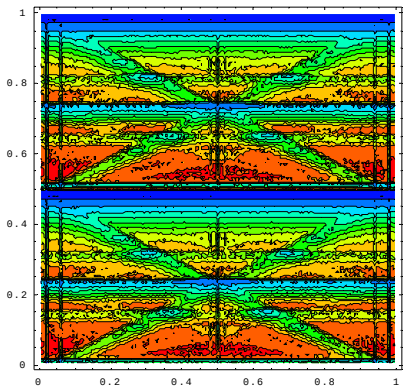

Figure 9: Luminosity, ϕ=18, $\beta_y = \sigma_z$

The next step is decreasing the β_y to its "nominal" value (see Table 1), to fit the overlapping area. Since the shift of CP due to X-betatron oscillations becomes now comparable with β_y, the vertical betatron phase at CP and

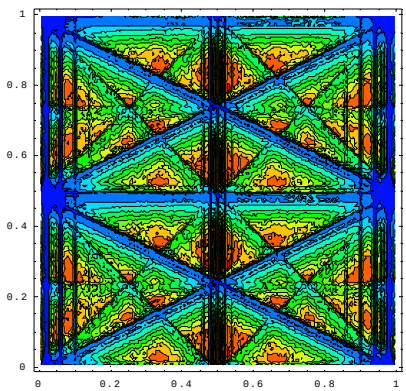

Figure 10: $\beta_y = 0.3$ mm, $L_{max} = 1.6 \cdot 10^{35}$

ξ_y are strongly modulated, thus exciting X-Y betatron resonances again. Actually, this is rather similar to synchro-betatron resonances exited by the hour-glass effect in head-on collisions. Simulation results are shown on Fig. 10. Here all the parameters are the same as listed in Table 1, except the bunch current which was reduced by a factor of 2.5 to get acceptable tune shifts (without Crab Waist). If we compare Figures 7b and 10, they look rather similar, but there are some differences. In the case of large ϕ the horizontal synchro-betatron resonances are enhanced, while the vertical ones are suppressed [4], as well as horizontal betatron ones. As for X-Y betatron resonances, their strength and width also changed, since the sources are different. For small ϕ it is an amplitude modulation of the vertical kick, coming from its dependence on X-coordinate. For large ϕ the main source is the Y-betatron phase modulation, plus amplitude modulation coming from ξ_y dependence on X-coordinate (due to hour-glass).

Finally, we introduce the Crab Waist (CW), which kills the vertical betatron phase modulation. According to [2]

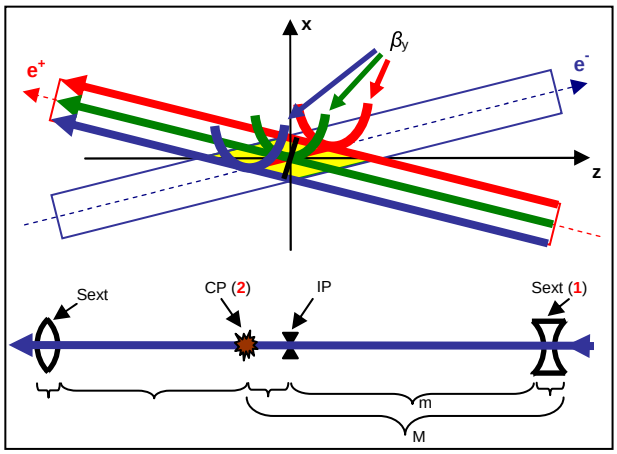

Figure 11: Crab Waist scheme.

the transport matrix ***M*** (see Fig. 11) from the entrance of the first sextupole (point 1) to the CP (point 2), vertical betatron motion only, can be written as:

$$M = \begin{pmatrix} 1 & L \\ 0 & 1 \end{pmatrix} \cdot \begin{pmatrix} m_{11} & m_{12} \\ m_{21} & m_{22} \end{pmatrix} \cdot \begin{pmatrix} 1 & 0 \\ V & 1 \end{pmatrix} \qquad (2)$$

where the first matrix corresponds to the drift space from IP to CP, L being the drift length, the last matrix corresponds to the sextupole, considered here as a thin linear lens, and in the middle is the unperturbed matrix ***m*** from the sextupole location to the IP. For this unperturbed matrix we have $m_{22} = 0$, since $\alpha_y = 0$ at the IP and $\Delta\mu_y = \pi/2$. As a result we get $M_{22} = 0$ as well. On the other hand, considering the "new" lattice (sextupoles included) we can write the standard formula for M_{22}:

$$M_{22} = \sqrt{\beta_y / \beta_{1y}} \cdot \left(\cos(\Delta\mu_{1y}) - \alpha_{1y} \cdot \sin(\Delta\mu_{1y})\right) \qquad (3)$$

where β_{1y} and α_{1y} are the beta- and alpha-functions at the CP. Since it is the waist at the CP, α_{1y} must be equal to zero, so we get $\cos(\Delta\mu_{1y}) = 0$, resulting in $\Delta\mu_{1y} = \pi/2$, that is exactly what we wanted. In the other words, the vertical betatron phase advance from the first sextupole to CP and then from CP to the second sextupole remains to be $\pi/2$ for all the particles independently on their X-coordinate. This feature allows increasing the beam-beam tune shift by a factor of about 2.5! Thus we return to the nominal bunch current (see Table 1). Simulation results for the nominal waist rotation are shown on Fig. 12.

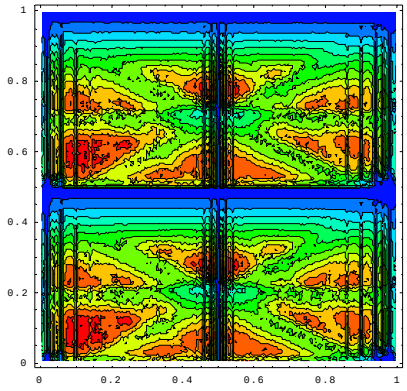

Figure 12: CW = 1, $L_{max} = 1.03 \cdot 10^{36}$

Now let us consider an amplitude modulation of the vertical beam-beam kick caused by the β_y modulation at the CP. The vertical tune shift depends on both "weak" and "strong" betas, as follows:

$$\xi_y \propto \frac{\beta_{yw}}{\sqrt{\varepsilon_{ys} \cdot \beta_{ys}}} \qquad (4)$$

Here in the numerator we have "weak" β_y, and in the denominator – "strong" beam size. Without Crab Waist both betas at the CP are actually the same, the difference is negligible when $\theta << 1$. It means that ξ_y scales as $(\beta_{ys})^{1/2}$. In the CW scheme $\beta_{yw} = const$ at the CP, so ξ_y scales as $(\beta_{ys})^{-1/2}$, that is inverse dependence of the one without CW, see Fig. 13. This means that if the waist rotation is smaller than the nominal value, the amplitude modulation should decrease while some phase modulation appears again. From here we can conclude that there is some optimum waist rotation angle, as a compromise between amplitude and phase modulations, which should depend on the other parameters (ξ, ϕ, etc.). Usually the optimum lies somewhere in the range of 0.6 to 0.8 of the nominal value.

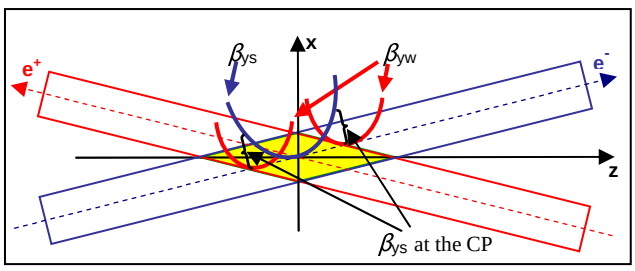

Figure 13: "weak" and "strong" betas at the CP with CW.

In order to check the Crab Waist idea we performed special simulations without β_{ys} modulations. This was

achieved by increasing β_{ys} by a factor of 100 and decreasing the "strong" vertical emittance ε_{ys} by the same factor, so the vertical beam size was not changed. In these conditions the optimum waist rotation must be shifted to the nominal value, and it was completely confirmed by our simulations. These rather specific simulations, of course, were not realistic, as the "weak" and "strong" beam parameters were very different. The only goal was to demonstrate how the X-Y betatron resonances are suppressed by the Crab Waist. The luminosity tune scans for these conditions without and with Crab Waist are shown on Fig. 14 (a, b).

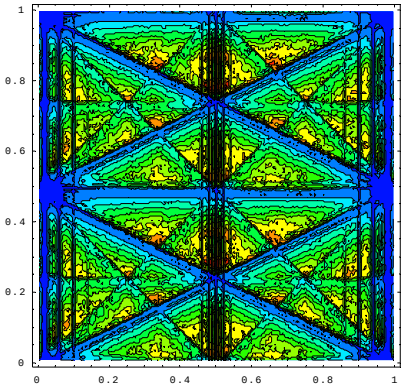

Figure 14a: CW=0, without β_{ys} modulations.

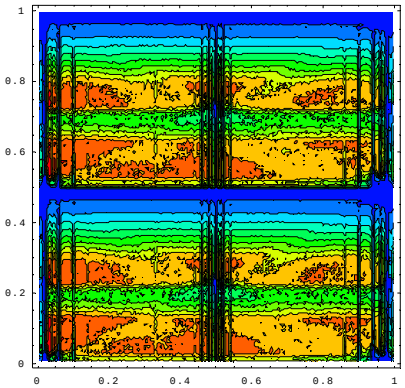

Figure 14b: CW=1, without β_{ys} modulations.

As one can see, without Crab Waist removing the β_{ys} modulations did not help at all, but with Crab Waist it results in actual vanishing of all X-Y resonances. We still can see the resonances $\nu_x \pm 2\nu_y = k$, but they became rather weak (note the color!). Though they look wide, it is simply due to a very large tune shift: $\xi_y = 0.17$. Also, this is the reason of "shifting" the resonances down.

Finally, we performed a tune scan for the nominal set of parameters with the optimal waist rotation, see Fig. 15. The optimal CW value can be recognized even clearer when performing the beam tails simulation [2]. As for the luminosity scan, the resonances $\nu_x \pm 2\nu_y = k$ become more emphasized for CW=0.8 (Fig. 15) as compared to CW=1 (Fig. 12), but on the other hand the "good" areas become larger for CW=0.8, especially the ones close to half-integer resonances.

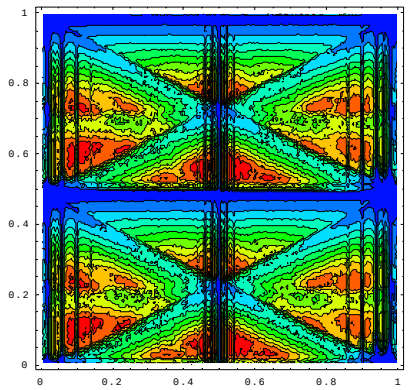

Figure 15: CW=0.8, $L_{max} = 1.05 \cdot 10^{36}$

CONCLUSIONS

We performed a number of beam-beam simulations for different collision schemes. The main sources of beam-beam resonances which affect the equilibrium particles distribution were recognized, and the luminosity tune scans allowed their clear visualization and identification.

The collision scheme with large Piwinski angle and Crab Waist looks the most promising, since it makes the X-Y modulations much smaller as compared to head-on collision scheme, thus the beam-beam limit ξ_y can be significantly increased, that was confirmed by the recent experimental results obtained on DAFNE [5].

ACKNOWLEDGEMENTS

All these simulations were performed on **lxcalc** cluster (LNF-INFN, Frascati, Italy). Thanks to LNF Computing Division for their support!

REFERENCES

[1] P. Raimondi, "Status on SuperB Effort", presentation at the 2nd Workshop on Super B-Factory, 2006, http://www.lnf.infn.it/conference/superb06/talks/raimondi1.ppt

[2] P. Raimondi, D. Shatilov, M. Zobov, "Beam-Beam Issues for Colliding Schemes with Large Piwinski Angle and Crabbed Waist", Preprint LNF-07/001, 2007, arXiv:physics/0702033.

[3] "SuperB Conceptual Design Report", 2007, arXiv:0709.0451.

[4] D.Pestrikov, "Vertical Synchrobetatron Resonances due to Beam-Beam Interaction with Horizontal Crossing", Nucl. Instr.&.Meth., A336:427-437, 1993.

[5] C.Milardi et al., "Crab Waist experiment results", this Workshop.

[*] P.Raimondi, M.Zobov (LNF, Frascati, Italy); D.Shatilov (BINP, Novosibirsk, Russia).

THE PROJECT OF T-CHARM FACTORY WITH CRAB WAIST IN NOVOSIBIRSK

A.Blinov, A.Bogomyagkov, A.Bondar, V.Kiselev, I.Koop, G.Kurkin, E.Levichev, P.Logachev, S.Nikitin, I.Okunev, V.M.Petrov, P.Piminov, Yu.Pupkov, D.Shatilov, S.Sinyatkin, V.Smaluk, A.Skrinsky, P.Vobly, BINP, Novosibirsk, Russia

Abstract

The project of a new-generation t-charm factory is now under consideration in Novosibirsk. A novel approach of the Crab Waist collision scheme allows reaching the luminosity of $1\div2\times10^{35}$ $cm^{-2}s^{-1}$. The other features of the facility are: variable energy from 2 GeV to 4.5 GeV (c.m.), longitudinal polarization of electrons at IP, usage of damping wigglers to keep high luminosity for all energy levels, etc. We discuss some of the challenges and opportunities available with the development of the project.

INTRODUCTION

A tau-charm factory can study the issues concerning the tau leptons, charmed particles, and light quark spectroscopy in a unique manner. Many of these issues can only be addressed to a t-charm factory and may not be substituted by the successfully operating B-factories.

A number of different projects of TCF were discussed in the '90s of the last century [1-6]. All these projects had more or less similar features: the maximum luminosity around 10^{33} $cm^{-2}s^{-1}$ and the single beam energy variable in the range ~1÷3 GeV. One of the representatives of this family, the Beijing Tau Charm Factory, has already started its operation.

In 1995 BINP also released a conceptual design of t-charm factory [7]. In the framework of the BINP TCF project, a new e^+e^- injection facility has been launched. An excavation work of the TCF main halls and tunnels was started in 1996 but then it was frozen. However, recently we decided to revive the TCF project in Novosibirsk and this time our optimism was inspired by (a) the invention of the Crab Waist collision concept that allows increasing the luminosity by factor of 10÷100 and (b) the exciting results from the B-factories, which enhance significantly an interest to the physics of charmed particles.

The following task list was formulated for the new TCF project:

- D-Dbar mixing
- CP violation search in charm decays
- Study of rare and forbidden charm decays
- Standard Model tests in tau lepton decays
- Searching for lepton flavor violation
- CP/T violation search in tau lepton decays
- Production of polarized anti-nucleons

This experimental program can be carried out at a facility with the basic features listed below:

- Collision energy from 2 GeV to 4.5 GeV (anti-nucleons – J/psi – charm barions)
- The luminosity $\geq10^{35}$ $cm^{-2}s^{-1}$
- Electrons polarized longitudinally at IP
- No energy asymmetry is required
- No beam monochromatization is required
- An accuracy of energy calibration ~5×10^{-4} can be achieved with the Compton back scattering technique realized at VEPP-4M [8], so the beam transverse polarization is not required.

Other constraints include the correspondence of the new factory performance with the capability of the injection facility, which is now entering the commissioning stage and matching of underground tunnels and halls already constructed for the previous TCF design.

CRAB WAIST COLLISION SCHEME

One of the key requirements of high luminosity colliders is extremely small β_y at the IP. But β_y cannot be made much smaller than the bunch length without encountering a "hourglass" effect, so this imposes a rigid limitation on the bunch length. But, unfortunately, it is very difficult to shorten the bunch length σ_z in a high current ring without facing the instabilities.

This problem can be overcome with the recently proposed Crab Waist collision scheme [9], which can substantially increase luminosity without the bunch length decrease, since it combines several potentially advantageous ideas. The first idea is the use of a large Piwinski angle

$$\phi = \frac{\sigma_z}{\sigma_x}\tan\frac{\theta}{2} \approx \frac{\sigma_z}{\sigma_x}\frac{\theta}{2},$$

where θ is the horizontal crossing angle, σ_z and σ_x are the rms bunch length and the horizontal beam size, respectively.

For collisions at the crossing angle ϕ, the luminosity L and the tune shifts ξ_x and ξ_y scale as [10]:

$$L \propto \frac{N\,\xi_y}{\beta_y} \propto \frac{1}{\sqrt{\beta_y}},$$

$$\xi_y \propto \frac{N\,\beta_y}{\sigma_x\sigma_y\sqrt{1+\phi^2}} \propto \sqrt{\beta_y} \quad \text{and} \quad \xi_x \propto \frac{N}{\varepsilon_x(1+\phi^2)},$$

where N is the number of particles per bunch, ε_x is the horizontal emittance and σ_y is the vertical rms beam size at IP. We consider here the case of flat beams, small horizontal angle $\theta << 1$ and large Piwinski angle $\phi >> 1$.

In the Crab Waist collision scheme, the Piwinski angle is increased by decreasing the horizontal beam size and increasing the crossing angle. In this way, the luminosity grows, and the horizontal tune shift due to the crossing angle decreases.

The most important effect is that the overlap area of colliding bunches is reduced, as it is proportional to σ_z/θ and β_y can be made comparable to the overlap area size (i.e. much smaller than the bunch length):

$$\beta_y \approx \frac{\sigma_x}{\theta} << \sigma_z.$$

A smaller spot size at IP and reduction of the vertical tune shift can be achieved at the same time, providing an increase in luminosity inversely proportional to β_y.

The main advantage in such a collision scheme is that the bunch length must not be shortened to increase the luminosity. This will certainly ease the problems of HOM heating, coherent synchrotron radiation of short bunches, excessive power consumption, etc.

However, a large Piwinski angle itself introduces new beam-beam resonances and may limit the maximum achievable tune shifts (see, for example, [11, 12]). This is where the Crab Waist innovation is required. The Crab Waist transformation boosts the luminosity, mainly by suppression of betatron (and synchrobetatron) resonances that usually arise through the vertical motion modulation by horizontal beam oscillations [13]. In this scheme the modulation becomes significantly smaller as compared to the head-on collision scheme, thus, the beam-beam limit ξ_y increases by a factor of about 2-3.

A sketch of the Crab Waist scheme is shown in Fig.1.

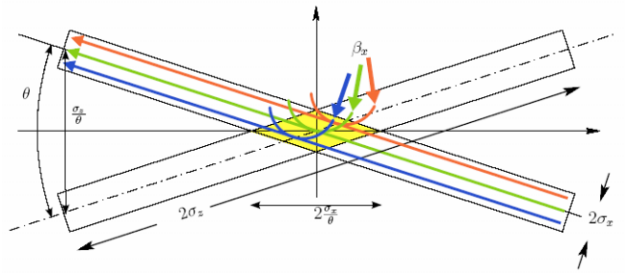

Fig.1 Sketch of large Piwinski angle and Crab Waist scheme. The collision area is shown in yellow.

The Crab Waist correction scheme is realized in practice with two sextupole magnets in phase with the IP in the x plane and at π/2 in the y plane, on both sides of the IP, as shown in Fig.2.

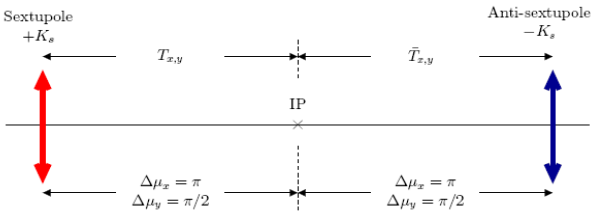

Fig.2 Scheme of Crab Waist correction by sextupoles

The position of such sextupoles in the ring lattice has to be studied with great care, minimizing nonlinearities that may induce a reduction of the ring dynamic aperture.

Recently the Crab Waist concept was proven experimentally at DAΦNE in Italy [14].

PHYSICS CHALLENGES

A schematic view of the TCF layout is shown in Fig.3. A two-ring configuration with the racetrack rings, single collision point and a system of the emittance damping and excitation wigglers is considered. A circumference of the machine is around 850 m, a straight section length is ~150 m and the arcs radius is ~90 m. In the design of the injection complex we use the already existing facilities and engineering infrastructures.

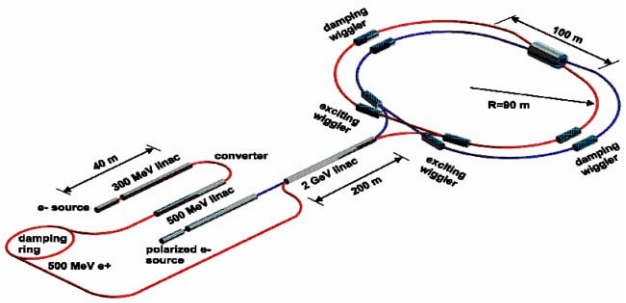

Fig. 3 Schematic view of the Novosibirsk TCF

The design of a high-luminosity TCF leads to physics challenges primarily in the areas of lattice design, IR design, e^- polarization technique, dynamic aperture optimization and the beam-beam interaction.

Luminosity

The peak luminosity has been optimized for the beam energy of 2 GeV. To reach the goal of $\geq 1\times10^{35}$cm^{-2}s^{-1}, the following essential parameters of the colliding beams should be met: small emittance ε_x = 10 nm-rad, small betas at IP β_x/β_y = 30 mm/0.75 mm and large crossing angle at IP $2\phi_x$ = 40 mrad.

Table 1 Main parameters of the Novosibirsk TCF

Energy, GeV	1.5	2.0	2.5
Hor. emittance, nm	10		
Coupling, %	0.5		
Bunch length, mm	10		
Bunch number	400	400	300
Particles/bunch	5.1×10^{10}	6.8×10^{10}	8.5×10^{10}
Bunch current, mA	3.1	4.0	5.0
Total current, A	1.2	1.6	1.51
Damping times, ms	30/30/15		
Betas at IP, mm	30/0.75		
Crossing angle, mrad	40		
Parameter ξ_y	0.15		
Luminosity, cm^{-2}s^{-1}	7.8×10^{34}	1.4×10^{35}	1.6×10^{35}

Table 1 lists the main machine parameters and the TCF luminosity at three energy levels.

It is worth mentioning that neither of the above parameters seems to be too excessive: even smaller emittance is typical for the latest generation synchrotron light sources; the total current of ~2 A was obtained in PEP II and DAΦNE; a few millimeter vertical beta, ξ_y = 0.1 or 10 mm bunch length can be attributed to KEKB. Undoubtedly, reaching all these figures is a challenge but all the accelerator technologies required for that already exist.

A sophisticated tracking of the beam-beam collision without and with the Crab Waist conditions by a LIFETRACK computer code [15] has shown the advantage of the last one.

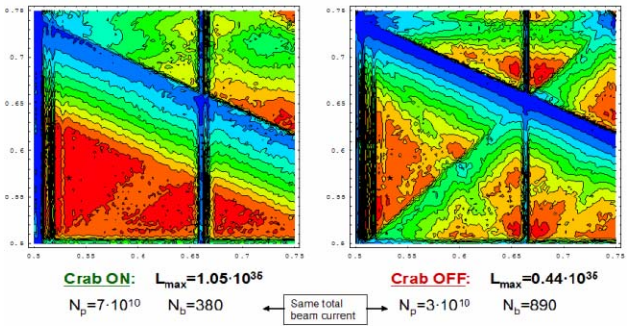

Fig. 4 Luminosity scan with the Crab-on and -off. Axes are the betatron tunes. The red color corresponds to the highest luminosity while the blue is the lowest.

At the luminosity scan presented in Fig.4, a suppression of betatron coupling resonances with the Crab Waist optics is clearly seen. As a result, the betatron tune region available for high luminosity is opened substantially. One should note that direct comparison in Fig.4 is, to some extent, incorrect because, if we tune the Crab Waist to the maximum luminosity and switch off the sextupole, the beam-beam effects will kill the beam. That is why we had to reduce particles number per bunch and increase bunch number to plot the right diagram in Fig.4.

Lattice design

Both rings of the TCF have the same racetrack design with two arcs (~280 m each) and two long straight sections (~150 m). The facility circumference (~850 m) is constrained by the tunnel that is now under construction at BINP. The lattice can be separated into the following sections: two arcs, producing the required emittance; IR with the Crab Waist optics and sextupoles; a long straight section opposite the IR intended to accommodate RF, injection and other technological equipment; several straights for wigglers to control the emittance with energy change and matching cells between all mentioned parts.

Key parts are the arcs producing the low emittance and the interaction region with the final focus and the Crab sextupoles.

Different cells (FODO, DBA, TME) have been considered as the candidates for the low emittance arcs and, finally, a simple FODO was selected because its focusing strength is enough to get the required emittance and, at the same time, to provide compact and reliable cell with a reasonable strength of chromatic sextupole.

An essential idea of the machine tuning is using the damping wigglers to control radiation parameters and to optimize the Crab Waist luminosity parameters in the whole energy range.

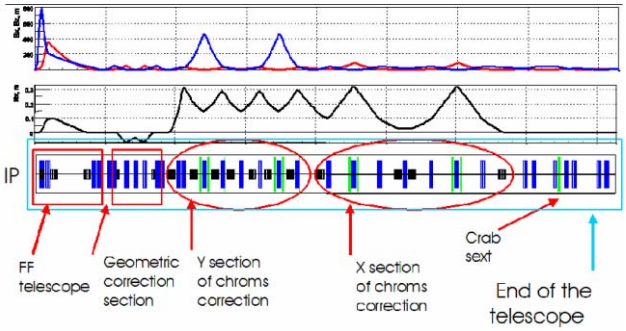

Fig.5 TCF FF lattice functions

The design of the IR with the low beta final focus and the Crab Waist optics is a most challenging task in the TCF lattice development because the following restrictions should be kept in mind: very small spot sizes at the IP; local correction for the very high chromaticity due to the highly focused beam; keeping chromatic and geometric aberrations small; separation of two beams from the rings as soon as possible; preventing synchrotron radiation production from hitting the beam pipe and the detector. Presently we have a solution based on the telescope approach with sextupole pairs spaced by –I in phase and compensation of the chromatic and the geometry aberrations locally (Fig.5). In our design a dispersion vector (η,η') is zero at the IP and at the Crab sextupoles location; and special dipoles introduce the dispersion to the location of the chromatic sextupoles. Such a design provides a rather large momentum bandwidth of ±2% (Fig.6).

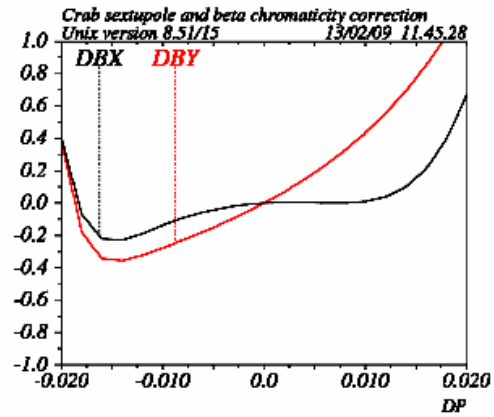

Fig.6 TCF bandwidth

Dynamic aperture and beam lifetime

Due to the very strong focusing, almost 50% of the horizontal and 80% of the vertical chromaticity is induced and corrected in the FF region. It requires high-strength sextupole magnets and the study shows that they, together with the Crab sextupoles, are the main source of the dynamic aperture (DA) limitation. A special technique of the weak DA correction sextupole pair interleaved with the strong chromatic pair was developed and provided a rather large transverse DA (Fig.7).

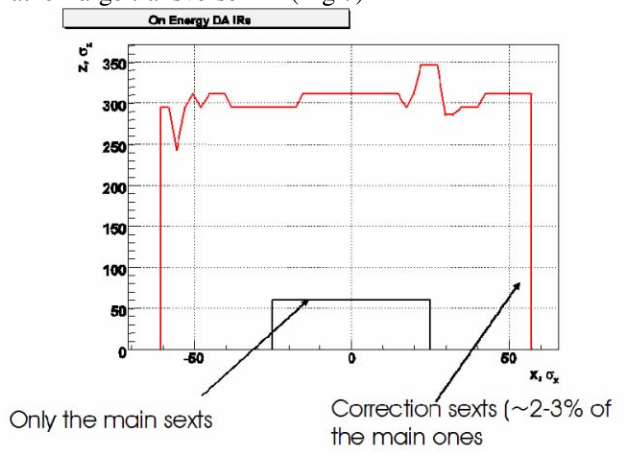

Fig.7 Correction sextupole pair opens the DA reduced by the strong chromatic sextupoles

There are two sources of the beam life time degradation in the TCF: the Touschek effect and the loss of particles due to scattering at the interaction point at a rate proportional to the machine luminosity. At the low energy the Toschek lifetime dominates (~1000 s) and this is an additional point for a further lattice optimization.

At the high energy the beam life time due to the Bhabha process (radiative and elastic), that scatters particles outside the ring acceptance, and the Touschek lifetime have approximately the same value of ~2000 s.

TECHNOLOGY CHALLENGES

Injection

To reach the specified luminosity, we have to provide a top-up injection of $2\div4\times10^9$ particles at 50 Hz repetition frequency.

At present a new Injection Facility is commissioned at BINP. It consists of the 300-MeV electron linac, the conversion system, the 510-MeV e^+e^- linac and the damping ring of the same energy (Fig.8).

Today the Facility produces 2×10^{10} e^-/pulse yielding at the 50 Hz repetition rate and with 1.5% conversion coefficient 1.5×10^{10} e^+/s. In the future we plan to use the Facility to supply the TCF with positrons. The following upgrade is available: new electron gun can increase the electron intensity by factor 3; more effective focusing system in the positron linac may enhance the positron current by 1.5; installation of a debuncher at the exit of the positron linac provides a better matching of the beam energy spread with the energy acceptance of the damping ring and, hence, increase twice the injection efficiency.

Fig.8 Damping ring under commissioning

Totally the positron production capacity can be enlarged up to 1.4×10^{11} e^+/s.

Experimental performance of the TCF requires longitudinally polarized electrons. To deliver such electrons we plan to use a Polarized Electron Source (PES) that was developed by BINP and operated successfully at AmPS (Netherlands) for many years [16]. The polarized electrons are accelerated to 510 MeV by the linac identical to the one of the Injection Facility. Finally, a 200 m long 2 GeV linac will be shared in turn between positron and electron beams to inject the particles in TCF at the energy of the experiment.

Beam polarization

To obtain longitudinally polarized electrons at IP, several options were considered. At the moment it seems that the most appropriate way is to produce polarized electrons by the PES [16] and manipulate them in the TCF with the Siberian Snakes as it is shown in Fig.9.

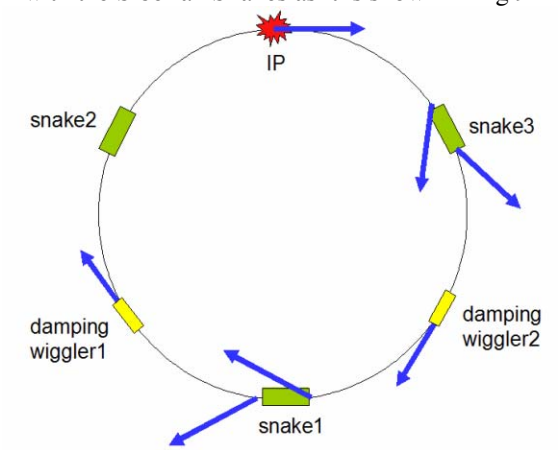

Fig.9 The odd-number Siberian Snakes spin manipulator

In our project we use 5 Snakes 12-m-long each. The Snake consists of two superconducting solenoids (L = 2.6 m, B = 5 T), rotating the spin by 90° each around the

beam velocity vector, and 7 quadrupoles providing condition for the local correction of the betatron coupling.

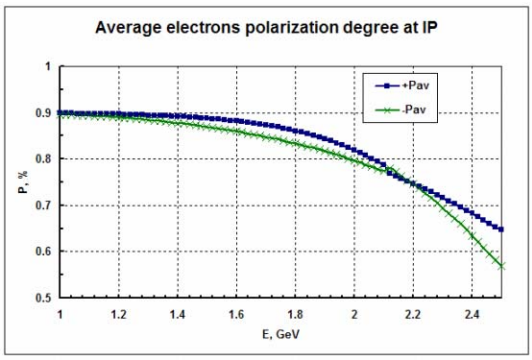

Fig.10 Average polarization degree (along and opposite the velocity vector) of the electron beam at IP vs. energy

The Snakes provide smooth (without the gaps at the spin resonance values) behavior of the average polarization degree at IP in the whole energy range. Fig.10 shows the polarization degree as a function of energy for the initial degree of 90% and the beam life time of 1000 s.

Infrastructure

One of the important constraints imposed on the new TCF project is using of the infrastructures already designed and partly constructed for the old TCF project. Besides the Injection Facility, it includes the underground tunnel for the longitudinally polarized source, 2.5 GeV linac injector (Fig.11) and halls for the storage rings.

Fig.11 A 800 m tunnel for 2.5 GeV linac

CONCLUSIONS AND OUTLOOK

Tau-charm factory with $L \geq 10^{35}$ $cm^{-2}s^{-1}$ seems to be an extremely attractive facility for HEP experiments. The Crab Waist crossing approach allows us to obtain this luminosity without going far beyond the present accelerator state-of-art with the already existing technology.

At BINP we have an advantage-ground to start the TCF project because the injection facility is under commissioning now, the tunnels for the linac and injection lines are ready, a lot of the solutions put in the core of the project are based on the existing wares and technologies.

Future plans for the project design include a further FF improvement, the dynamic aperture optimization, the beam-beam study, Touschek lifetime increase, etc.

REFERENCES

[1] E. Perelshtein et al. Proc. of the 3rd Workshop on the TC Factory, Marbella, Spain, 1-6 Jun 1993, 557-570
[2] M.V. Danilov et al. Int. J. Mod. Phys. A, Proc. Suppl. 2A (1993) 455-457
[3] E.Berger et al. ANL-HEP-TR-94-12, Feb 1994. 28pp
[4] Yu.Aleksahin, A.Dubrovin, A.Zholents. In EPAC 90 Proc., vol. 1, 398-400
[5] He-Sheng Chen. Nucl. Phys. Proc. Suppl. 59: 316-323, 1997
[6] A. Faus-Golfe and J. Le Duff. NIM A372:6-18, 1996
[7] C-Tau in Novosibirsk: Conceptual Design Report, BINP, Novosibirsk, 1995
[8] N.Yu. Muchnoi, S. Nikitin, V. Zhilich. Proc. of EPAC 2006, Edinburg, Scotland
[9] P. Raimondi, Status of the SuperB Effort, presentation at the 2nd Workshop on Super B Factory, LNF-INFN, Frascati, March 2006
[10] P. Raimondi and M. Zobov, DAΦNE Technical Note G-58, April 2003; D. Shatilov and M. Zobov, ICFA Beam Dyn. Newslett. 37, 99 (2005)
[11] D.V.Pestrikov, NIM Phys. Res., Sect. A 336, 427 (1993)
[12] K. Ohmi et al., Phys. Rev. ST Accel. Beams 7, 104401 (2004)
[13] P. Raimondi, D. Shatilov, M. Zobov, LNF-07/003 (IR), 2007
[14] M.Zobov (INFN LNF), for DAFNE Collaboration Team, DAFNE Operation Experience With Crab Waist Collision, arXiv:0810.2211v1
[15] D.Shatilov, Part.Accel., 1996, Vol.52, pp. 65-93
[16] L.G. van Amersfoort et.al. Proc. PAC'97, v.1, pp. 1063-1065

IR DESIGHN FOR SUPER-CT-FACTORY

A. Bogomyagkov*
BINP SB RAS, Novosibirsk

Abstract

Interaction region of Super-ct-factory is designed to bring stored electron-positron beams into collision with luminosity of 10^{35} cm^{-2}sec^{-1}. In order to achieve that CRAB waist collision scheme is implemented, which requires cross angle collision with high Piwinski angle. The small values of the beta functions at the interaction point and distant final focus lenses are the reasons for high nonlinear chromaticity which limits energy acceptance of the whole ring. The present design is based on chromatic properties of telescopic transformation, on local chromaticity correction schemes and on as close as possible placement of CRAB sextupole.

INTRODUCTION

The project of Super-ct-factory is designed to provide electron positron collisions with luminosity of 10^{35} cm^{-2}sec^{-1} in the central mass energy range of 3÷4.5 GeV. Invention of the crab waist collision scheme [1, 2] allows to achieve desired luminosity without utmost parameters of the accelerator. However, there are strong constraints on the size of the ring, because of the cost of the project and available space for the tunnel. This constraints limit the size of the interaction region to be less than 200 meters.

So far there are only two designs of the interaction region with crab waist — DAFNE and SuperB factory in Italy [3, 4]. The length of the interaction region of this project is about 300 meters which is not suitable for Super-ct-factory. Therefore new design of the interaction region has been done, however interaction region of SuperB project has been studied carefully.

PARAMETERS OF THE INTERACTION REGION

Basic parameters of the interaction region presented in Table 1 allow to achieve desired luminosity with nonextreme beam current, beta function values at the interaction point and beam-beam tune shift Table 2.

The chosen coupling coefficient of 1% is providing nonextreme beam-beam tune shift thus giving freedom for possible increase of luminosity by decreasing coupling.

The interaction region (IR) must also satisfy the following constraints.

- Due to collision with crossing angle there would be undesired synchrotron radiation background from the incoming beam in the final lens, therefore the lens is shifted to provide on axis trajectory of the incoming beam and eliminate synchrotron radiation background.
- Since accelerator is designed to operate at different energies there should be no longitudinal field integral over the final focus lenses.
- Integral of the detector longitudinal field should be compensated before each final focus lens.
- The length of the IR must be less than 200 meters.
- CRAB sextupole should be placed as close as possible to IP and at the position with low chromaticity of beta functions and phase advances to minimize its influence on dynamic aperture.

Table 1:

Energy, GeV	2
Beam current, A	1.36
Number of bunches	295
β_x, mm	20
β_y, mm	0.76
ε_x, nm rad	10
Coupling $\varepsilon_y/\varepsilon_x$, %	**1**
Beam length σ_z, cm	1
Crossing angle, mrad	34

Table 2:

Tune shift ξ_y	**0.13**
Particles per bunch	$7 \cdot 10^{10}$
Luminosity, cm^{-2}sec^{-1}	$1 \cdot 10^{35}$
Hour glass $\frac{\sigma_z}{\theta\beta_y}$	1.095
Piwinski angle $\varphi = \frac{\sigma_z\theta}{\sigma_x}$	12.021

BLOCKS OF THE INTERACTION REGION

Interaction region consist of several blocks:

1. final focus telescope — provides final demagnification of the beam, consist of two symmetrical triplets;
2. vertical chromaticity correction section — one pair of sextupoles with $n\pi$ phase advance from the first final focus lens (defocusing) and separated by -I transformation;

* A.V.Bogomyagkov@inp.nsk.su

3. horizontal chromaticity correction section — one pair of sextupoles with $n\pi$ phase advance from the second final focus (focusing) lens and separated by -I transformation;

4. CRAB sextupole section — cancels dispersion and provides place with appropriate phase advances ($\mu_x = \pi m$ and $\mu_y = \pi(2n+1)/2$) for CRAB sextupole;

5. ending telescope section — symmetrical triplet closing IR so that there is a telescopic transformation from IP to the end of the IR;

6. matching section — matches optical functions with the arcs of the accelerator.

The structure and optical functions are shown on Fig.1

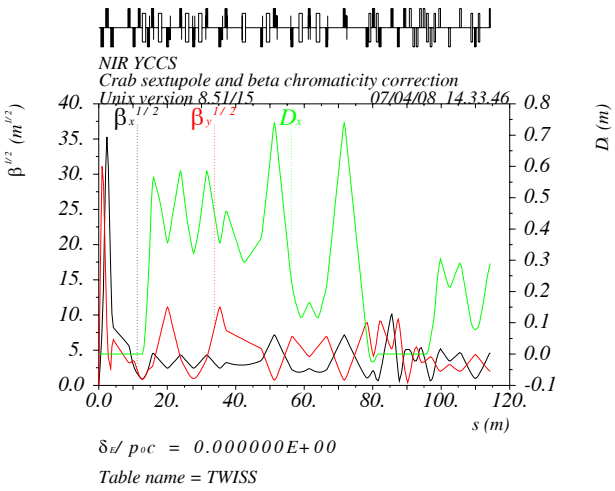

Figure 1: Optical functions of the interaction region.

The basic block of the IR is chosen to be telescopic transformation. This is done because the transfer matrix of the telescope is diagonal

$$R = \begin{pmatrix} R_{11} & 0 \\ 0 & R_{22} \end{pmatrix},$$

thus providing following relations between entering and exiting optical functions:

$$\begin{aligned} \beta &= R_{11}^2\beta_0 \\ \alpha &= \alpha_0 \quad = \quad 0 \\ \gamma &= R_{22}^2\gamma_0\,. \end{aligned}$$

The shown relations allow to change beta function at the IP with the help of matching section lenses without changing strengths of the IR quadrupoles. Another quality of the telescope is zero beta function chromaticity at the exit [5] with zero chromaticity at the entrance. Also symmetrical properties of the telescope provide simple relations for first and second order chromaticity of phase advance μ, beta function β and alpha function α:

$$\frac{d\mu_x}{d\delta} = \frac{T_{126}}{\beta_0 R_{11}}\,, \tag{1}$$

$$\frac{d^2\mu_x}{d\delta^2} = \frac{2U_{1266}}{\beta_0 R_{11}} - 2\frac{T_{126}T_{116}}{\beta_0 R_{11}^2}\,, \tag{2}$$

$$\begin{aligned} \beta = R_{11}\beta_0 + \delta\Big[2R_{11}T_{116}\beta_0\Big] + \\ +\delta^2\left[(T_{116}^2 + 2R_{11}U_{1166})\beta_0 + \frac{T_{126}^2}{\beta_0}\right], \end{aligned} \tag{3}$$

$$\begin{aligned} \alpha = \delta\left[-R_{11}T_{216}\beta_0 - \frac{T_{126}R_{22}}{\beta_0}\right] + \\ +\delta^2\Big[-\beta_0\Big(R_{11}U_{2166} + T_{116}T_{216}\Big) - \\ -\gamma_0\Big(R_{12}U_{2266} + T_{126}T_{226} + U_{1266}R_{22}\Big)\Big], \end{aligned} \tag{4}$$

where T_{ijk} and U_{ijks} denote second and third order matrices as in $R_{11}(\delta) = R_{11} + T_{116}\delta + U_{1166}\delta^2$. The above relations are true and for the vertical plane with appropriate change of the indices.

TRAJECTORIES AND APERTURES OF THE FINAL FOCUS LENSES

The final focus telescope is made of two symmetrical triplets. Trajectories of the particles of incoming and outgoing beams in the first two lenses are shown on Figure 2. Analyse of the shown trajectories allows to choose apertures of the final focus lenses. Also the cone of matter free space for the detector is shown, limiting an outside dimensions of the magnets. Detailed parameters of the final focus lenses are shown in Table 3 at 2.5 GeV.

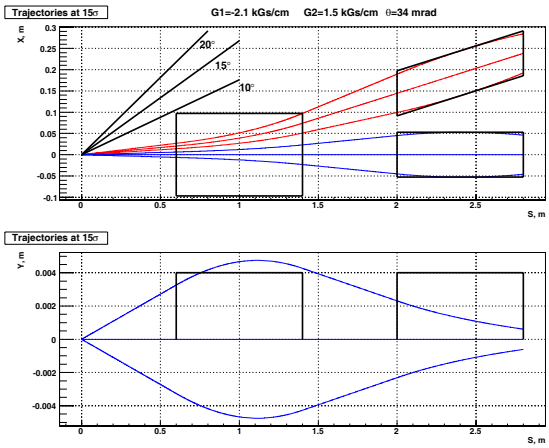

Figure 2: Horizontal and vertical trajectories of incoming and outgoing beams. Shown are central trajectories and distant at 15σ of respectful beam size. Rectangles show position of the lenses and net aperture.

EMITTANCE

The IR possesses strong bending magnets in order to couple sextupoles with chromatic functions. In order to minimize emittance growth in the IR all bending magnets are placed at the positions with minimum dispersion. However, the first final focus lens for outgoing beam (off axis)

Table 3: Parameters of the final focus symmetrical triplet at 2.5 GeV

Name	Q0	Q1	Q2
Position	0.6 m	2 m	3.4 m
Length	0.8 m	0.8 m	0.8 m
Gradient	-2.1 kGs/cm	1.5 kGs/cm	-2.1 kGs/cm
Bend	0.083 rad		
Net aperture	10 cm	5 cm	
β_x/β_y	66 / 970 m	1241 / 67 m	110 / 32 m

provides strong deflection of its trajectory. Combining with high values of beta functions and excited dispersion it gives rise to high value of H interval (Figure 3). Designed emittance of Super-ct-factory is $\varepsilon = 10$ nm and about 40% of it comes from IR bending magnets.

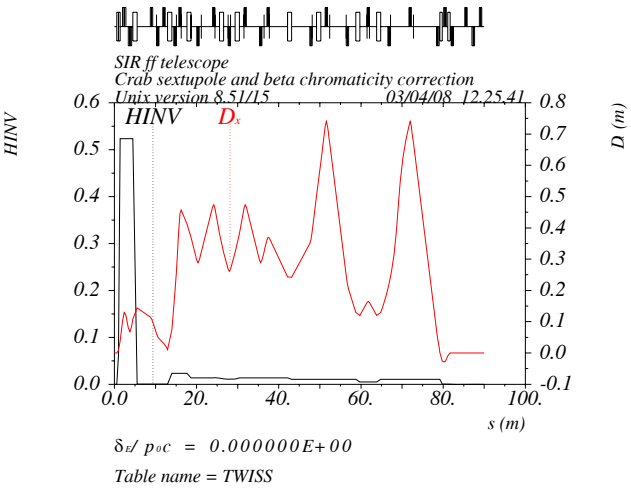

Figure 3: H invariant and dispersion the IR.

ENERGY ACCEPTANCE

High beta functions and strong quadrupoles of final focus telescope give rise to nonlinear chromatic terms in phase advance and optical functions. To cancel chromaticity of the final focus lenses two pairs of sextupoles are placed at $n\pi$ phase advance from each lens respectfully. However, as it is shown on figures (4, 5, 6) they are not suffiecent to compensate high order phase advance chromaticity. Therefore additional sextupoles and octupoles have been inserted in the structure with following principles:

- additional sextupoles — low beta functions but high beta chromaticity, high second order dispersion, weaker than main sextupoles;
- octupoles — high beta and dispersion.

The energy acceptance of $[-0.35, +0.55]\%$ was obtained (Figure 7) with the presented IR and its chromaticty tuning.

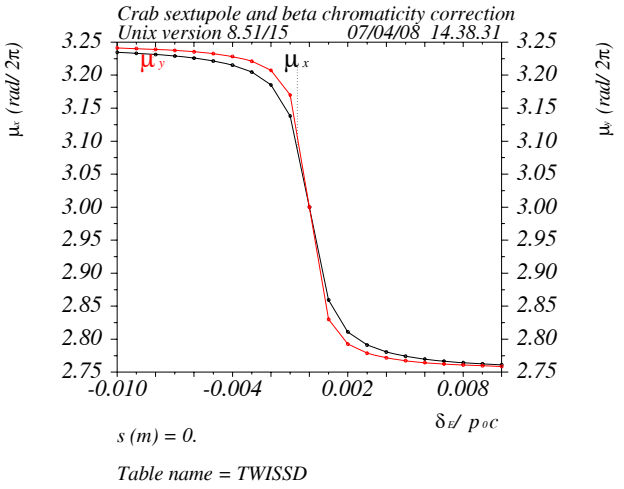

Figure 4: Phase advance at the exit of ending telescope. All sextupoles are off.

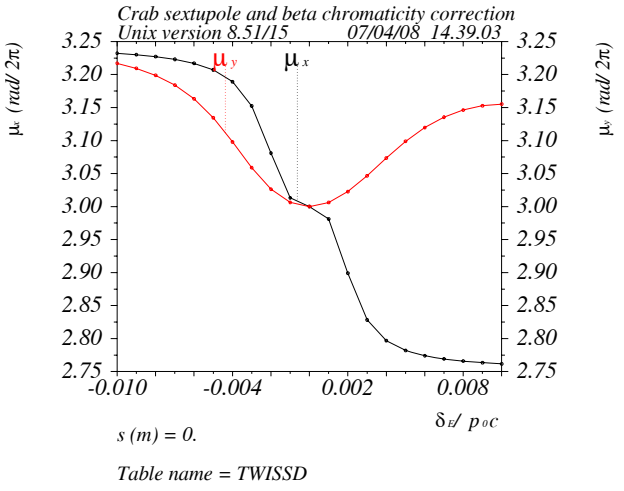

Figure 5: Phase advance at the exit of ending telescope. Only main sextupoles are on.

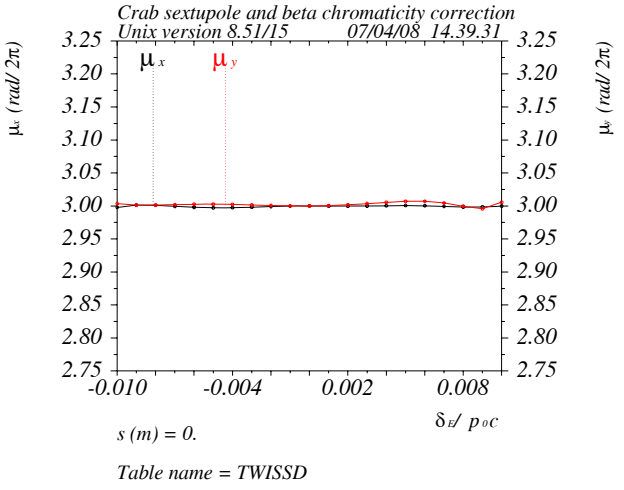

Figure 6: Phase advance at the exit of ending telescope. All sextupoles and octupoles are on.

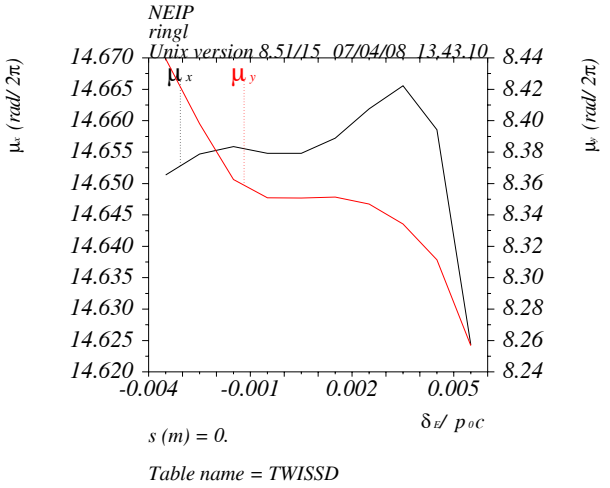

Figure 7: Phase advance of the whole ring versus energy deviation.

CONCLUSION

Designed interaction region provides luminosity of 10^{35} cm^{-2}sec^{-1} with not utmost parameters. There is freedom in beam-beam tune shift, which allows to reduce the coupling coefficient and increase the luminosity. The presented interaction region satisfies all geometrical constraints. Obtained energy acceptance of the Super-ct-factory is small and requires further optimization of the nonlinear chromaticity correction schemes in the interaction region and in the arcs.

REFERENCES

[1] P.Raimondi, Status on SuperB Effort, presentation at the 2nd Workshop on Super B-Factory, http://www.lnf.infn.it/conference/superb06/talks/raimondi1.ppt

[2] P. Raimondi, D. Shatilov, M. Zobov, .Beam-Beam Issues for Colliding Schemes with Large Piwinski Angle and Crabbed Waist., Preprint LNF-07/001, http://arxiv.org/physics/0702033

[3] C. Milardi "Crab waist experiment results", present workshop.

[4] SuperB conceptual design report, INFN/AE-07/2, SLAC-R-856, LAL 07-15, March 2007.

[5] Karl L. Brown, SLAC-PUB-3381, "First and Second Order Charged Particle Optics".